UNIVERSIDAD NACIONAL AUTÓNOMA DE MÉXICO

PROGRAMA DE POSGRADO EN ASTROFÍSICA

Instituto de Astronomía

Stellar Rotation of Young Stars

THESIS DISSERTATION TO OBTAIN THE:

DOCTORAL DEGREE IN SCIENCES (ASTROPHYSICS)

PRESENTS:

Javier Serna Quiñones

ADVISOR:

Dr. Jesús Omar Hernández Alarcón
Instituto de Astronomía - UNAM

Ensenada, B. C., September 2023.

Dissertation jury committee:

Dr. Cesar Briceño Avila
Cerro Tololo Inter-American Observatory.

Dra. Karla Peña Ramírez
Universidad de Antofagasta.

Dr. Carlos Carrasco González
Instituto de Radioastronomía y Astrofísica, UNAM.

Dr. Luis Alberto Zapata González
Instituto de Radioastronomía y Astrofísica, UNAM.

Dra. Amelia Maria Bayo Aran
The European Southern Observatory.

Dedicatory

To my family and friends

Acknowledgements

I want to express my gratitude to my family, Marien Quiñones, Weiner Serna, and Valentina Serna, for supporting me throughout. Despite the distance that separates us, you will always be close to my heart.

A special thank you to Jesús Hernández; it is an honor and true privilege to have come this far, thanks to him.

A special thanks to Margarita Pereyra, who has been by my side, supporting me in this journey, and has offered her advice and motivation with great affection.

I appreciate UNAM, especially the Instituto de Astronomía headquarters in Ensenada, for providing me with all the necessary spaces and infrastructure to complete my postgraduate studies. I also extend my gratitude to the PAPIIT IA102319 project, "Studies of Young Stars and their Protoplanetary Disks in the GAIA-APOGEE-WISE Era," the PAPIIT CG101723 project, "Caracterización y modelación de grupos estelares jóvenes en la era del big data," the CONACyT CF-86372 project, "CitlalCoatl: A multiscale study at the new frontier of the formation and early evolution of stars and planetary systems" and, of course, to the funding from the government of Mexico through CONACYT.

The discussions and recommendations improved the advances and results of this thesis and its products in the following collaborative research groups: Activity and Rotation in Young Stellar Objects (ARYSO), Models and Observations of Disk Evolution in Latin America (MODELA), and the Star Formation group of the Instituto de Astronomía, Ensenada, México.

To all of them ¡Pura Vida!

Contents

List of Figures

List of Tables

Abbreviations

TESS Transiting Exoplanet Survey Satellite

OSFC Orion Star-Forming Complex

HR Hertzprung Russell

AM Angular Momentum

CTTS Classical T-Tauri Star

Gaia DR3 Gaia Data Release 3

PMS Pre-Main Sequence

SDSS Sloan Digital Sky Survey

WTTS Weak T-Tauri Star

YSO Young Stellar Object

WTTS Weak T-Tauri Star

FOV Field of View

APOGEE-2 Apache Point Observatory Galactic Evolution Experiment 2

Myr Million Year

AM Angular Momentum

LC Light Curve

RUWE Renormalized Unit Weight Error

ONC Orion Nebula Cluster

CWTTS Classical Weak T Tauri Star (Briceño et al., 2019)

RV Radial Velocity

IN-SYNC INfrared Spectra of Young Nebulous Cluster

FT Fourier Transform

FFI Full Frame Image

SAP Simple Aperture Photometry

CBV Cotrending Basis Vector

LSP Lomb Scargle Periodogram

DSS2 Digital Sky Survey 2

FAP False Alarm Probability

ASAS-SN All Sky Automated Survey for SuperNovae

2MASS Two Micron All Sky Survey

SB2 Spectroscopic Binary

IQR InterQuartile Range

K-S Kolmogorov Smirnov

DL Disk Locking

MHD Magnetohydrodynamics

APSW Accretion-Powered Stellar Winds

ABC Approximation Bayesian Computation

LAMOST Large Sky Area Multi-Object Fiber Spectroscopic Telescope

MAD Median Absolute Deviation

ARYSO Activity and Rotation of Young Stellar Objects Group

ULLYSES Ultraviolet Legacy Library of Young Stars as Essential Standards Program

ODYSSEUS Outflows and Disks around Young Stars: Synergies for the Exploration of Ullyses Spectra Team

HARPS High Accuracy Radial Velocity Planet Searcher

WISE Wide-field Infrared Survey Explorer

Nomenclature

T_{eff} Effective temperature

$M_{\odot}$ Units of solar mass

A_v Visual extinction

R Spectral resolution

$v \sin(i)$ Projected rotational velocity

P_{rot} Rotational period

$EW(H_{\alpha})$ Equivalent width of H_{α}

$\log(g)$ Surface gravity

[Fe/H] Metalicity

$\sin(i)$ Sine of inclination

ω Angular velocity

χ Branching ratio

B_* Dipolar magnetic field

I Moment of inertia

k Gyration radius

R_{co} Corotation radius

r_A Alfvén radius

τ_* Torque

v_{esc} Escape velocity

$\dot{M}_{wind}$ Stellar winds rate

Resumen

El complejo de formación estelar de Orión es un laboratorio astrofísico ideal con un gran número de estrellas confirmadas espectroscópicamente como objetos jóvenes de baja masa (estrellas T Tauri) en un amplio rango de edades (1-10 Myr), muy adecuado para realizar un estudio sistemático de la rotación estelar durante los primeros millones de años de vida estelar. En esta fase, los discos protoplanetarios que están vinculados mediante columnas de acreción a las estrellas regulan la evolución del momento angular. El objetivo central de esta tesis doctoral es embarcarse en una exploración sin precedentes de la rotación estelar de las estrellas T Tauri. Este trabajo se realizó desde las perspectivas observacional y teórica, desarrollando herramientas para la estimación robusta de medidas de rotación estelar:

Desde una perspectiva observacional, utilizamos estimaciones de velocidad de rotación proyectada ($v \sin(i)$) de la colaboración APOGEE-2, así como masas y edades individuales derivadas del diagrama HR y modelos evolutivos. Las estimaciones de $v \sin(i)$ fueron comprobadas con una herramienta propia que usa métodos de Transformada de Fourier. Nuestro estudio también incluye períodos de rotación estimados a partir del análisis de la curva de luz de TESS. Para las estrellas de baja masa, encontramos una tendencia evolutiva empírica de $v \sin(i)$, que indica que los discos de acreción regulan la rotación estelar en escalas de tiempo de aproximadamente 6 Myr, que es la escala de tiempo en la que la mayoría de las estrellas T Tauri pierden su disco interno. Nuestros resultados proporcionan importantes limitaciones a los modelos de rotación en las primeras fases de la evolución de estrellas jóvenes y sus discos. Este trabajo se publicó en la revista ApJ (Serna et al., 2021).

Desde una perspectiva teórica, desarrollamos una herramienta que permite la generación de redes de modelos de rotación estelar, que incluyen evolución de la estructura estelar, la interacción estrella-disco y las eyecciones magnetosféricas en el marco de vientos estelares potenciados por acreción. De esta forma estudiamos la evolución de la tasa de rotación estelar en función de la masa, el campo magnético y el viento estelar. Nuestros resultados confirman que las mediciones de $v \sin(i)$ en T Tauri stars concuerdan con las tasas de rotación proporcionadas por nuestros modelos. Adicionalmente, encontramos que la evolución de $v \sin(i)$ con

la edad podría ser regulada por variaciones en (a) la intensidad del campo magnético y (b) la fracción del flujo de acreción expulsado en los vientos magnéticos. Este trabajo se encuentra actualmente en su segunda revisión en la revista ApJ [2].

Además, presentamos la aplicación web TESSExtractor, que facilita de forma intuitiva la extracción y el análisis de curvas de luz TESS para diversos estudios astrofísicos, incluida la rotación estelar. Esta herramienta ya esta disponible y la publicación asociada se presentará en la revista AJ este año [3]. De hecho, TESSExtractor ya se utiliza intensivamente en dos proyectos Ph.D. de nuestros grupos de colaboración (por ejemplo, Rodríguez-Feliciano et al. (2023), Batista et al. en preparación).

Esta investigación ha proporcionado una comprensión general de la rotación en estrellas jóvenes en relación con sus discos, proporcionando información valiosa sobre los procesos físicos involucrados en las estrellas T Tauri. Además, este trabajo ofrece modelos para pronosticar parámetros físicos como el campo magnético y la tasa de pérdida de masa para las estrellas T Tauri. Además, proporciona herramientas para estimar observables de rotación utilizando fotometría y espectroscopía, extendiendo su utilidad a diversos usuarios.

Abstract

The Orion star-forming complex is an ideal astrophysical laboratory with a large number of spectroscopically confirmed stars as low-mass young objects (T Tauri stars) in a wide range of ages (1-10 Myr), well suited to perform a systematic study of stellar rotation during the first million years of stellar life. In this phase, protoplanetary disks that are linked via accretion columns to the stars regulate the evolution of angular momentum. The central objective of this doctoral thesis is to embark upon an unprecedented exploration of stellar rotation within T Tauri stars. To achieve this, we combine two approaches to conduct this study, developing tools for the robust estimations of stellar rotation measurements:

From an observational perspective, we use projected rotational velocity ($v \sin(i)$) estimations from the APOGEE-2 collaboration, as well as individual masses and ages derived from the HR diagram and evolutionary models. The $v \sin(i)$ estimates were checked using a tool developed in this thesis that uses Fourier Transform methods. Our study also includes rotational periods estimated from TESS light curve analysis. For low-mass stars, we found an empirical evolutionary trend of $v \sin(i)$ that indicates that accreting disks regulate stellar rotation on timescales of about 6 Myr, which is the timescale in which most of the T Tauri stars lose their inner disk. Our results provide important constraints to models of rotation in the early phases of the evolution of young stars and their disks. This work was published in the ApJ Journal (Serna et al., 2021).

From a theoretical perspective, we developed a tool to generate grids of stellar rotation models, incorporating the star-disk interaction and magnetospheric ejections in the accretion-powered stellar winds framework to investigate the evolution of the stellar rotation rate as a function of the mass, the magnetic field, and stellar wind. Our results confirm that T Tauri stars' $v \sin(i)$ measurements agree with the rotation rates provided by our models. Additionally, we find that the evolution of $v \sin(i)$ with age might be regulated by variations in (a) the intensity of the magnetic field and (b) the fraction of the accretion flow ejected in magnetic winds. This work is currently under its second revision in ApJ Press [2].

In addition, we present a user-friendly web application called TESSExtractor, which facilitates the extraction and analysis of TESS light curves for various astrophysical studies, including stellar rotation. This tool is already available and is within the scope of any person. The paper related to TESSExtractor will be submitted to AJ Journal this year [3]. Indeed, TESSExtractor is already intensively used in two Ph.D. projects of our collaboration groups (e.g., Rodríguez-Feliciano et al. (2023), Batista et al. in preparation).

This research has provided a general understanding of rotation in young stars in connection with their disks, providing valuable insights into the physical processes involved in T Tauri stars. Furthermore, this work offers models to forecast physical parameters such as magnetic field and mass loss rate for T Tauri stars. Moreover, it provides tools to estimate rotation observables using photometry and spectroscopy, extending their utility to diverse users.

1 Introduction

Stellar rotation is fundamental to studying the formation and evolution of stars and planets (Bouvier, 2013; Pinzón et al., 2021; Strugarek et al., 2015). In this context, it is a key piece for understanding the early evolution of angular momentum and its relationship to various stellar processes, such as the stellar structure, magnetic fields, stellar activity, stellar winds, and protoplanetary disks. Angular momentum and its evolution is one of the more challenging open problems of modern stellar astrophysics. Nowadays, thanks to the large surveys and the unprecedented precision of available data (e.g., APOGEE, TESS, *Gaia*), the community is making valuable efforts and significant progress in this area (Kounkel et al., 2023).

Young stars, also known as T Tauri stars (ages ≤ 10 Myr), are born from vast clouds of gas and dust (Briceño et al., 2019; Hernández et al., 2014), and even at their earliest stages, they exhibit inherent rotation (Covey et al., 2005). As they form, the material from their natal cores is transferred through protoplanetary disks onto the central protostar (Hartmann et al., 2016). Consequently, the rotational velocity of these stars is expected to increase due to the conservation of angular momentum. However, the rapid angular momentum loss observed in these stars has been an enigma for decades (Bouvier et al., 1993). Most stars with disks exhibit rotation rates significantly below their theoretical break-up limits (Stassun et al., 1999). This paradox suggests that these stars lose angular momentum at an astonishing rate during their first million years (Kounkel et al., 2023), challenging our understanding of the underlying mechanisms driving this phenomenon. Thus, it is crucial to perform studies of stellar rotation in young stellar pre-main sequence populations in which large angular momentum loss is expected.

One of the physical phenomena that could induce the diminishing of the angular momentum is disk-locking, where a star's magnetic field interacts with its surrounding protoplanetary disk, resulting in a redistribution of angular momentum. Despite it being a conceivable scenario to explain the braking, the efficiency of this disk-locking mechanism in counteracting the spin-up caused by accretion remains a subject of debate. Observations indicate that stars with protoplanetary disks exhibit slower rotation rates than diskless stars, supporting the

notion of disk-locking. However, not all studies have confirmed this trend, and contradictory results have been reported (see Serna et al., 2021).

Previous studies have proposed models based on the disk-locking mechanism, in which stellar angular velocity remains constant as long as stars are in the presence of disks (Amard et al., 2016, 2019; Gallet and Bouvier, 2013, 2015). However, new models such as Accretion-Powered Stellar Wind (APSW) suggest that even in the presence of an accreting disk, the stellar angular velocity can change (Gallet et al., 2019; Matt et al., 2012; Pinzón et al., 2021). This paradigm provides an excellent opportunity to build models and explore the influence of the physical mechanisms such as magnetic fields (B_*) and mass-loss rate via stellar winds ($\chi = \frac{\dot{M}_{wind}}{\dot{M}_{acc}}$) in relation to observables of CTTS, e.g., Rotational period (P_{rot}), Projected rotational velocity ($v \sin(i)$), Mass, Age, among others.

Nowadays, we know that the relationship between rotation and physical phenomena in stars depends heavily on age, stellar mass, and even metallicity, which increases the complexity toward a better understanding of the origin and evolution of the angular momentum of stars. However, we are in a golden era in which the stellar characterization of young stars can be robustly and homogeneously derived thanks to large spectroscopic surveys, such as SDSS-APOGEE (e.g., Kounkel et al., 2018), combined with the kinematic information available in the data release of *Gaia*. Additionally, multi-epoch large-scale photometric surveys, such as TESS, can provide precise information about the rotation of spotted stars, such as T Tauri stars.

In this dissertation, we present a multifaceted study that seeks to provide a general perspective on the stellar rotation of young stars. From an observational perspective, we contribute to the ongoing discussion about the role of accreting disks in shaping the observed trends of angular momentum in pre-main-sequence stars. More details about this work are found in Chapter 2. From a theoretical perspective, we explore the influence of astrophysical processes in young stars such as (B_*, χ) in relation to the stellar rotation through a comprehensive grid of models developed for disk stars or Classical T Tauri Stars. The reader can find more details about this work in Chapter 3. The TESSExtractor tool developed in this work is presented in the Chapter 4. In the Chapter 5, we present our conclusions, contributions to research papers, and my ongoing/future work.

2 Stellar Rotation of TTS in the OSFC (Serna et al., 2021)

The analysis presented in this section constitutes my first publication during the second year of my doctoral program. This manuscript, titled "Stellar Rotation of T Tauri Stars in the Orion Star-forming Complex" by Serna et al. (2021), was published in ApJ Press and constitutes an integral part of this dissertation. While a significant portion of the findings in this publication originated from my master's degree, crucial components, such as mass and age determination, the estimation and comparative analysis of projected rotational velocities in existing literature, post-processing of the TESS light curves and period determination with errors, as well as the development of the software introduced herein, were refined and expanded upon during my doctoral studies.

Abstract: We present a large-scale study of stellar rotation for T Tauri stars in the Orion Star-Forming Complex. We use the projected rotational velocity ($v \sin(i)$) estimations reported by the APOGEE-2 collaboration as well as individual masses and ages derived from the position of the stars in the HR diagram, considering Gaia-EDR3 parallaxes and photometry plus diverse evolutionary models. We find an empirical trend for $v \sin(i)$ decreasing with age for low-mass stars ($0.4M_{\odot} < M_{*} < 1.2M_{\odot}$). Our results support the existence of a mechanism linking $v \sin(i)$ to the presence of accreting protoplanetary disks, responsible for regulating stellar rotation in timescales of about 6 Myr, which is the timescale in which most of the T Tauri stars lose their inner disk. Our results provide important constraints to models of rotation in the early phases of evolution of young stars and their disks.

2.1 Introduction

Stellar rotation is a fundamental parameter in star formation and stellar evolution, and it plays a crucial role in the origin of planetary systems. Understanding the origin and early evolution of stellar angular momentum is one of the most challenging problems of modern stellar astrophysics. This study is a cross-sectional tool for multiple stellar physical processes

(Amard et al., 2019; Bouvier, 2013; Bouvier et al., 2014; Spada and Lanzafame, 2020).

While rotational velocities of most main-sequence stars decrease with age ($v \sin(i) \propto t^{-\frac{1}{2}}$) due to angular momentum (AM) losses by stellar winds (Skumanich, 1972), in very young stars there are mechanisms not yet well understood that can affect the angular momentum (e.g., disk-locking effect, core-envelope decoupling, stellar winds; Littlefair, 2013). Thus, finding Skumanich-type relations for pre-main-sequence stars (PMS) becomes more problematic. Regardless of these complexities, and based on observations from different young stellar associations, it has been possible to progress in AM evolutionary models for low-mass stars at the PMS phase (Amard et al., 2016, 2019; Gallet and Bouvier, 2013, 2015; Matt et al., 2012). The characterization of critical parameters related to the interaction between a star and its protoplanetary disk, mass accretion rate, stellar winds, and other mechanisms of AM loss, needs to be improved to better understand AM evolution during the early stages (Bouvier et al., 2014), when disk dissipation and planet formation occur (e.g. Hernandez et al., 2007; Testi et al., 2014; Williams and Cieza, 2011).

AM evolutionary models consider a disk-locking mechanism that keeps a constant stellar angular velocity as long as stars have accreting disks (Amard et al., 2016, 2019; Gallet and Bouvier, 2013, 2015). However, accretion-powered stellar wind models suggest that the stellar angular velocity could change even in the presence of an accreting disk (Gallet et al., 2019; Matt et al., 2012; Pinzón et al., 2021). Most observational studies support a scenario in which magnetic star-disk coupling has a fundamental impact on young stars rotational properties. Thus, stars with accreting disks rotate, on average, slower than stars without accreting disks (e.g., Biazzo et al., 2009; Davies et al., 2014; Jayawardhana et al., 2006; Rebull et al., 2006, 2014; Venuti et al., 2017). In contrast, other studies found no significant differences between rotation properties and the presence of accretion disks, even reporting contradictory results to the disk-locking scenario (Blanc et al., 2011; Karim et al., 2016; Makidon et al., 2004; Nguyen et al., 2009; Stassun et al., 1999). Thus, additional studies are needed to determine the role of accreting disks, stellar magnetic fields, and stellar winds on the evolutionary trends of angular momentum observed in PMS stars.

The Orion Star-Forming Complex (OSFC) is one of the best-known young regions in the solar neighborhood. It is located at a distance of $d \sim 400$ pc (Großschedl et al., 2018; Kuhn et al., 2019) and has a wide variety of stellar populations in different environments, with ages spanning from 1 to 10 Myr (Briceño, 2008; Briceño et al., 2019; Kounkel et al., 2017, 2018; Zari et al., 2019). The OSFC has several well-known stellar clusters such as the Orion Nebula Cluster (ONC; 1-2 Myr), the σ Orionis cluster (3-4 Myr), the λ Orionis cluster (4-6 Myr)

and the 25 Ori cluster (7-10 Myr), mainly located in two OB associations, the Orion OB1 association (Warren and Hesser, 1977) and the λ Orionis association (Murdin and Penston, 1977). This makes the OSFC an ideal astrophysical laboratory to perform general studies of star formation and early stellar evolution. Thus, the OSFC is well suited to perform a systematic study of stellar rotation during the first million years of the stellar life, when protoplanetary disks with magnetospheric accretion can affect the AM evolution.

Several works have focused on detecting and characterizing young stellar objects (YSOs) on/off clouds of the OSFC. Briceño et al. (2019) identified more than 2000 T Tauri stars in the Orion OB1 association using optical spectra. The detection of the Li1 line in absorption confirms the youth of the sample, while measurements of the equivalent width of the Hα emission line were used to identify stars with accreting disks (e.g., Classical T Tauri Stars; CTTS), as well as those without accreting disks (e.g., Weak-lined T Tauri Stars; WTTS). Using similar methods for characterizing young stellar populations, Hernández et al. (2014) and Hernandez et al.(in preparation) present exhaustive spectroscopic censuses of the stellar population in the σ Orionis cluster and in the ONC, respectively. In addition, combining the second data release of the Gaia space mission (Gaia-DR2; Gaia Collaboration et al., 2018) and Apache Point Observatory Galactic Evolution Experiment (APOGEE; Majewski et al., 2017) high resolution near infrared spectra obtained in the OSFC (Cottaar et al., 2014), Kounkel et al. (2018) have detected $\sim$2400 kinematic members using 6-dimensional analysis (positions, parallax and proper motions from Gaia-DR2 and radial velocities from APOGEE; hereafter known kinematic members).

Photometric variability is widely used to identify and characterize YSOs (e.g.; Bouvier et al., 1993; Briceño, 2008; Cody and Hillenbrand, 2018; Herbst et al., 2002; Morales-Calderón et al., 2011). In addition to periodic light curves (LCs) modulated by stellar rotation and the presence of magnetic spots on a stellar surface, other mechanisms contribute to the observed variability in YSOs such as dimming by the dust in the disk, fluctuations in the accretion rate of the disk, eclipses caused by stellar companions or planets, and stellar pulsations (Cody and Hillenbrand, 2010; Cody et al., 2014). Nowadays, space missions have revolutionized the sky photometric monitoring, providing unprecedented information on the variable sky. Particularly, the Transiting Exoplanet Survey Satellite (TESS), which has finished its second year of operations providing very high-quality photometric data, is one of the most powerful large-scale astrophysical space missions. It focuses primarily on detecting transits of planets orbiting bright host stars relatively close to the earth (Ricker et al., 2014). TESS has provided accurate photometry with a cadence of 30 minutes during 27 days of observations for the entire OSFC. In this work, we use TESS data to build LCs and measure rotational

periods of T Tauri stars, which normally range from 1 to 10 days (Karim et al., 2016).

Making use of large-scale spectroscopic, photometric, and kinematic surveys in the OSFC (Briceño et al., 2019; Kounkel et al., 2018), we perform here an evolutionary study of the stellar rotation for low-mass stellar members ($0.4M_{\odot} < M_{*} < 1.2M_{\odot}$) in this star-forming complex. We investigate stellar rotation in T Tauri stars and the relation to their protoplanetary disks. We also provide new rotational periods for kinematical and spectroscopic members of the OSFC, derived from TESS data. In §2.2, we define our sample of spectroscopic and kinematic members. We provide a brief description of the TESS observations and the LC analysis extraction, and we also describe the derivation and compilation of the stellar parameters such as $v\sin(i)$, effective temperature (T_{eff}), rotation period ($P_{\rm rot}$), mass, and age. In §3.3 we present the derived relationships of $v\sin(i)$ against period, $v\sin(i)$ versus age, and $v\sin(i)$ versus Hα line equivalent width (EW_{H_α}). Also, we discuss the influence of disks on the rotation measurements of the OSFC, including evidence of disk-locking effects. Finally, in §2.4 we summarize the results and present our main conclusions.

2.2 OSFC sample and measurements of stellar parameters

2.2.1 Kinematic Members

The Gaia mission has opened the possibility of detecting young stars by studying their kinematic properties with unprecedented precision and accuracy (Godoy-Rivera et al., 2021; Kounkel et al., 2018; Kuhn et al., 2019; Soubiran et al., 2019; Zari et al., 2019). Recently, the Early Third Data Release (hereafter Gaia-EDR3) of the Gaia mission became available. It includes significant improvements with respect to previous releases (Gaia Collaboration et al., 2020). We cross-matched the known kinematic members reported by Kounkel et al. (2018) with the Gaia-EDR3 catalog. Based on the distributions of Gaia-EDR3 parallaxes (ϖ) and proper motion modulus ($|\mu| = \sqrt{\mu_\alpha^2 + \mu_\delta^2}$) of the known kinematic members, we define the following membership region: 2.00< ϖ < 3.14 mas and $|\mu|$ <3.5 mas/yr. These limits were defined using the mean and the standard deviation applying a 3σ criteria. Our sample of kinematic members includes stars with APOGEE infrared spectra (Cottle et al., 2018; Kounkel et al., 2018; Majewski et al., 2017) that fall in the membership region. Thus, we include stars with reliable astrometric solutions in Gaia-EDR3, not included in the previous Gaia release. We require stars with relative errors in parallax smaller than 20%. We also apply cuts based on the photometric and astrometric quality suggested for Gaia-EDR3 data

(Lindegren et al., 2020b). In brief, we select all kinematic members with renormalized unit weight error (RUWE) smaller than 1.4 and satisfying the Lindegren et al. (2020b) relation:

$$0.001 + 0.039 \times (BPmag - RPmag) < \log E < 0.12 + 0.039 \times (BPmag - RPmag) \quad (2.1)$$

where E is the excess flux ratio [1] and $BPmag$ and $RPmag$ are the magnitudes in the filters BP and RP, respectively. Kinematic members that do not fulfill equation (2.1) could have inconsistent Gaia-EDR3 photometric fluxes due to blends, contamination by a nearby source or a sign of the extended nature of the source. Finally, using the GAIADR3_ZEROPOINT python package, we estimate the value of the parallax zero-point for Gaia-EDR3. This software applies the analytical functions to compute the expected parallax zero-point as a function of ecliptic latitude, magnitude and color (Lindegren et al., 2020a). To reduce systematics, we subtract the parallax zero-point from the Gaia-EDR3 parallaxes. The left panel of Figure 2.1 shows the spatial distribution of the kinematically selected YSOs in the complex. The resulting sample has 2204 kinematic members of the Orion Complex that will be used in this work.

2.2.2 Spectroscopic Members

An extensive optical spectroscopic study in the Orion OB1 associations was performed by Briceño et al. (2019). Using several instruments with similar spectral resolution (R$\sim$ 1000-2000), they obtained optical spectra for a sample of 11200 candidate PMS stars selected by their photometric variability and location in optical and optical-near-IR color-magnitude diagrams. Using the IRAF/IDL based SPTCLASS tool (Hernandez et al., 2017; Hernández et al., 2004), Briceño et al. (2019) analyzed the mentioned sample of candidates and reported 2062 T Tauri Stars (TTSs) that were listed with their spectral types and equivalent widths of Li1 λ6708Å and Hα lines. Similarly, and using the same tools, Hernández et al. (2014) and Hernandez et al., (in preparation) performed a systematic optical spectroscopic census of YSOs, reporting 221 TTS in the σ Orionis cluster and 909 TTS in the ONC (see also Manzo-Martínez et al., 2020). The middle panel of Figure 2.1 shows the spatial distribution of the spectroscopically-confirmed TTS.

Using a classification scheme based on the relation between the equivalent widths of the Hα line and spectral types, Briceño et al. (2019) reported 1696 WTTS, 214 CTTS, and 152 CWTTS in the Orion OB1 association. The CWTTS are considered stars evolving from an active CTTS accretion phase to a non-accreting WTTS stage. Briceño et al. (2019) proposed that CWTTS is likely composed of a mix of objects that are accreting at modest or low levels, constituting the weak tail of the CTTS and a few objects in a quiescent stage between periods

[1] $E = \frac{I_{BP}+I_{RP}}{I_G}$; where I_{BP},I_{RP} and I_G are the fluxes in the Gaia filters BP, RP and G, respectively

of enhanced accretion. In this work, we apply the same classification scheme to split the σ Ori and the ONC samples of TTS into WTTS, CTTS, and CWTTS. This information about the accretion status of spectroscopically confirmed TTS is crucial to examine the relation between the stellar rotational properties and the presence of accreting protoplanetary disks (see §2.3.3).

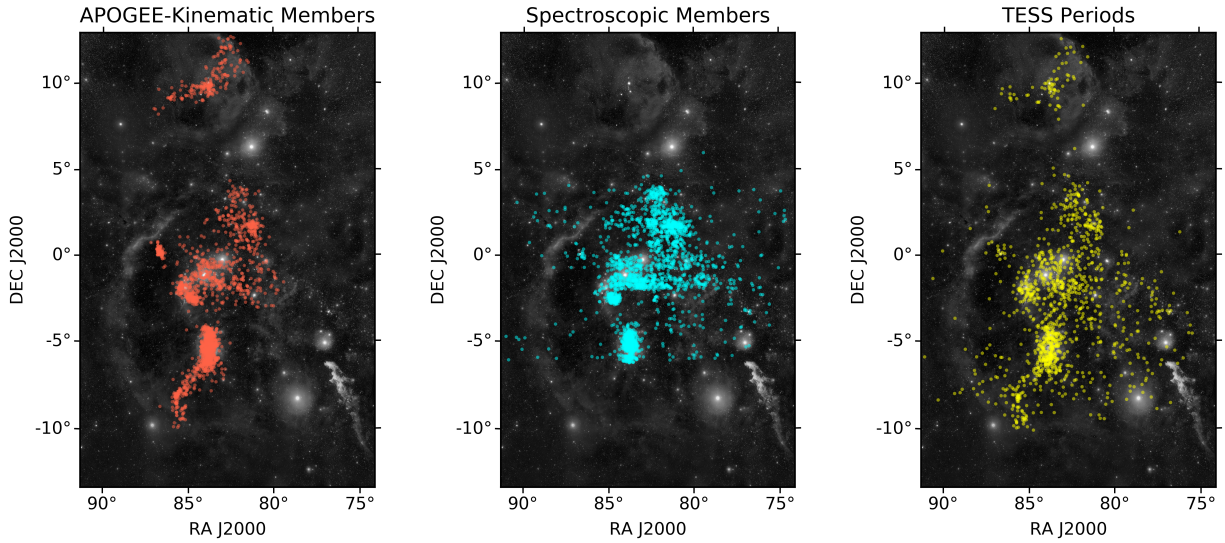

Figure 2.1: Spatial distribution of Orion's APOGEE sources with counterparts in the kinematic members sample (red dots in the left panel), spectroscopic members (middle panel, cyan dots), and kinematic or spectroscopic members with TESS LCs (right panel, yellow dots) in the OSFC sample. The gaps observed in the middle panel are due to a selection effect of the spectroscopic sample (see, Briceño et al., 2019). The background image is an astrophotograph in optical filters as a reference, courtesy of Rogelio Bernal Andreo (modified to grayscale).

2.2.3 Rotational Velocity and Effective Temperature

The effective temperatures (T_{eff}), surface gravities ($\log g$), and radial velocities (RV) of the stars in the OSFC sample (Cottle et al., 2018) were reported by Kounkel et al. (2018) using the IN-SYNC pipeline (Cottaar et al., 2014)[2]. IN-SYNC was designed to analyze APOGEE spectra of YSOs as an alternative to the APOGEE Stellar Parameter and Chemical Abundances Pipeline (ASPCAP; García Pérez et al., 2016), which is primarily optimized for giants stars. The IN-SYNC code fits to each APOGEE spectrum T_{eff}, $\log g$, RV, veiling and $v \sin(i)$, using a synthetic grid, and interpolating between the grid points (Kounkel et al., 2018).

Olney et al. (2020) find that the stellar parameters estimated by Kounkel et al. (2018) could

[2]The $v \sin(i)$ for this sample was reported in Kounkel et al. (2019)

still include some non-physical systematics due to mismatches between the empirical and theoretical spectra. Thus, using a deep convolutional neural network, the APOGEE-net pipeline was designed to correct most of these issues, providing more reliable predictions of $\log g$, T_{eff} and [Fe/H] for solar and lower mass regime ($T_{eff} \leq 6700$ K; Olney et al., 2020). Since Olney et al. (2020) studied only stars within the APOGEE DR14 data set, not all APOGEE fields in the OSFC and the ones studied in Kounkel et al. (2018); Kounkel et al. (2019) were included in their work. Thus, we use the APOGEE-net to obtain the best estimates for the stellar parameters of the entire kinematic members selected in §2.2.1. Since the APOGEE-net does not predict $v \sin(i)$, we made use of the $v \sin(i)$ values obtained from Kounkel et al. (2019). In general, the differences between the stellar parameters determined in Kounkel et al. (2018) with the IN-SYNC pipeline and the APOGEE-net pipeline are less than 500 K for T_{eff} and less than 1.0 dex for $\log g$. To investigate whether these differences could produce systematic errors in the $v \sin(i)$, we made a quality check for $v \sin(i)$ values reported in Kounkel et al. (2019), using the Fourier Transform (FT) method, which does not require the use of spectroscopic templates (Carroll, 1933).

The FT method is widely used to study stellar rotation in different ranges of stellar masses (Royer et al., 2002; Simón-Díaz and Herrero, 2007; Thanathibodee et al., 2020). In short, the observed star's spectrum can be written as a convolution of the intrinsic stellar spectrum, the broadening function, and the instrumental function (Carroll, 1933; Royer, 2005). The rotational broadening function produces zeros in the FT space in which the first zero is correlated with $v \sin(i)$. Other broadening functions such as Stark, thermal, macro-turbulence broadening do not create zeroes in the FT space, and do not affect the derivation of $v \sin(i)$ (Carroll, 1933; Royer, 2005). The instrumental function does not add zeroes in the FT space but it is related to the lower limit of $v \sin(i)$ that we can measure in a given spectral resolution. In order to estimate the rotational velocity using the FT method, an interactive tool was designed in Python and Qt as a part of a suite of tools for stellar rotation (Serna et al., in preparation). To obtain robust estimations of $v \sin(i)$, the FT method requires the selection of single spectroscopic lines (not blended), with good signal to noise (S/N) to get a reliable normalization (Royer, 2005). The tool enables the user to select and analyze the shape of the spectral line of interest. The tool automatically gets the line center and width by fitting a Gaussian function to the spectral line and the continuum using the routine *lmfit* (Newville et al., 2014). Thus, the line profile is properly normalized and convolved using the Fast Fourier Transform (FFT) algorithm to get zeroes at the FT space. We use only the first zero (σ_1), which, with the APOGEE spectral resolution, provides reliable $v \sin(i)$ (Reiners and Schmitt, 2002). Thus, the rotational velocity is computed as $v \sin(i) = \frac{k_1(\epsilon)}{\sigma_1}$. Following Reiners and Schmitt (2002) prescription, we use the following approximation based on

Table 2.1: OSFC rotational velocities and rotational periods.

2MASS ID	$v \sin(i)$[a] (km/s)	$v \sin(i)$[b] (km/s)	Binary[a]	Kinematic Class	Accretor	EW[H_α] (Å)	TIC (mag)	Tmag (days)	Period[c] (days)	Period[d]	References[d]
05180280-0106222	16.7 ± 0.7		1		W	-5.3					
05181171-0001356					W	-3.7	249067805	13.16	1.65 ± 0.01	1.65	7
05181457+0010095					W	-5.6	454223248	14.21	6.70 ± 0.03		
05185716-0256047	78.3 ± 6.0		0	1							
05190273-0032274					W	-7.7	249074941	14.79	8.23 ± 0.01	8.21	7
05191214-0242275	13.5 ± 0.6		1		W	-3.6					
05191549-0204529	7.4 ± 1.2		1	1							
05192175-0217193	16.4 ± 0.6		1	1			4011038	13.03	4.88 ± 0.01		
05194010-0121224	28.2 ± 5.9		0	1							
05194349-0116397	10.2 ± 0.6		1	1							
05194988-0408068					W	-5.9	4068446	14.06	0.52 ± 0.01		
05195655-0520227					W	-4.2	4069106	13.75	3.36 ± 0.01		
05195766-0301262	16.4 ± 0.4		1	1							
05200104-0100101	198.9 ± 21.8		0	1							

[a] Kounkel et al. (2018); Kounkel et al. (2019): 0- Undeconvolvable cross-correlation function (CCF); 1- Only a single component in the CCF; 2- Multiple components in the CCF; -1- Spotted pairs or SB2 Uncertain
[b] Fourier Method, §2.2.3
[c] TESS periods §2.2.4
[d] Known periods: 1) Stassun et al. (1999); 2) Rebull (2001); Rebull et al. (2006); 3) Carpenter et al. (2001, ; J-band); 4) Herbst et al. (2002); 5) Cody and Hillenbrand (2010); 6) Morales-Calderón et al. (2011); 7) Karim et al. (2016, 7)
Only a portion of the table is shown here. The full version is available in electronic form.

the limb-darkening coefficient (ϵ): $k_1(\epsilon) = 0.610 + 0.062\epsilon + 0.027\epsilon^2 + 0.012\epsilon^3 + 0.004\epsilon^4$. To evaluate the robustness of the method and to obtain uncertainties for our measurements, the tool creates an ensemble of synthetic lines for each measure, resampling 1000 times the input line, taking into account the uncertainties of the flux and the wavelength, with the limb-darkening coefficient varying randomly from 0.4 to 0.6 (Gilhool et al., 2018). The program then computes $v \sin(i)$ from the median value and the associated uncertainty from the standard deviation.

To guarantee proper line shapes in the FT analysis, we have measured $v \sin(i)$ for 271 kinematic members (§2.2.1) with APOGEE spectra presenting S/N>200. We analyzed at least 5 of the most intense lines within the APOGEE spectroscopic range for each star, avoiding lines with apparent mixing with other lines. The final values (the median of the set of individual results) are shown in Table 2.1[3]. All measurements with $v \sin(i) < 13.3$ km s^{-1} provided by FT method are considered upper limits. The left panel of Figure 2.2 compares the $v \sin(i)$ derived by (Kounkel et al., 2019) and the $v \sin(i)$ estimated from the FT method. In general, both sets of measurements, above the APOGEE velocity resolution, are in good agreement within 5 km s^{-1}. Similarly, the right panel of Figure 2.2 compares the $v \sin(i)$ derived by

[3]Appendix **??** includes velocity measurements for stars located in the general region of the OSFC not included as kinematic (§2.2.1) or spectroscopic(§2.2.2) members

(Kounkel et al., 2019), to those derived using the ASPCAP pipeline, which uses different spectral theoretical libraries and analyzes the combined spectra obtained from multi-epoch APOGEE observations (García Pérez et al., 2016). The comparison shows a good agreement and does not reflect any biases; We also made some comparisons with the literature (Frasca et al., 2009; Pinzón et al., 2021; Sacco et al., 2008; Sicilia-Aguilar et al., 2005; Wolff et al., 2004). In general, we have a good agreement with Kounkel et al. (2019).
Most stars with the larger differences in Figure 2.2 are spectroscopic binaries detected by Kounkel et al. (2019). The $v \sin(i)$ estimation in binary stars can be affected by blended spectroscopic features from the binary components. Since we can not obtain reliable $v \sin(i)$ in stars with low signal to noise (S/N<200) using the FT method and ASPCAP $v \sin(i)$ are available only for stars in the APOGEE DR14 data set, we use in the following sections the $v \sin(i)$ values derived by Kounkel et al. (2018) and reported in Kounkel et al. (2019).

2.2.4 The TESS Data and Light Curves

TESS is an all-sky survey mission focused on searching for transit exoplanets. To date, TESS has covered $\sim 75\%$ of the sky with at least 27 days of continuous observation with a cadence of 30 minutes and a pixel size projected into the sky of 21×21. Since TESS was optimized to survey stars in the spectral range F5-M5 (Ricker et al., 2014), these data present a golden opportunity for photometric variability studies in solar-type and low-mass stars. Particularly, in this work, we use the high quality and cadence of TESS photometric data to estimate stellar rotational periods of TTS in the OSFC, which is widely covered by TESS Sectors 5 & 6.

We developed the *TESSExtractor* tool specially optimized for periodical variability searches of YSOs using TESS data. It can use as input the Full Frame Images (FFIs) directly, or use the *TESScut* (Brasseur et al., 2019) service to downloads 10×10 squared pixels cutouts, centered on each target.
To extract and process LCs of selected stars, it selects an optimal aperture to perform simple aperture photometry (SAP) using Python *Photutils* package (Bradley et al., 2019). The optimal photometric aperture depends on the star's brightness and can vary from 1.0 to 3.5 pixels radii. The annulus used for the background estimation depends on the selected aperture, with the inner and outer radius varying from 2.5 to 4.0 pixels, and 3.5 to 5.0 pixels, respectively. Also, the TESS quality flags were used to avoid any anomaly in the photometry (e.g., Cosmic rays, Popcorn noise, Fireworks, etc.)[4].

[4]TESS Data release notes: https://archive.stsci.edu/tess/tess_drn.html

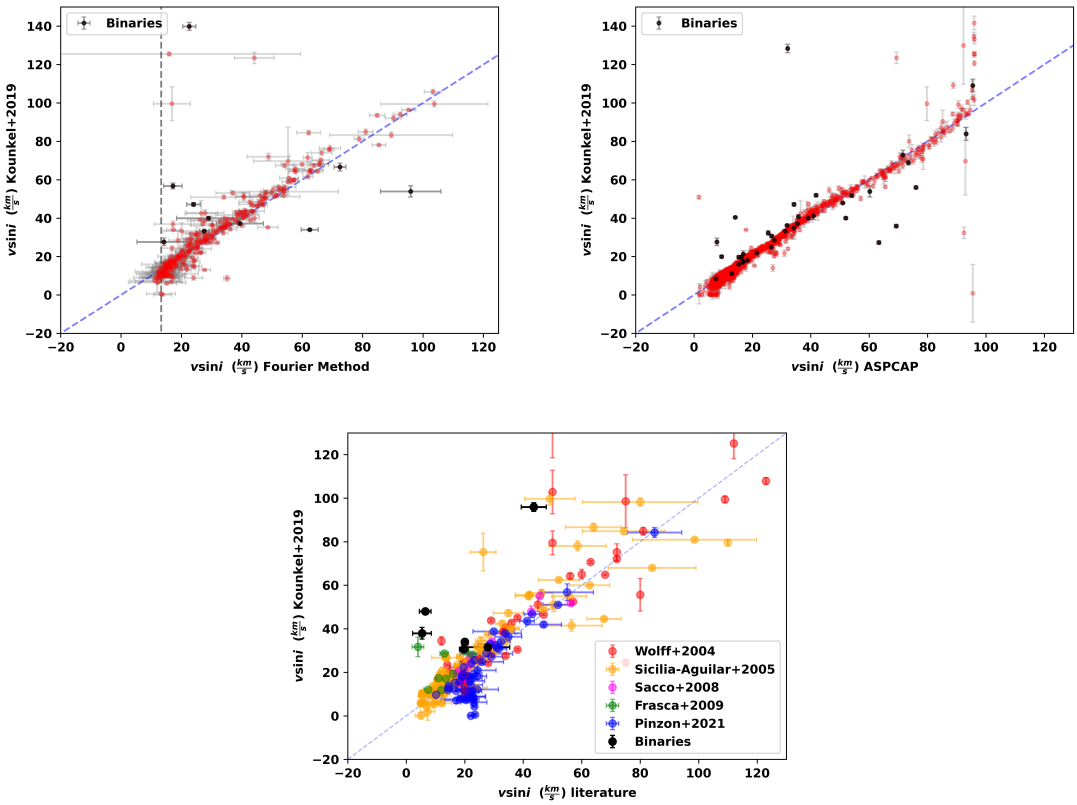

Figure 2.2: Quality check for vsin(i) measurements: The upper left panel shows a validation between the $v\sin(i)$ measurements of Kounkel et al. (2019), which we used in this work, and the measurements that we made with the Fourier Method. The upper right panel shows a comparison of Kounkel et al. (2019) versus ASPCAP. Notice that the ASPCAP does not estimate $v\sin(i)$ larger than 100 km s^{-1}. The lower panel shows a comparison of Kounkel et al. (2019) versus other works in the literature. Black dots denote confirmed spectroscopic binaries (Kounkel et al., 2019). The slope of the blue dashed line in each box is one, and the vertical black dashed line in the upper left box marks the APOGEE velocity resolution $\sim$ 13.3 km s^{-1}.

We implemented the task *kepcotrend* of PyKE package (Still and Barclay, 2012) in our tool, and the first four Cotrending Basis Vectors (CBVs) provided by TESS to identify and reject LCs dominated by systematics. To avoid possible contamination from scattered light patterns on the TESS detector, we reject all data points with a strong sky variability, above 95% of the median background estimation. Finally, each LC was calibrated to the TESS photometric system based on Stassun (2019, TIC v8.0).

Given the relatively large TESS pixel size, some LCs may be contaminated by point sources located inside the selected photometric aperture. To consider this issue we computed, the ratio between the flux of the target and the the sum of the fluxes of Gaia-sources that fall within the aperture ($\frac{f_{in}}{f_*}$). The fluxes are based on the G filter of Gaia-EDR3. We flag the targets with $\frac{f_{in}}{f_*} > 20\%$ as stars contaminated by nearby sources. Additionally, to facilitate visual inspection and verify if neighboring sources contaminate the target source, *TESSExtractor* generates an image per each studied target, where one can compare the DSS2 image and TESS image with a field of view of 210×210 corresponding to a TESS image of 10×10 pixels (see Figure 2.3).

TESS Rotational Periods

Using the Lomb-Scargle periodogram (LSP; Lomb, 1976; Scargle, 1982) within the *TESSExtractor* tool, we obtain stellar rotational periods for a sample of kinematic members and spectroscopic members in the OSFC (§2.2.1 & 2.2.2). We use a grid of 1000 periods in the interval of $0.04 < P < 25$ days. Our minimum period is twice the TESS cadence, and the maximum period of 25 days is the average length of the TESS time series. We use the bootstrap technique as a proper way to estimate the period uncertainty. Each LC was re-sampled 100 times within the magnitude uncertainties and the rotational period was recomputed in each iteration. At the end, we have an ensemble of measurements, where the reported period is the median of the individual values, and the standard deviation is adopted as the period uncertainty. Given the highest peak in the periodogram and assuming Gaussian noise, we have obtained the maximum False Alarm Probability (FAP) of the estimated period, based on the Baluev method (Baluev, 2008) using the task *statistics.false_alarm_probability* from astropy package (Astropy Collaboration et al., 2013b). As a result, we have FAPs below 0.01%, indicating that the period measurements are highly reliable. We perform phase folding of the LCs at the estimated period (Figure 2.3). Additionally, we select those stars that show a clear periodicity by visual inspection since their LCs show a regular pattern. Rotational

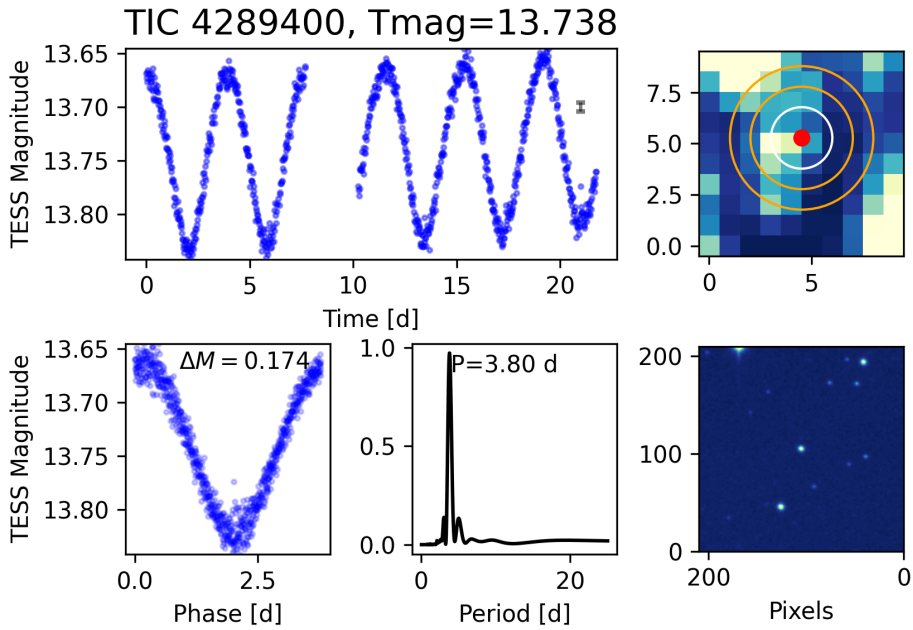

Figure 2.3: An example of a TESS light curve and its analysis. From the left to the right in top: (A) Light curve in TESS magnitudes with a representative error bar. The legend at top refers to the star identification, and the mean TESS magnitude. (B) Field of view (210 x 210 sq arcsec) corresponding to a TESS image of 10x10 pixels. The white circle shows the photometric aperture, and the orange circles the sky annulus. The red dot marks the centroid of the star. In the bottom panels from the left to the right: (C) Phase-folded light curve to the estimated best period. The legend shows the amplitude. (D) Lomb-Scargle periodogram, with the estimated period. (E) 210 x 210 pixels Digital Sky Survey (DSS2) thumbnail, same field of view as (B).

periods are reported for this sample in Table 2.1 [5].

We compile stellar rotation periods from some multi-epoch and multiband studies performed in selected regions of the OSFC. Table 2.2 lists the studied regions with the respective nominal stellar ages, the analysis method used to obtain the rotational period, and the photometric band used for each selected reference. We have included rotational periods obtained from the All-Sky Automated Survey for Supernovae (ASAS-SN) database that provides ~ 4 years baseline LCs for sources brighter than V ≤ 17 (Jayasinghe et al., 2018, 2019). Figure 2.4 shows comparisons between the compiled periods and the TESS periods derived in this work regardless of different databases for the LCs (e.g., cadence, photometric bands, observational windows, range of brightness, sensitivity, and technique). We found that 80% of the sources have TESS periods that differ by less than 5% from the literature values.

Table 2.2: Compilation of rotational periods in the OSFC.

Region	Age (Myr)	Filter Band	# stars	Reference
ONC	1-2	I_c	254	Stassun et al. (1999)
ONC	1-2	J, H, K	233	Carpenter et al. (2001)
ONC	1-2	I_c	138 a	Rebull (2001); Rebull et al. (2006)
ONC	1-2	[3.6], [4.5], I_c, J, K	150	Morales-Calderón et al. (2011)
ONC	1-2	ESO filter 851$\sim I_c$	369	Herbst et al. (2002)
ONC	1-2	V, R, I, J, H, K	29	Frasca et al. (2009)
ONC	1-2	V, R, I	148	Parihar et al. (2009)
σ Ori	3	I_c	84	Cody and Hillenbrand (2010)
Orion OB1 Association	4-10	V, R_c, I_c	564	Karim et al. (2016)
OSFC	...	B, V	40	Marilli, E. et al. (2007)
OSFC	...	V	$\sim$1000	Jayasinghe et al. (2018, 2019)

a) Sources of Rebull (2001) with periods reported in Rebull et al. (2006)

2.2.5 Reddening, masses, and ages

We use the *MassAge* code (Hernandez et al. in preparation) to obtain reddening, luminosities, stellar ages, and masses for each kinematic member (with T_{eff} <6500 K) of the OSFC. The *MassAge* code uses the effective temperature from the APOGEE-net pipeline

[5] Appendix **??** includes TESS rotational periods for stars located in the general region of the OSFC not included as kinematic (§2.2.1) or spectroscopic(§2.2.2) members

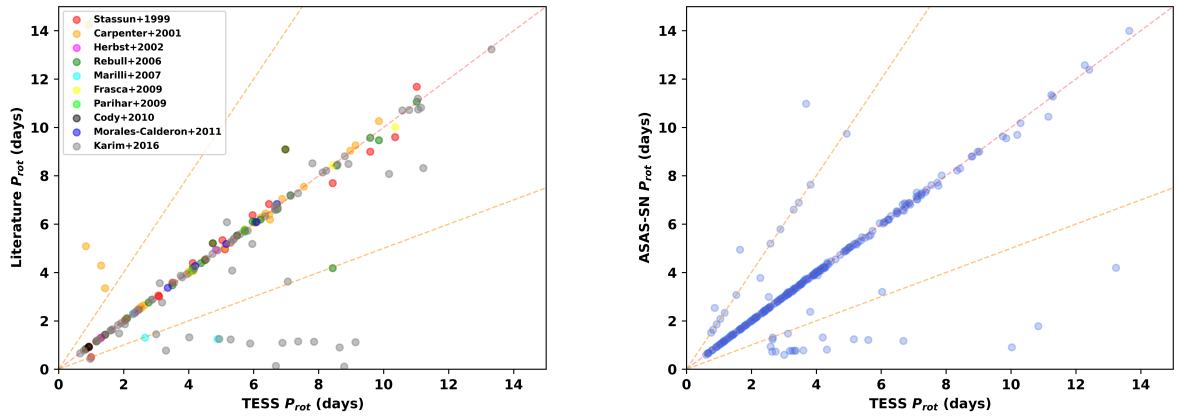

Figure 2.4: Left panel: TESS periods versus periods from the literature. Right Panel: TESS Periods versus ASAS-SN periods (Jayasinghe et al., 2018, 2019). Error bars for TESS periods are smaller than the marker size. Dotted lines represent 1:2, 1:1, and 1:1/2 relationships, respectively.

(§2.2.3), photometry (Gp, Rp, and Bp), and parallax from Gaia-EDR3 (Gaia Collaboration et al., 2020), and the J and H magnitudes from 2MASS (Cutri et al., 2003)[6]. The uncertainties in the estimated values are obtained using the Monte Carlo method of error propagation (Anderson, 1976), assuming Gaussian distribution for the uncertainties in the input parameters to generate 500 artificial points per each source. The adopted final results and uncertainties of the estimated values are the median and the median absolute deviation (MAD; 1σ=1.4826×MAD), respectively.

To estimate the reddening to each star of our sample, the *MassAge* code tests several values of A_V until we obtain the best match between the observed colors ($[M_{\lambda i} - M_0]_{obs}$) and the standard colors affected by reddening ($[M_{\lambda i} - M_0]_{std} + [A_{\lambda i}/A_V - A_0/A_V] \times A_V$), where $M_{\lambda i}$ are the Gaia/2MASS magnitudes (Bp, Rp, G, J, H) and $A_{\lambda i}$ is the extinction in magnitudes in those photometric bands. The standard colors were taken from Luhman and Esplin (2020) and the adopted reddening law $A_{\lambda i}/A_V$ values from Fitzpatrick et al. (2019), assuming a canonical interstellar reddening law (R_V=3.1). The effective wavelength for each filter (λi) was calculated using the filter transmission (T_λ) and the stellar flux (S_λ) in the respective bandpass as in equation 2.2 (e.g., Brown et al., 2016). The stellar flux was approximated using a PHOENIX synthetic reddened spectrum (Husser et al., 2013) with a T_{eff} similar to the target star. The reddening effect on the synthetic spectra correspond to the values of A_V that we tested and the extinction law comes from Fitzpatrick et al. (2019).

[6]Since K-band photometry could be contaminated by emission from disks on the OSFC sources, it was not included in this procedure

$$\lambda i = \frac{\int \lambda T_\lambda S_\lambda d\lambda}{\int T_\lambda S_\lambda d\lambda} \tag{2.2}$$

Once each star of our sample is located in the HR diagram, we estimated its stellar age and mass using three different evolutionary models: Baraffe et al. (2015), Dotter (MIST; 2016), and Marigo et al. (PARSEC-COLIBRI; 2017). Note that the adopted luminosities were derived from the reddening-corrected J band photometry, with the J band bolometric correction for PMS stars from Pecaut and Mamajek (2013), and the corrected Gaia-EDR3 parallaxes. For each of the 500 artificial points, we selected the stellar mass and the stellar age corresponding to the closest theoretical point in the evolutionary model grid. Table 2.3 includes the stellar parameters derived for the kinematic sample. It is important to mention that masses and ages derived using this method can be affected by unresolved binaries or stellar variability. Figure 2.5 shows comparisons between the stellar ages derived by the *MassAge* code using the different evolutionary models. Stellar ages from MIST are in good agreement with those derived from Baraffe et al. (2015). In contrast, stars with stellar masses $\sim$0.5 $M_\odot$ or smaller have stellar ages from PARSEC-COLIBRI models systematically larger than those derived from MIST.

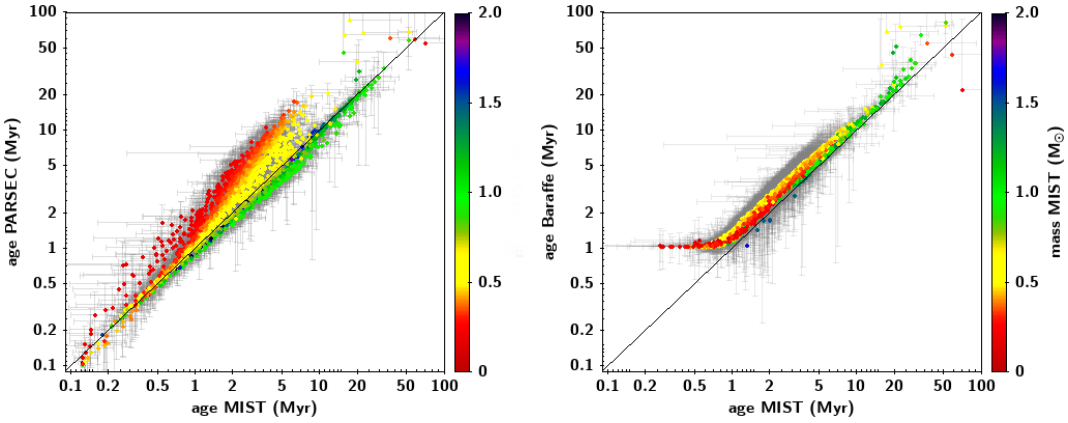

Figure 2.5: Comparison between the stellar ages derived by the MassAge code using different evolutionary models. Left panel: ages derived using PARSEC-COLIBRI (Marigo et al., 2017) versus MIST (Dotter, 2016). Right Panel: ages derived using Baraffe et al. (2015) and MIST (Dotter, 2016). The color bar represents masses derived using MIST models.

Table 2.3: Masses and ages for kinematic members with $T_{eff} < 6500\,K$

2MASS ID	T_{eff} (K) [K]	L_* [$L_\odot$]	Av [mag]	Mass[a] [$M_\odot$]	Age[a] [Myr]	Mass[b] [$M_\odot$]	Age[b] [Myr]	Mass[c] [$M_\odot$]	Age[c] [Myr]
05365409-0253155	4335.9 ± 51.3	1.08 ± 1.04	0.36 ± 0.07	0.94 ± 0.06	1.98 ± 0.32	0.81 ± 0.05	1.55 ± 0.24	1.04 ± 0.06	2.27 ± 0.40
05391151-0231065	3755.3 ± 48.6	0.52 ± 1.05	0.80 ± 0.11	0.50 ± 0.04	1.30 ± 0.21	0.56 ± 0.04	1.53 ± 0.28	0.62 ± 0.05	1.75 ± 0.41
05355077-0516291	4135.2 ± 49.8	0.97 ± 1.05	0.85 ± 0.11	0.75 ± 0.05	1.37 ± 0.23	0.71 ± 0.02	1.26 ± 0.15	0.84 ± 0.04	1.57 ± 0.26
05415845-0115486	3945.3 ± 50.3	0.86 ± 1.06	3.43 ± 0.20	0.59 ± 0.04	0.98 ± 0.17	0.60 ± 0.04	1.01 ± 0.17	0.74 ± 0.03	1.24 ± 0.20
05392147-0723300	3509.5 ± 51.4	0.78 ± 1.09	4.84 ± 0.24	0.33 ± 0.03	0.38 ± 0.14	0.30 ± 0.03	0.36 ± 0.16		
05365014-0641292	4039.1 ± 47.3	0.95 ± 1.07	3.52 ± 0.17	0.66 ± 0.04	1.08 ± 0.19	0.66 ± 0.04	1.09 ± 0.18	0.78 ± 0.03	1.25 ± 0.21
05320778-0655368	3540.2 ± 51.7	0.21 ± 1.08	0.00 ± 0.16	0.39 ± 0.04	2.81 ± 0.63	0.58 ± 0.04	5.03 ± 1.12	0.44 ± 0.05	3.55 ± 0.91
05392519-0238220	3917.5 ± 50.0	1.08 ± 1.06	1.39 ± 0.13	0.55 ± 0.04	0.64 ± 0.09	0.54 ± 0.04	0.67 ± 0.09		
05353907-0508564	4252.3 ± 92.9	1.57 ± 1.05	0.96 ± 0.10	0.80 ± 0.09	0.88 ± 0.23	0.73 ± 0.05	0.78 ± 0.14	0.97 ± 0.06	1.09 ± 0.16
05314751+0217129	5954.1 ± 52.1	3.83 ± 1.04	0.00 ± 0.15	1.43 ± 0.04	10.53 ± 0.97	1.47 ± 0.04	9.85 ± 0.87		

[a] MIST Dotter (2016)
[b] PARSEC Marigo et al. (2017)
[c] Baraffe et al. (2015)
Only a portion of the table is shown here. The full version is available in electronic form.

2.3 Results and Discussion

2.3.1 $v\sin(i)$ vs $P_{\rm rot}$

In Figure 2.6 we plot the rotational period ($P_{\rm rot}$) obtained from our TESS LC analysis versus the $v\sin(i)$ parameter measured for 277 stars that are OSFC kinematic members. Assuming a solid body rotation, these parameters are related to the stellar radius (R) as follows:

$$v\sin(i) = \frac{2\pi R \sin(i)}{P_{\rm rot}} \tag{2.3}$$

As reference, we also plot the theoretical upper limit of $v\sin(i)$ for each $P_{\rm rot}$ assuming a maximum stellar radius of 2.5 $R_\odot$ and a rotation axis inclination of i=90. Using solar metallicity MIST models (Dotter, 2016), this corresponds to a maximum stellar mass of 1.2 $M_\odot$ with an age of 1 Myr, that of the youngest sub-associations in the OSFC.
We have considered $v\sin(i)$ measurements for double-line spectroscopic binaries (SB2) in Figure 2.6 reported by Kounkel et al. (2019). As expected, $v\sin(i)$ estimations could be strongly affected by stellar companions. In this sense, Figure 2.6 can be used as a diagnostic plot to detect potential candidates for spectroscopic binaries. To inspect possible binaries in our sample, we have added stars that did not pass the binarity criteria of the Kounkel et al. (2019) analysis, reported as unresolved SB2 or star dominated by starspots (SB2/sp). In the latter case, one does not expect a $v\sin(i)$ larger than the one derived from the rotation period and the typical radius at 1 Myr (blue dashed line in Fig. 6). Generally, we expect binary stars or stars younger than 1 Myr to be located above the blue dashed line. Two of the stars above the blue dashed line have ages younger than 1 Myr (§2.2.5), and eight stars results possible SB2, an spectroscopic follow up is required to confirm the nature of these

targets.

An anti-correlation between $v\sin(i)$ and $P_{\rm rot}$ is expected according to equation 2.3. The scatter in this trend is mainly produced by different spin axis inclinations (i) and different stellar radii in the sample. Undetected stellar companions could also affect the anti-correlation of Figure 2.6. There is a possibility that broader spectral features are produced by unresolved combined features from both components in binary stars instead of those produced by fast rotation (e.g., Hernández et al., 2014; Maxted et al., 2008). Additional scatter can be produced by latitudinal differential rotation, which increases toward smaller inclination angles (Reiners and Schmitt, 2002). However, Barnes et al. (2005) show that differential rotation decreases with temperature. In particular, differential rotation is low for stars with T_{eff} <5000K and disappears at 3500K. Since most stars in our sample have T_{eff} <5000K, we expect this effect to be minimal in our sample. In addition, the inhibition of convective transport of energy by stellar magnetic fields and/or the presence of cool magnetic starspots can produce the so-called radius inflation effect (Jackson and Jeffries, 2014; Lanzafame et al., 2017; Somers et al., 2020). This effect is expected to be below 15% (Kesseli et al., 2018). Regardless of these effects, plots like Figure 2.6 can be used as a tool for searching binary candidates, as these would fall above the reference line.

Combining $v\sin(i)$ measurements (§2.2.3), the TESS rotational periods (§2.2.4), and the L_* and T_{eff} estimations (§2.2.5), we derived the ratio of projected radius to the model radius ($\frac{R\sin(i)}{R'_*}$) as follows:

$$\frac{R\sin(i)}{R'_*} = \frac{v\sin(i)P_{\rm rot}}{2\pi} \times \sqrt{\frac{4\pi\sigma}{L_*}T_{eff}^2} \tag{2.4}$$

where the second term is the inverse of the model radius (R'_*) derived from the luminosity and T_{eff} according to the Stefan-Boltzmann law. In the subsequent analyses, the sample is restricted to those objects with $v\sin(i) > 13$ km s^{-1} (the instrumental resolution limit).

We found that stars trace a sequence on the $\frac{R\sin(i)}{R'_*}$ versus $P_{\rm rot}$ diagram, with $\frac{R\sin(i)}{R'_*}$ tending to increase with $P_{\rm rot}$. A similar trend was reported before for CTTS and WTTS (e.g., Artemenko et al., 2012; Venuti et al., 2017). We include in Figure 2.7 stars of the Pleiades cluster (age=125 Myr; e.g., Somers and Stassun, 2017), using the measurements of $v\sin(i)$, $P_{\rm rot}$, and stellar radii reported by Hartman et al. (2010). It is apparent that stars in Pleiades and stars in the OSFC share similar behavior in Figure 2.7. There are a significant number of stars showing a larger projected rotational radius than the expected theoretical radius. This radius inflation effect has been observed previously and has been attributed to enhanced

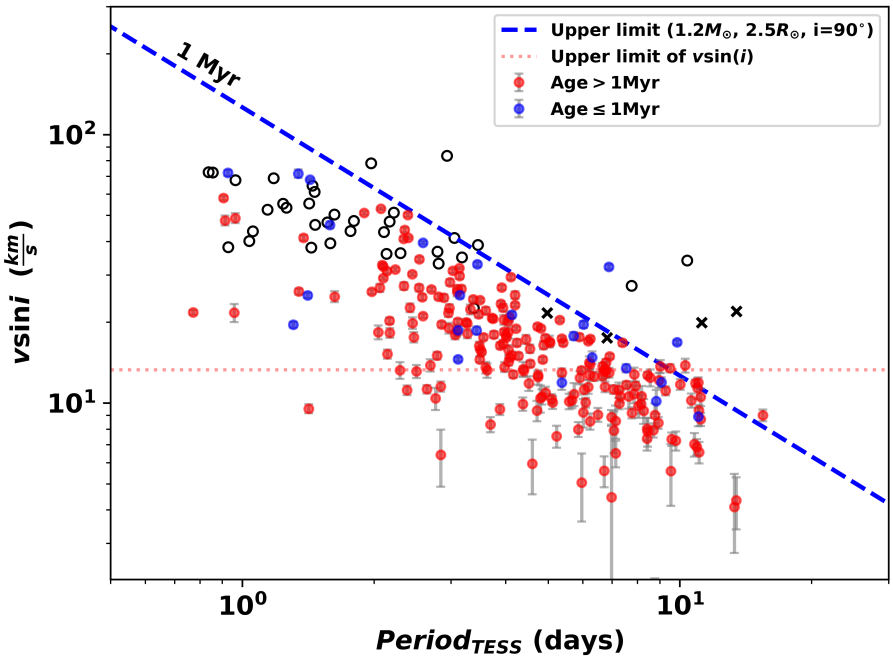

Figure 2.6: $v \sin(i)$ versus $P_{\rm rot}$ derived in this work. The blue dashed line shows a solid body model of $1.2 M_\odot$, $2.5 R_\odot$ at 1 Myr, $\sin i = 1$. Black crosses are double-line spectroscopic binaries (SB2), and black open circles are uncertain SB2 (Kounkel et al., 2019). The red dotted line shows the upper limit to $v \sin(i)$=13.3 km s^{-1}. The period error bars are smaller than the marker size.

magnetic activity and the presence of stellar spots (e.g. Bouvier et al., 2016; Jackson, R. J. et al., 2016; Jaehnig et al., 2019; Lanzafame et al., 2017; Somers and Pinsonneault, 2015; Somers et al., 2020). Other effects can increase the $\frac{R\sin(i)}{R'_*}$ parameter. e.g., systematic offsets of T_{eff} and L_* due to starspots, plages, or contamination by binaries (Somers and Stassun, 2017). Also, systematic errors in the estimation of $v\sin(i)$ can be introduced by unresolved binaries (Kesseli et al., 2018) or by using a not suitable limb darkening law in pre-main-sequence stars (Rhode et al., 2001). Finally, It is challenging to detect photometric rotational modulation for stars with a low inclination, especially for those with longer periods. Low values of $\frac{R\sin(i)}{R'_*}$ are frequent at low $P_{\rm rot}$ and diminish with the increase of $P_{\rm rot}$. Exploring the origin of stars with $\frac{R\sin(i)}{R'_*} > 1$ is beyond the scope of this paper. A detailed analysis of the radius inflation effect and the derived inclination pole distributions will be addressed in future works.

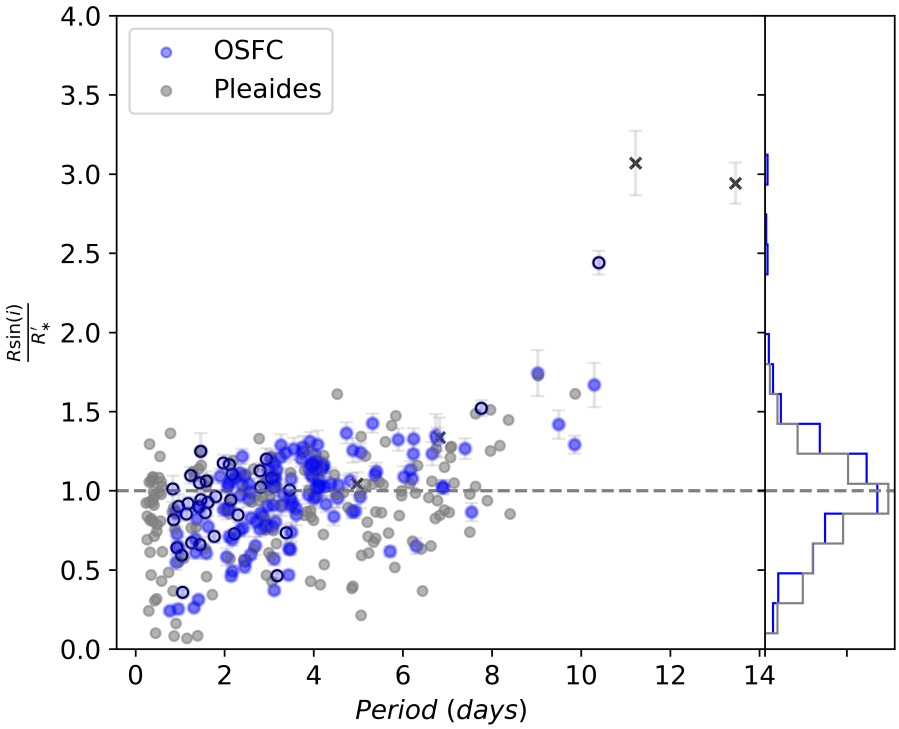

Figure 2.7: $\frac{R\sin(i)}{R'_*}$ of the OSFC compared with the Pleiades both as a function of $P_{\rm rot}$. The left panel show the OSFC stars with $\frac{R\sin(i)}{R'_*}$ and periods estimated in this work (blue dots). The grey dots represent the Pleiades stars with $\frac{R\sin(i)}{R'_*}$, and periods compiled from (Hartman et al., 2010). Black crosses are double-line spectroscopic binaries (SB2) and black open circles are uncertain SB2 or spotted star (Kounkel et al., 2019). The dashed line represent the mathematical limit for the inclination ($\sin(i) = 1$). Right panel: Normalized histogram of the vertical axis.

2.3.2 Rotational Evolution

We use $v\sin(i)$ and individual stellar ages of the kinematic members in the OSFC sample (§2.2.1) to examine evolutionary trends during the first million years of their life. We consider $v\sin(i)$ measurements that have fractional errors smaller than 10%. Additionally, stars identified as multiple stellar systems (Kounkel et al., 2019) were excluded from our sample. We prefer the use of $v\sin(i)$ instead of rotational periods because it is difficult to obtain rotational periods from TESS LCs in clustered young stellar regions (e.g., σ Ori, ONC). Moreover, the complex brightness variability in stars with accreting disks prevents obtaining estimations of rotational periods in most CTTS.

Figure 2.8 shows the evolution of $v\sin(i)$, considering ages derived with three different evolutionary models (Baraffe et al., 2015; Dotter, 2016; Marigo et al., 2017) as described in §2.2.5. We find a large scatter of $v\sin(i)$ at all ages. This is caused by several factors (e.g. Stassun et al., 1999), among them, variations on inclination angles ($\sin(i)$), on stellar masses, uncertainties in the determination of ages, and differing initial conditions of angular momentum evolution (e.g. the distribution of initial rotational periods).
To investigate the general evolution of stellar rotation for the kinematic members, we plot the median $v\sin(i)$ values (solid line) and the interquartile range (IQR) estimated for different age bins; The IQR corresponds to 50% central confidence interval (gray zones). We select the age bins to contain approximately the same number of stars per bin (0→1, 1→2, 2→3, 3→4, 4→5, 5→7, 7→10, y 10→20 Myr).

Gallet and Bouvier (2015) present parametric spin-evolution models ranging from 1 Myr to 10 Gyr for slow, medium, and fast rotators for three selected stellar masses (0.5, 0.8, and 1.0 $M_{\odot}$). These models include star-disk interaction, a magnetized stellar wind, core-envelope decoupling, and structural stellar evolution (i.e., mass, radius, moment of inertia) of the inner radiative core, and the outer convective envelope provided by Baraffe et al. (1998). During the accreting disk lifetime, the angular velocity for the stellar surface is constant as a consequence of the balance between the angular momentum added to the star from disk accretion and that extracted from it through the magnetic star-disk interaction (Matt et al., 2012). After the end of the accretion phase, the angular velocity evolution for PMS low-mass stars is regulated mainly by the structural stellar evolution and magnetized stellar winds, once the star arrives to the main sequence (Kawaler, 1988). By transforming angular velocities (ω) into rotational velocities ($V_{rot} = R_{*}\omega$), we plot in Figure 2.8 the prediction of the models for medium rotators (Gallet and Bouvier, 2015). Each model is associated to a stellar mass of 0.5, 0.8, and 1.0 $M_{\odot}$, that in turn is related to a disk lifetime, 3, 5, and 6 Myr,

respectively. Regardless of the stellar evolution models used for estimating stellar ages, the general rotational behavior of the kinematic members follows the general trend predicted by these models reasonably well.

For reference, we over-plot in the upper-left panel of Figure 2.8, a couple of "toy models" showing extreme scenarios for angular momentum evolution (dotted lines). Model "A" describes a star with an accreting disk. The disk-locking effect keeps a constant angular velocity up to 20 Myr. We assume a solid body with a constant period of 6 days, similar to that adopted by Gallet and Bouvier (2015) in their 0.8 $M_{\odot}$ model. The evolution of $v\sin(i)$ is proportional to the stellar radius ($v_{rot} = \frac{2\pi R_*(t)}{P_{\rm rot}}$), which is reduced by 50% between 1-10 Myr (Baraffe et al., 2015). In contrast, the model "B" describes a diskless star. The $v\sin(i)$ evolution is derived only from the stellar radius evolution and the AM conservation. As a starting point, we use the AM (J_0) derived from the empirical model of Kawaler (1987) and referred in Landin et al. (2016, Equation (1)):

$$J_0 = I\omega = 1.566 \times 10^{50} \left(\frac{M_*}{M_{\odot}}\right)^{0.985} [cgs].$$

We consider a solid body rotator with a moment of inertia $I = k^2 M_* R_*^2$; The gyration radius (k) and the stellar radius (R_*) are obtained from the stellar evolutionary models of Baraffe et al. (2015). In this case, the $v\sin(i)$ evolution is inversely proportional to the stellar radius ($v_{rot} = \frac{J_0}{k^2(t) M_* R_*(t)}$).

In agreement with Gallet and Bouvier (2015), the $v\sin(i)$ statistical trend observed in the kinematic members of the OSFC (see Figure 2.8) suggests the existence of two phases in the early PMS evolution. The transition time between these phases is similar to the inflection point observed in the evolution of the disk frequency, where the fraction of low-mass accretors decreases about 90% during the first 5-6 Myr (Briceño et al., 2019; Fedele et al., 2010; Hernandez et al., 2007; Manzo-Martínez et al., 2020). During the first phase (age 5-6 Myr), $v\sin(i)$ decreases in spite of the rapid contraction. The torques originated from the magnetic coupling between the star and the disk remove efficiently the angular momentum from the system. Although details about these mechanisms are still uncertain due to the lack of knowledge of the interplay between accretion and ejection phenomena. In the second phase (age 5-6 Myr), the disk effect on the angular momentum evolution has stopped, causing the stellar rotation to be regulated by the structural stellar evolution and stellar winds.

The key takeaways from the present subsection are the following:

- $v\sin(i)$ decreases statistically for the first 5-6 Myr of the star's life, which suggests

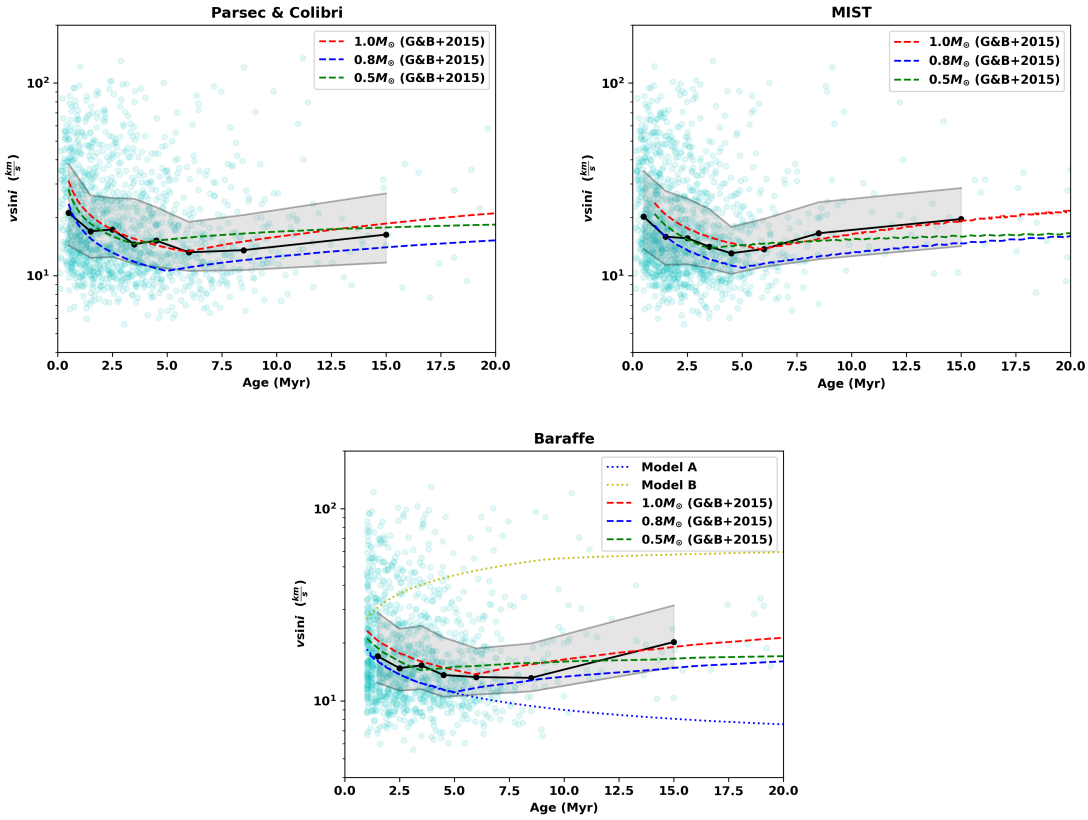

Figure 2.8: Evolution of $v \sin(i)$ versus age derived using the evolutionary models by PARSEC-COLIBRI (Marigo et al., 2017), MIST (Dotter, 2016), and Baraffe (Baraffe et al., 2015) for the sample of Orion's kinematic members (aqua green dots). The median of all points is represented by the black points joined by solid lines, while the gray zones define the interquartile range. Model A (disk-locking model up to 20 Myr) is represented by the blue dotted line. Model B (diskless star model) is shown as the yellow dotted line. Results from Gallet and Bouvier (2015) models are transformed to rotational velocities, assuming solid body rotation, $\sin i = 1$, and radius evolution from the respective evolutionary models. These are represented with dashed lines. Model A coincides with 0.8 $M_\odot$ (Gallet and Bouvier, 2015) model during the first 5 Myr. Model A and B are shown only in the third plot for illustrative purposes.

the existence of mechanisms that extracts angular momentum from the stars. Likely, disk-locking is the most important of these mechanisms.

- Beyond 5-6 Myr, the disk disappears, and $v\sin(i)$ tends to increase due to stellar contraction and angular momentum conservation.

2.3.3 Rotation and accretion

Using the classification of TTS derived from the equivalent width of $H\alpha$ (§2.2.1), we analyze the $v\sin(i)$ distributions of the CTTS, WTTS, and CWTTS samples. For all the samples of TTS (Figure 2.9), we plot a statistical limit that separates the slow rotators from the fast rotators (gray dashed line), the limit is defined so that 25% of WTTS have $v\sin(i)$ greater than this limit (i.e, $v\sin(i) = 28$ km s^{-1}).
In general WTTS show a large range of stellar rotation velocities, such that 25% (96/383) of the stars are considered fast rotators. In contrast, only 12% (24/206) of the CTTS can be classified as fast rotators (lower panel of Figure 2.9). Excluding binary stars and binary candidates reported by Kounkel et al. (2019), the fractions of fast rotators are 16% (52/330) and 7% (13/194) for WTTS and CTTS samples, respectively. In general, single CTTS have $v\sin(i) \leq 50$ km s^{-1}.

A visual inspection of the TTS distributions suggests that CTTS exhibit distinct rotation properties from WTTS. A Kolmogorov-Smirnov (K-S) test applied to both populations, rejecting binary candidates, supports this idea of statistically distinct rotation properties for the two groups. Indeed, the test yields a probability of only 0.03 that the two distributions in $v\sin(i)$ corresponding to CTTS and WTTS are extracted from the same parent distribution (Figure 2.9). These results provide a clear indication of a statistical connection between disk and rotation properties across the OSFC.

Jayawardhana et al. (2006) found similar results in the η Cha and the TW Hydrae ($\sim$ 6-8 Myr) stellar groups. They report that all accretors are slow rotators ($v\sin(i) \leq 20$ km s^{-1}), while non-accretors cover a larger range in rotational velocities. These results suggest a clear signature of disk-braking on the CTTS sample.

In spite of small numbers of CWTTS stars in comparison to WTTS, our results do not show any statistical difference between CWTTS class and WTTS. From the p-value of 0.7 obtained from the K-S test, we are not allowed to discard the null hypothesis that the two populations are extracted from the same parent distribution. The fast rotator fraction of CWTTS is 26% (16/61) in comparison with the 25% of the WTTS suggests that CWTTS are stars reaching

the end of their accretion phase, and could be less affected by the disk-braking effect than accreting stars.

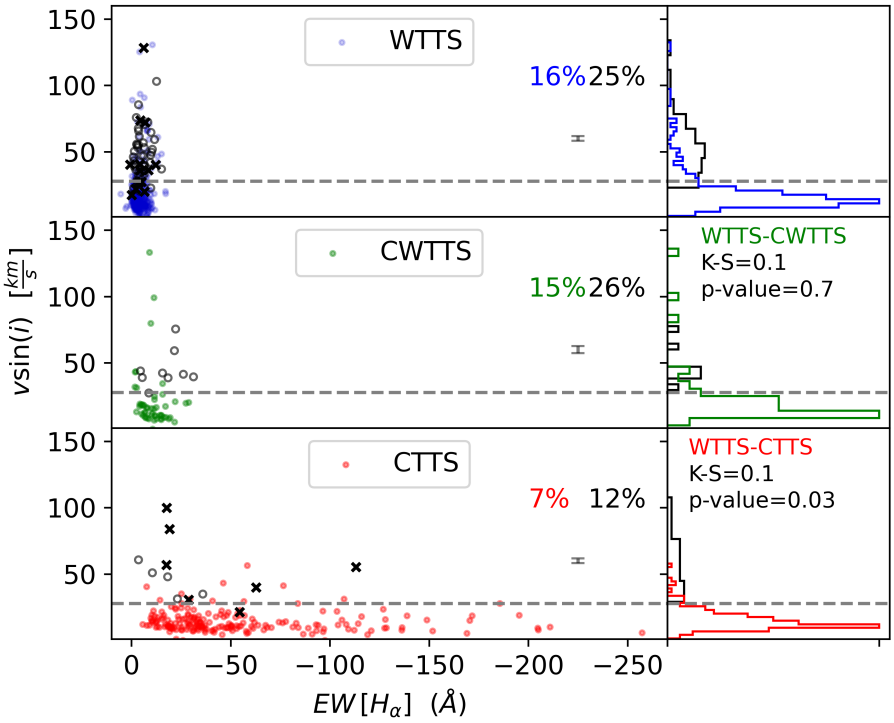

Figure 2.9: Left panels: $v\sin(i)$ versus EW_{H_α} for TTS. Black crosses are double-line spectroscopic binaries (SB2) and black open circles are uncertain SB2 or spotted star (SB2/sp) (Kounkel et al., 2019). The dashed line split our slow rotators from the fast ones, noted as 28 km s^{-1}. The colored percentages show the fraction of single stars above the dashed line, and the black percentage shows the fraction for the whole sample (single, binaries and multiple systems) above dashed line. Right panels: histograms of $v\sin(i)$ for both the single stars and SB2 or SB2/Sp. The results of the K-S test between WTTS, CWTTS, and CTTS are displayed above histograms.

Following the same methodology described in §2.3.2, we plot $v\sin(i)$ as a function of age for our sample of TTS (Figure 2.10). The results suggest that, statistically, CTTS rotate slower than WTTS during the first 1.5 Myr, when the separations in $v\sin(i)$ between these two classes are larger than the Poisson uncertainties $\frac{\sigma_{v\sin(i)}}{\sqrt{N}}$. This result also suggests that the disk locking scenario applies for TTS in the OSFC. In addition, the decrease in the rotation rate of WTTS suggests that, although stars have recently lost their inner disk, they have not had enough time to increase their rotation, as suggested by other studies (Biazzo et al., 2009; Jayawardhana et al., 2006; Nguyen et al., 2009). After 2 Myr, the rotational velocities of CTTS are comparable with those observed in WTTS. Other causes of angular momentum loss in WTTS such as the stellar winds are expected to play important roles in

the angular momentum evolution. Theoretical modelling suggest that winds may be present even at low stellar accretion rates, specially in stars that are magnetically active with strong non-axisymmetric fields that promove angular momentum losses via flaring events (Nicholson et al., 2018). The absence of a disk creates favorable conditions for wind formation with higher mass-loss rates that may spin-down the star in time scales of the same order than the CTTS-WTTS transition time (Sauty et al., 2011). Additional studies of confirmed TTS older than 4 Myr are needed to obtain a statistically robust comparison between CTTS and WTTS at the end of the disk evolution phase.

The key takeaways from the present subsection are the following:

- In general, CTTS's have a smaller rotational velocity than WTTS supporting the scenario in which the accreting disk regulates the angular momentum of disk bearing-stars.
- The distribution of $v\sin(i)$ of CWTTS resembles that of the WTTS instead of CTTS. This suggests that the rotation rate of these stars, which are nearly at the end of their accretion phase, could be less affected by the disk-braking effect.

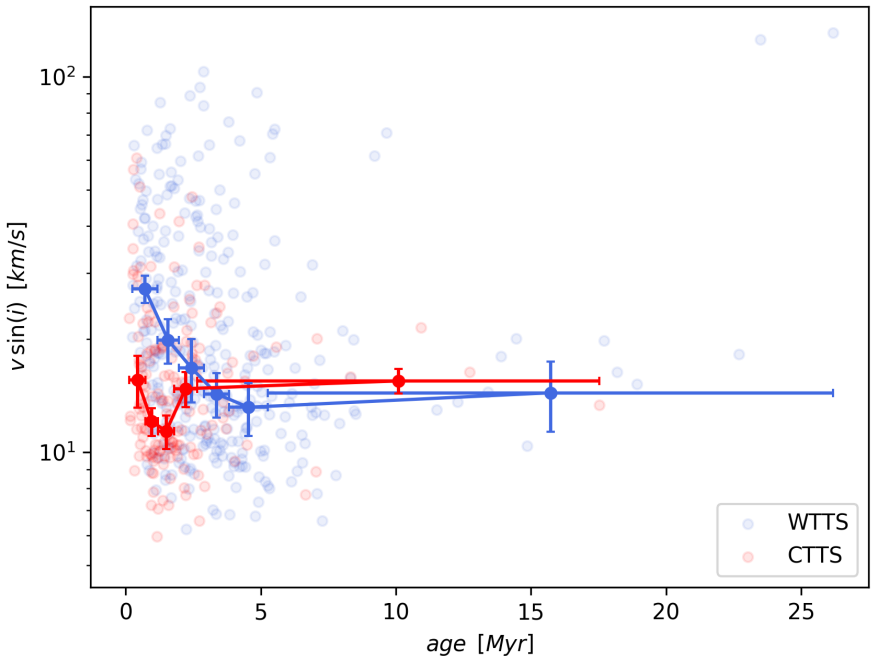

Figure 2.10: $v\sin(i)$ evolution for CTTS and WTTS in OSFC. Each solid dot represents the median per bin. The error bars are obtained considering Poissonian uncertainties. Differences between CTTS and WTTS are found to be significant only during the first ∼1.5 Myr in agreement to the disk-locking scenario.

2.4 Summary and Conclusions

We have presented an evolutionary study of the stellar rotation in the Orion star forming complex for a very robust sample of kinematical members and spectroscopically confirmed TTS to date. We processed and analyzed 3501 LCs from TESS observations along the OSFC. Throughout a visual inspection to each LC, we have classified 1157 stars as periodic variables. We have studied the measurements of $v \sin(i)$ for 1935 stars with stellar masses and ages estimations using different evolutionary models.

The main results of this work are summarized as follows:

1. We found an empirical trend of stellar rotation $v \sin(i)$ with age. It clearly shows a transitional phase on the stellar rotation at 5-6 Myr. This result is consistent with the disk lifetime used by Gallet and Bouvier (2015) in their AM evolutionary models for stars with masses between $0.8 M_{\odot}$ and $1 M_{\odot}$, and in agreement with the timescale for disk dissipation obtained by studies of protoplanetary disks (Carpenter et al., 2006; Hernandez et al., 2007).

2. Analysis of the $v \sin(i)$ distributions shows that CTTS are slow rotators suggesting that disk-braking effect regulates the angular momentum evolution of accreting stars, maintaining the rotation rates substantially below the ($v \sin(i) < 28$ km s^{-1}). In addition our data suggest that CTTS with $v \sin(i) > 28$ km s^{-1} are likely binary systems.

3. Stars reaching the end of their accretion phase (CWTTS) have similar statistical properties than WTTS, suggesting that this sample could be less affected by the disk-braking effect.

3 Rotational Evolution of Classical T Tauri Stars: Models and Observations

The analysis presented in this section constitutes my second publication as first author, titled "Rotational Evolution of Classical T Tauri Stars: Models and Observations" by Serna et al. (2023), which was carried out as part of this dissertation. This work is still under revision by ApJ Press. We expect this second review is going to be positive and the paper will be accepted this month. By now, this is a compilation of the last manuscript sent.

Abstract: We developed a grid of stellar rotation models for low-mass and solar-type Classical T Tauri stars (CTTS) ($0.3M_{\odot} < M_{*} < 1.2M_{\odot}$). These models incorporate the star-disk interaction and magnetospheric ejections to investigate the evolution of the stellar rotation rate as a function of the mass of the star M_{*}, the magnetic field (B_{*}), and stellar wind ($\dot{M}_{wind}$). We compiled and determined stellar parameters for 208 CTTS, such as projected rotational velocity $v\sin(i)$, mass accretion rate $M_{\odot}$, stellar mass M_{*}, ages, and estimated rotational periods using TESS data. We also estimated a representative value of the mass-loss rate for our sample using the [O1] λ6300 spectral line. Our results confirm that $v\sin(i)$ measurements in CTTS agree with the rotation rates provided by our spin models in the accretion-powered stellar winds (APSW) picture. In addition, we used the Approximate Bayesian Computation (ABC) technique to explore the connection between the model parameters and the observational properties of CTTS. We find that the evolution of $v\sin(i)$ with age might be regulated by variations in (1) the intensity of B_{*} and (2) the fraction of the accretion flow ejected in magnetic winds, removing angular momentum from these systems. The youngest stars in our sample ($\sim$1 Myr) show a median branching ratio $\dot{M}_{wind}/\dot{M}_{acc} \sim 0.16$ and median $B_{*} \sim$ 2000 G, in contrast to ~ 0.01 and 1000 G, respectively, for stars with ages 3 Myr.

3.1 Introduction

Low mass ($< 1.2 M_{\odot}$), Classical T Tauri Stars (CTTS) are young systems, still contracting and accreting gas from their circumstellar disks through the stellar magnetic field. Despite crossing a phase of gravitational contraction, the rotation rates of the majority of CTTS lie well below 10% of their break-up limit (Bayo et al., 2012; Bouvier et al., 1993; Herbst et al., 2002; Jayawardhana et al., 2006; Nguyen et al., 2009; Pinzón et al., 2021; Serna et al., 2021), indicating that these stars lose angular momentum expeditiously during the first million years (Myr).

In the so-called Disk-Locking (DL) scenario, angular momentum in CTTS is transferred outward from the star to the disk regions beyond the corotation radius through the stellar magnetic field closed lines anchored to the star surface (Collier Cameron and Campbell, 1993b; Ghosh and Lamb, 1979). Nevertheless, the stellar spin-down efficiency in the DL model is substantially reduced due to the turbulent diffusion of the field inside the disk, which results in more realistic magnetic field topologies with open field regions (Matt and Pudritz, 2005b). These regions allow the appearance of stellar winds, which are an alternative source of angular momentum loss (Matt and Pudritz, 2008a).

CTTS exhibit energetic stellar and disk winds traced through the blue-shifted absorption profiles of their most prominent lines and by the presence of intense forbidden line emission of low ionization species in their spectra (Alencar and Basri, 2000; Edwards et al., 2003; Hartmann et al., 1982; Kuhi, 1964). The correlation between the forbidden line emission and stellar accretion suggests that such winds are somehow powered by disk accretion (Hartigan et al., 1995). However, how the energy is transferred from the accretion flow to a stellar wind through the corona is still unknown.

Magnetohydrodynamic (MHD) simulations of CTTS, including stellar and disk wind scenarios, have shown that stellar rotation can reach an equilibrium around 10% of the break-up limit at the end of the Hayashi track for X-wind models (Shu et al., 1988). Mass loss mechanisms such as stellar wind models (Tout and Pringle, 1992), accretion-powered stellar winds models (APSW, Matt and Pudritz, 2008a,b), and disk wind models (Ercolano et al., 2021; Zanni and Ferreira, 2013) can be involved to reach this equilibrium. While all these models rely on the basis that a fraction of the accretion luminosity powers the stellar wind, only APSW establishes an upper limit for the so-called branching ratio between the mass loss rate in the stellar wind and the disk accretion rate ($\chi \equiv \dot{M}_{wind}/\dot{M}_{acc}$). This upper limit of $\chi \sim 0.6$ has been confirmed by (Watson et al., 2016) using infrared forbidden line emission

from the Spitzer and Herschel observations. The authors obtain a distribution of χ centered close to 0.1 with a tail towards lower values ($\chi < 0.6$), whose effect on the angular momentum evolution of CTTS has not been properly explored.

In this work, we computed synthetic rotational velocities for low-mass stars ($0.3M_{\odot} < M_{*} < 1.2M_{\odot}$) in the framework of APSW models with the aim of obtaining the branching ratio distribution of a well-characterized CTTS sample with available rotation rates and accretion indicators. We use a Bayesian approach to investigate the connection between the branching-ratio parameter, the stellar magnetic fields, rotational evolution, and internal structure. This paper is organized as follows. In §3.2, we describe the observations and data sources used to study our sample of CTTS. In §3.3, we estimate the rotation periods using the TESS light curves. We derive the stellar mass accretion rate based on the H_{α} spectral line and identify wind tracers (e.g., [O1] λ6300) to estimate the mass-loss rate by winds ($\dot{M}_{wind}$). We also build and present the spin models for CTTS and use the Approximate Bayesian Computation (ABC) technique to investigate the connection between the model parameters and available observable distributions of CTTS. In §3.4, we discuss the implications of our results. Finally, in §3.5, we present the conclusions of this work.

3.2 T Tauri Stars Sample And Data Sources

3.2.1 CTTS Sample

We use the sub-sample of 208 CTTS studied in Serna et al. (2021). This sub-sample has been confirmed and characterized by Briceño et al. (2019) and Hernández et al. (2014). It includes low-mass accretors of the on/off cloud population in the Orion OB1 association, which span ages from 1 to 10 Myr (e.g., ONC, σ Ori, 25 Ori). Each of these targets has measurements of the H_{α} equivalent width, $v \sin(i)$, as well as masses and ages derived using the `MassAge` code (Serna et al., 2021, Hernández et al., in preparation). The list of parameters can be seen in Table 3.1.

3.2.2 APOGEE-2 Data and Stellar Parameters

The APOGEE-2 northern spectrograph (APOGEE; Majewski et al., 2017) is located on the 2.5 m SDSS telescope at the Apache Point Observatory and observed thousands of stars for the APOGEE-2 Young Cluster Survey. This instrument can simultaneously observe up to 300 objects at high resolution ($R \sim 22500$) in the H-band (15100–17000Å) across a 1.5 deg

radius field-of-view.

Kounkel et al. (2018) analyzed data from the APOGEE-2 survey in the Orion Star-Forming Complex and reported nearly 2400 kinematic members using six-dimensional analysis (positions, parallax, and proper motions from *Gaia*-DR2 and radial velocities (RV) from APOGEE-2). Additionally, for each one of these members, Kounkel et al. (2019) report (effective temperature T_{eff}, surface gravity $log(g)$, $v\sin(i)$, RV). However, the authors warn that there are likely systematic features in the parameter space due to theoretical templates not offering a perfect match to the real data. To reduce these issues on the estimated parameters, Olney et al. (2020), based on a deep learning analysis, have provided more reliable predictions of $\log g$, T_{eff}, and [Fe/H] for low-mass stars. More recently, Serna et al. (2021) estimated $v\sin(i)$ using the Fourier method, an independent method that does not require theoretical templates, and found that measurements are in agreement with the estimations of Kounkel et al. (2019), indicating that the systematic features in the parameter space suggested by these authors do not affect their $v\sin(i)$ derivation. Since the Fourier method requires a high signal-to-noise ratio, applying this method to the entire CTTS sample was not possible. Thus, we adopt Kounkel et al. (2019) measurements for our sample of CTTS.

3.2.3 LAMOST

We use the data archive from the Large Sky Area Multi-Object Fiber Spectroscopic Telescope (LAMOST; Liu et al., 2020; Luo et al., 2015), located on the 4-meter quasi-meridian reflecting Schmidt telescope at the Xinlong station of the National Astronomical Observatory. We downloaded 55 spectra of our CTTS sample at low-resolution (R$\sim$1800) in the wavelength range 3650–9000Å, and 7 spectra at medium-resolution (R$\sim$ 7500) in two bands, which cover the wavelength ranges 4950-5350Å, and 6300-6800Å. From these spectra, only 24 have the presence of the [O1] λ6300 line, which was used for the mass-loss rate estimations §3.3.1. The remaining spectra of the 55 stars without [OI] were not used in the analysis. The details of the LAMOST data and plots of the [O1] λ6300 profile are presented in Appendix **??**.

3.2.4 X-Shooter and Giraffe/ESO

We download spectra for 25 CTTS using the ESO Archive Science Portal. From this sample, there are 15 stars with resolution $R < 18340$ (X-Shooter) and 10 stars with $R = 24000$ (Giraffe); both instruments are installed in the ESO Very Large Telescope (Vernet et al., 2011). We rejected three stars observed with Giraffe that do not exhibit the [O1] λ6300 line. We

Table 3.1: Stellar parameters of the CTTS sample

2MASS ID	$v \sin(i)$[a] (km s^{-1})	M_* ($M_\odot$)	Age (Myr)	P_{rot}[b] (days)	P_{rot}[c] (days)	$\log \dot{M}_{acc}$ ($\log M_\odot$ yr^{-1})	$\log \dot{M}_{wind}$ ($\log M_\odot$ yr^{-1})	Binary[a]
05390878-0231115	12.8 ± 0.6	0.3 ± 0.03	2.36 ± 0.53			-9.37 ± 0.31	-11.13 ± 0.83	1
05380097-0226079	16.2 ± 0.5	0.37 ± 0.03	3.77 ± 0.85			-9.01 ± 0.3	-10.43 ± 0.84	1
05344178-0453462	10.7 ± 0.7	0.44 ± 0.04	1.73 ± 0.33			-8.95 ± 0.3	-10.05 ± 0.84	1
05373094-0223427	7.7 ± 0.6	0.36 ± 0.03	6.66 ± 1.46			-8.93 ± 0.3	-10.38 ± 0.84	1
05391151-0231065	13.7 ± 0.5	0.5 ± 0.04	1.3 ± 0.21			-8.89 ± 0.3	-9.76 ± 0.84	1
05332852-0517262	8.1 ± 1.2	0.5 ± 0.04	1.56 ± 0.27			-8.7 ± 0.29	-10.26 ± 0.83	1
05380826-0235562	8.8 ± 0.5	0.4 ± 0.03	1.03 ± 0.18			-8.68 ± 0.29	-9.9 ± 0.84	1
05384027-0230185	18.3 ± 1.1	0.49 ± 0.03	0.8 ± 0.11	7.69 ± 0.01		-8.67 ± 0.29	-9.37 ± 0.85	1
05402461-0152309	14.4 ± 0.5	0.54 ± 0.04	1.9 ± 0.34			-8.66 ± 0.29	-10.02 ± 0.84	1
05393938-0217045	14.1 ± 0.5	0.6 ± 0.04	0.98 ± 0.16		13.52 ± 0.01	-8.61 ± 0.29	-9.93 ± 0.83	1
05343395-0534512	22.3 ± 0.5	0.54 ± 0.04	0.82 ± 0.12			-8.56 ± 0.29	-9.03 ± 0.85	1
05395362-0233426	0.1 ± 0.6	0.35 ± 0.03	2.68 ± 0.55			-8.56 ± 0.29	-10.75 ± 0.83	1
05324196-0539239	60.7 ± 1.7	0.75 ± 0.07	0.41 ± 0.07	1.7 ± 0.01	1.69 ± 0.01	-8.56 ± 0.29	-9.29 ± 0.84	-1
05400195-0221325	8.8 ± 0.5	0.36 ± 0.03	0.96 ± 0.15			-8.54 ± 0.28	-10.71 ± 0.83	1
05391883-0230531	47.9 ± 2.6	1.1 ± 0.18	2.45 ± 1.33		1.83 ± 0.01	-8.53 ± 0.28	-9.79 ± 0.83	-1
05380674-0230227	15.3 ± 2.1	0.52 ± 0.03	0.77 ± 0.11			-8.51 ± 0.28	-9.05 ± 0.85	1
05401274-0228199	50.9 ± 1.4	0.45 ± 0.03	0.52 ± 0.05	1.53 ± 0.01		-8.49 ± 0.28	-10.86 ± 0.81	-1
05354600-0057522	10.3 ± 0.7	0.65 ± 0.05	1.75 ± 0.32			-8.49 ± 0.28	-10.01 ± 0.83	1*
05341420-0542210	5.4 ± 1.1	0.62 ± 0.05	2.53 ± 0.52			-8.42 ± 0.28	-9.12 ± 0.85	1
05394017-0220480	16.1 ± 0.8	0.77 ± 0.05	1.6 ± 0.27	5.8 ± 0.01	5.64 ± 0.01	-8.4 ± 0.28	-9.73 ± 0.84	1

[a] Kounkel et al. (2018); Kounkel et al. (2019): 0- Undeconvolvable cross-correlation function (CCF); 1- Only a single component in the CCF; 2- Multiple components in the CCF; -1- Spotted pairs or SB2 Uncertain
[b] TESS Sector 6
[c] TESS Sector 32
* Tokovinin et al. (2020) visual binaries
Only a portion of the table is shown here. The full version is available in electronic form.

use the data reduced and flux-calibrated by the ESO calibration pipelines available in the ESO archive. Additionally, we used the `Molecfit` tool (Kausch et al., 2015) to correct each spectrum from telluric lines. Table 3.2 shows a summary and observations details.

3.2.5 TESS Data

From the initial sample of 208 CTTS, we have 194 stars observed by TESS at 10 min and 30 min cadences for at least ∼25 days. We build each light curve (LC) using the `TESSExtractor`[1] application (Serna et al., 2021), which uses simple aperture photometry (SAP) to extract the stellar fluxes from the Full-frame images (FFI) provided by TESScut (Brasseur et al., 2019). Also, we use the Cotrending basis vectors (CBVs) from TESS and the task `kepcotrend` of the PyKE package (Still and Barclay, 2012) to correct the LCs from any systematic effect on the data. Once LCs were adequately processed, we performed a visual inspection and flagged the sources that exhibited periodic or quasi-periodic events as candidates for their posterior period analysis. Figure 3.1 shows an example of the graphical product generated

[1] `https://www.tessextractor.app`

Table 3.2: Summary of ESO archival spectroscopy

Target	Instrument*	Spectral Resolution	Obs. Date (UT)	Exp. time (s)	SNR	ESO Program ID
SO 73	XSHOOTER	8935	2019-11-18	2400	106	0104.C-0454(A)
SO 299	GIRAFFE	24000	2009-02-04	2775	22	082.C-0313(B)
SO 341	XSHOOTER	1029	2020-02-07	90	28	0104.C-0454(A)
SO 362	XSHOOTER	1512	2020-02-07	200	41	0104.C-0454(A)
SO 662	XSHOOTER	1512	2020-02-07	60	38	0104.C-0454(A)
SO 908	GIRAFFE	24000	2010-01-03	2775	39	084.C-0282(A)
SO 927	GIRAFFE	24000	2010-01-03	2775	62	0103.C-0887(B)
SO 984	XSHOOTER	18340	2019-11-17	420	83	0104.C-0454(A)
SO 1036	XSHOOTER	1512	2019-10-11	60	37	0104.C-0454(A)
SO 1075	GIRAFFE	24000	2010-01-03	2775	26	084.C-0282(A)
SO 1152	XSHOOTER	18340	2019-10-12	800	73	0104.C-0454(A)
SO 1153	XSHOOTER	1512	2021-02-13	60	37	106.20Z8.002
SO 1156	XSHOOTER	1512	2019-10-28	60	44	0104.C-0454(A)
SO 1260	GIRAFFE	24000	2010-01-03	2775	40	084.C-0282(A)
SO 1267	XSHOOTER	1512	2019-11-17	60	33	0104.C-0454(A)
SO 1327	GIRAFFE	24000	2010-01-03	2775	33	084.C-0282(A)
SO 1368	GIRAFFE	24000	2010-01-03	2775	79	0103.C-0887(B)
SO 1361	XSHOOTER	1512	2019-12-09	60	40	0104.C-0454(A)
CVSO 58	XSHOOTER	1512	2020-12-02	65	27	106.20Z8.002
CVSO 90	XSHOOTER	18340	2020-12-04	740	80	106.20Z8.002
CVSO 107	XSHOOTER	18340	2020-12-04	740	80	106.20Z8.002
CVSO 146	XSHOOTER	1512	2020-12-09	40	42	106.20Z8.002
CVSO 1876	GIRAFFE	24000	2010-01-03	2775	72	084.C-0282(A)
CVSO 1885	GIRAFFE	24000	2010-01-03	2775	49	084.C-0282(A)
V605 Ori B	GIRAFFE	24000	2010-01-03	2775	39	084.C-0282(A)

*The spectral coverage for the X-Shooter data 533.7-1020 nm and Giraffe 611.38-640.37 nm.

by the `TESSExtractor` application. This product includes the light curve, the phase-folded curve, and the periodogram used to obtain rotational periods. For more details, see section 3.3.1.

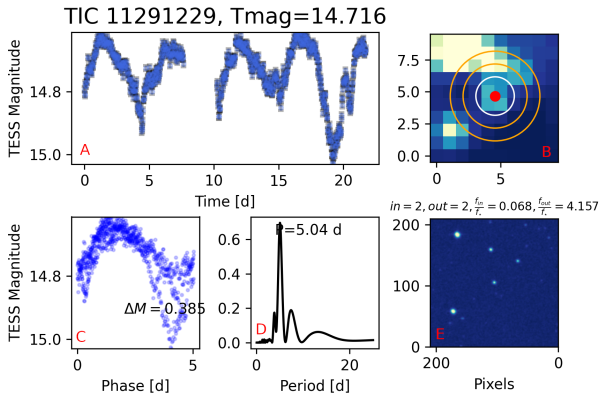

Figure 3.1: TESS light curve and analysis for the target TIC 11291229. *Top*: (A) Light curve in TESS magnitudes, the error bars are contained in the marker symbols. The label on top refers to the star identification and the mean TESS magnitude. (B) Field of view (210 x 210 sq arcsec) corresponding to a TESS image of 10x10 pixels. The white circle shows the photometric aperture, and the orange circle shows the sky annulus. The red dot marks the centroid of the star. *Bottom*: (C) Phase-folded light curve to the estimated best period. The legend shows the amplitude. (D) Lomb-Scargle periodogram, with the estimated period. (E) 210 x 210 pixels Digital Sky Survey (DSS2) thumbnail, same field of view as (B).

3.3 Analysis and Results

3.3.1 Stellar Parameters

Rotation Period

Several variability studies in young stellar objects (YSOs) have revealed that most CTTS exhibit complex flux variations on timescales of hours, days, and even years (Bouvier et al., 1993; Cody and Hillenbrand, 2010; Roggero et al., 2021). In some cases, brightness fluctuations are observed at levels of 1% to 10%, with fading or brightening events and quasi-periodic structures in most instances (Cody et al., 2014). It has been proposed that these flux variations are generated by various mechanisms, such as the rotation of hot and cold starspots, accretion bursts (e.g., Espaillat et al., 2021), occultations by dusty disk structures (e.g., Ansdell et al., 2019), and accretion streams falling at random locations on the star (Kurosawa and Romanova, 2013). These processes may be acting at once in CTTS, challenging the estimations of P_{rot} for most stars. However, according to the DL model, the magnetic

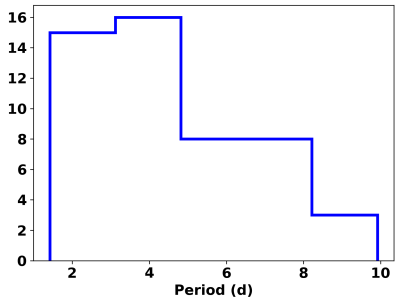

Figure 3.2: Rotational periods for the CTTS sample obtained through TESS light-curve analysis. The bin size used in the histogram follows Scott's rule (Scott, 1979).

connection between the star and its inner disk results in synchronization between the stellar angular velocity and the Keplerian velocity at the corotation radius (Artemenko et al., 2012), particularly for the first 3 Myr of the CTTS evolution (Matt et al., 2010, 2012). Then, assuming a Keplerian rotation regime, any periodic signal produced at the corotation zone could proxy the stellar rotation at the stellar surface. Therefore, under this assumption, we have estimated rotation periods for those candidates that show an apparent periodicity in the TESS data (§3.2.5).

From the sample of LCs in §3.2.5, only 51 stars exhibit periodic behavior to study rotation. We have selected light curves with a false alarm probability (FAP) below 0.01%, indicating that the period measurements are highly reliable. We use the task `statistics.false_alarm_probability` from the astropy package (Astropy Collaboration et al., 2013b). We use the Lomb-Scargle periodogram (Lomb, 1976; Scargle, 1982) to estimate the rotational period from the LC. We use a resolution of 1000 steps within the interval $0.01 < P < 25$ days. The best period was selected as the highest peak in the periodogram (see lower middle panel of Figure 3.1). These periods have been confirmed by checking the periodic pattern using the phase-folded LC at the estimated period, as shown in Figure 3.1. The P_{rot} are listed in Table 3.1. We plot the histogram of the periods in Figure 3.2. The range of periods estimated in this section will be used as input in the models §3.3.2, see Table 3.3.

Mass Accretion Rate

We determined mass accretion rates for the 208 stars of the sample in §3.2.1 based on the Hα equivalent width (EWH_α), spectral types, and reddening A_V reported by Briceño et al. (2019); Hernández et al. (2014, Hernández et al., in preparation). Also, we use the *Gaia* DR3 parallax measurements corrected by systematics and the *Gaia* G, G_{BP}, and G_{RP} photometry (Gaia Collaboration et al., 2022; Lindegren et al., 2021). Using the relationship between the

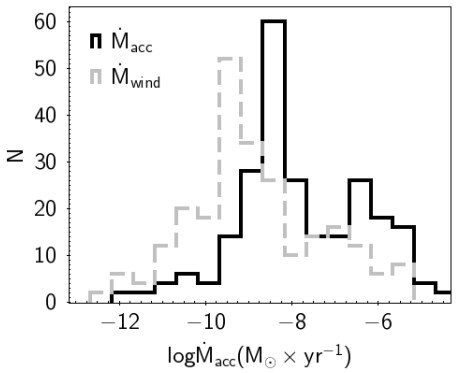

Figure 3.3: Mass accretion and mass loss rates for the sample of CTTS.

Johnson-Cousins photometric system and the *Gaia* photometry[2], we obtain the V magnitude. Given the spectral type and using the V magnitude corrected by extinction, the $I_{c,0}$ magnitude is obtained from the intrinsic $[V - I_c]_0$ color from Pecaut and Mamajek (2013). To obtain the continuum flux at the Hα line (F_{cont}), we estimate the fluxes at the $V(0.55\ \mu m)$ and I_c $(0.79\mu m)$ bands and interpolate the flux at 0.6563 μm. Using the Hα equivalent width and distance estimated by the inverse relation with the parallax, we estimate the luminosity of the Hα as follows:

$$L_{H\alpha} = 4\pi d^2 \times (EW H_\alpha) \times F_{cont} \tag{3.1}$$

Subsequently, we obtain the accretion luminosity using the following relation (Ingleby et al., 2013):

$$\log(L_{acc}) = 1.0(\pm 0.2)\log(L_{H\alpha}) + 1.3(\pm 0.7). \tag{3.2}$$

Finally, the mass accretion rate is obtained from $L_{acc} = GM_*\dot{M}_{acc}/R_*$, where M_* and R_* are determined using the MIST evolutionary models (Dotter, 2016). The mass accretion rates distribution is shown in Figure 3.3, and corresponding values are included in Table 3.1.

Mass loss Rate Determination

We computed mass loss rates for a sub-sample of the CTTS described in §3.2.1 via the forbidden emission line of [O1] λ6300, which has been widely used as a tracer of bi-polar jets, stellar and disk winds (e.g., Cabrit et al., 1990; Edwards et al., 2003; Pascucci et al., 2022; Watson et al., 2016). Specifically, we compute mass loss rates for 24 CTTS with LAMOST spectra (§3.2.3), 15 CTTS with X-Shooter spectra and 7 CTTS with Giraffe spectra (§3.2.4). Luminosities of [OI] emission lines are computed from equivalent widths and dereddened

[2]from Table 5.8 of the *Gaia* data release 2 documentation https://gea.esac.esa.int/archive/documentation/GDR2/

fluxes at wavelengths near 6300Å and used as indicators of the amount of mass in the outflow (Hartigan et al., 1995). Forbidden lines typically exhibit two components: a low-velocity component (LVC), which is symmetric and slightly blue-shifted, and a high-velocity component (HVC), with its peak either blue or red-shifted and separated from the LVC just a few tens of $\mathrm{km\,s^{-1}}$ (e.g., Banzatti et al., 2019; Hartigan et al., 1995; Natta et al., 2014; Simon et al., 2016).

Following the physical treatment to the mass-loss rate in the Appendix A1 of Hartigan et al. (1995) and references therein, we use the luminosity of the [O1] λ6300, identified in the optical spectra of our CTTS to estimate the mass-loss rate ($\dot{M}_{wind} = MV_{\perp}/l_{\perp}$), where M is the mass in the flow whose dependence with the [O1] λ6300 luminosity was taken from Hartigan et al. (1995), the $V_{\perp}$ is the component of the velocity of the projected wind in the plane of the sky, and $l_{\perp}$ corresponds to the size of the slit projected in the sky. In what follows, we assume $V_{\perp} = 150\ \mathrm{km\,s^{-1}}$ as an average for all the stars (Hartigan et al., 1995), and based on the average distance to Orion ($d \sim 400$pc), we adopt $l_{\perp} = 6 \times 10^{15}\ cm$ for X-shooter and Giraffe observations. For the case of the LAMOST spectra, the slit at the output end of the fibers is assumed to be equal to 2/3 of the fiber width leading to marginal differences relative to $l_{\perp}$. Thus, the correlation of Hartigan et al. (1995) may be written as follows:

$$\log_{10}\left(\dot{M}_{wind}\right) = -4.65 + \log_{10}\left(\frac{L_{\lambda 6300}}{L_{\odot}}\right) \tag{3.3}$$

Before analyzing any optical forbidden line profiles, we first remove any telluric and photospheric absorption contaminating the region of interest in the spectra. We used the `Molecfit` tool (Smette et al., 2015), which corrects for telluric absorption lines based on synthetic modeling of the Earth's atmospheric transmission. To remove telluric lines, each spectrum was normalized and corrected by radial velocity (RV), using the RV reported in Hernández et al. (2014); Kounkel et al. (2018). Based on the effective temperature and $\log(g)$ of the star, we selected templates from the PHOENIX spectral library (Husser et al., 2013). In the specific case of the X-Shooter data, we use the XSL DR2 (Gonneau et al., 2020) to select a proper template for each star. Once spectra were corrected by RV, all the templates were broadened by their reported $v\sin(i)$ using the rotational kernel implemented in the `PyAstronomy` package (Czesla et al., 2019b). Then, the broadened templates were subtracted from each observed spectrum.

In Figures 3.4, and 3.5 we show the line profiles. In order to get the luminosity of the line [O1] λ6300 ($L_{\lambda 6300}$), we have used the distances of *Gaia* DR3, the equivalent width of

[O1] λ6300 (EW[OI]) obtained with the task *splot* of `IRAF`, a continuum flux estimation around the [O1] λ6300, and the equation (3.1). In particular, for LAMOST and Giraffe spectra, the flux at the continuum was estimated interpolating two bands around 6300Å as described in section 3.3.1. For the X-shooter spectra, we directly measure the flux because the spectra have been properly flux calibrated. Subsequently, using the equation (3.3), we estimate the mass-loss rate $\dot{M}_{wind}$ of our sample and their uncertainty following the error propagation procedure.

This analysis remains valid as long as we have the presence of HVC in the [O1] λ6300 line profiles. In some cases, our spectral resolution is insufficient to distinguish the HVC. We warn the reader to be cautious with results because the mass-loss rates for some sources could be overestimated. However, our results provide a helpful statistical estimation of the mass loss rate for this study. We summarize our results in Table 3.1.

Using the mass accretion rates estimated in §3.3.1 and the mass-loss rates of our sample, we roughly estimate the branching ratio χ of these systems. We plot in Figure 3.6 the accretion and mass-loss rates for our sample compared to other estimations of CTTS in the literature. Considering the limited mass and age intervals covered by our sample, accretion rates values range between $10^{-9} - 10^{-8}$ $M_{\odot}\, yr^{-1}$ and mass-loss rates between $10^{-10} - 10^{-8}$ $M_{\odot}\, yr^{-1}$ as shown in Figure 3.3. To have a more comprehensive view of a diverse population of CTTS, we included reported measurements for CTTS in Taurus (Herczeg and Hillenbrand, 2008), Lupus (Natta et al., 2014), active CTTS systems from Gullbring et al. (1998); Hartigan et al. (1995), and CTTS in nine molecular cloud complexes studied by Watson et al. (2016) using Spitzer data. According to Figure 3.6, most of our CTTS remain below the APSW boundary (long-dashed black line), confirming that APSW is a suitable scenario to explain the observed rotation rates.

Although age information is not available in Figure 3.6, some studies have suggested evidence of temporal evolution between the $\dot{M}_{acc}$ and $\dot{M}_{wind}$ relationship. For instance, Watson et al. (2016) mostly includes objects younger than CTTS (e.g., Class 0 and Class I) and demonstrated that different classes of young objects, used as an age proxy, are naturally separated into different plot regions (see Figure 7 of Watson et al., 2016). Our study supports that evidence, providing more CTTS to the sample and showing even better how CTTS are well positioned in the plot.

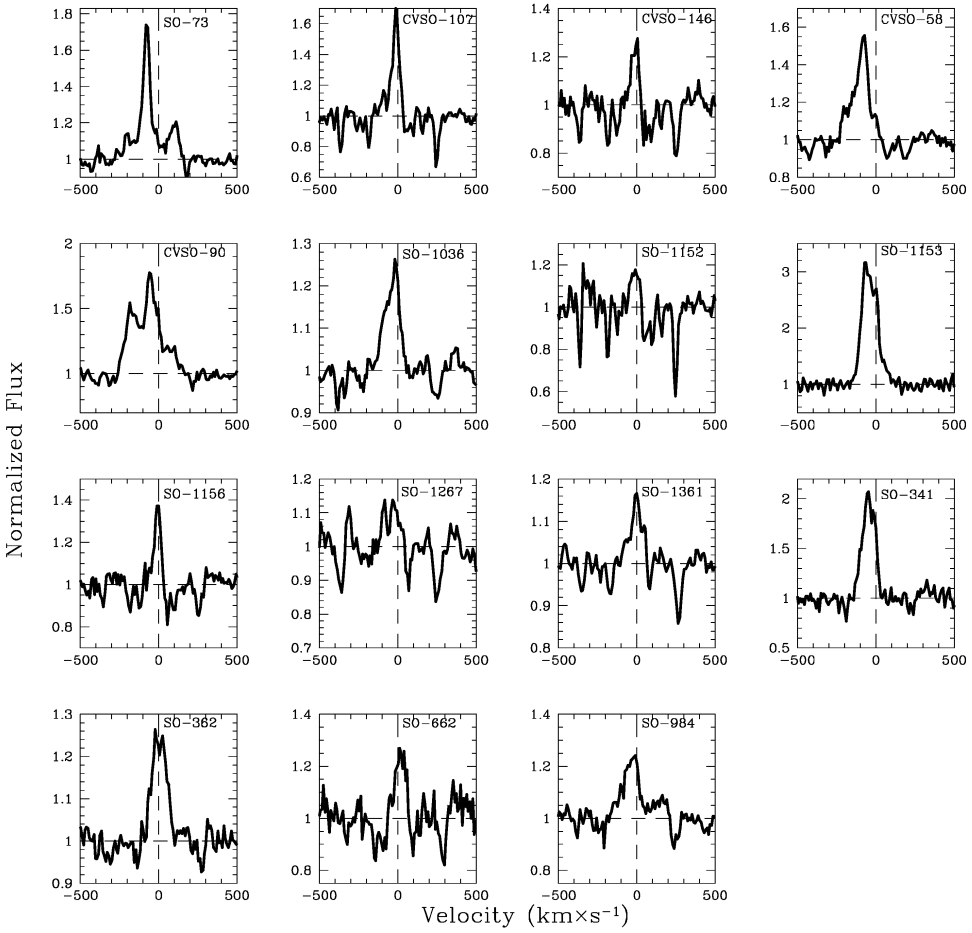

Figure 3.4: [O1] λ6300 residual line profiles for 15 CTTS found in the X-Shooter data archive. The stellar rest velocity is indicated with a vertical dashed line. Residual emission lines were obtained by subtracting photospheric contributions using Phoenix templates and posterior removing telluric lines.

Magnetic field topology and evolution

Observations indicate that the surface magnetic fields of young stars have high-order multipolar components rather than magnetic dipoles. While stars more massive than $0.5M_{\odot}$ exhibit toroidal and non-axisymmetric poloidal components, low-mass stars below $0.5M_{\odot}$ show strong poloidal large-scale magnetic fields, which are mainly axisymmetric (Donati and Landstreet, 2009), where most CTTS have typical intensities of the order of 1-3 kG (Johns-Krull, 2007), and significant star spot coverages (Cao and Pinsonneault, 2022; Somers et al., 2020). These magnetic fields are expected to impact CTTS, their accretion disks, and planets (Strugarek et al., 2015).

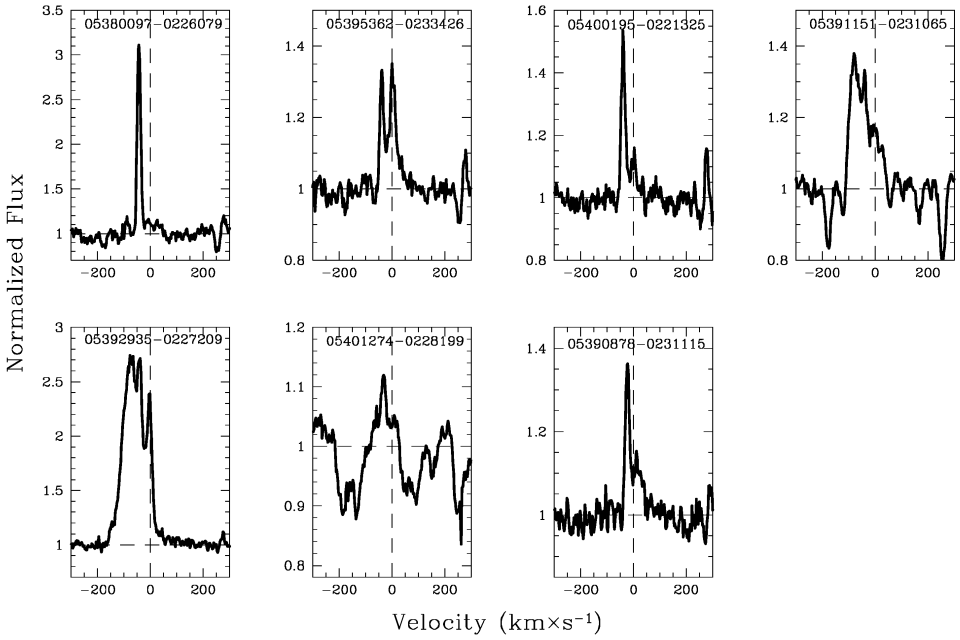

Figure 3.5: [O1] λ6300 residual lines profiles for 7 CTTS found in data archive of Giraffe.

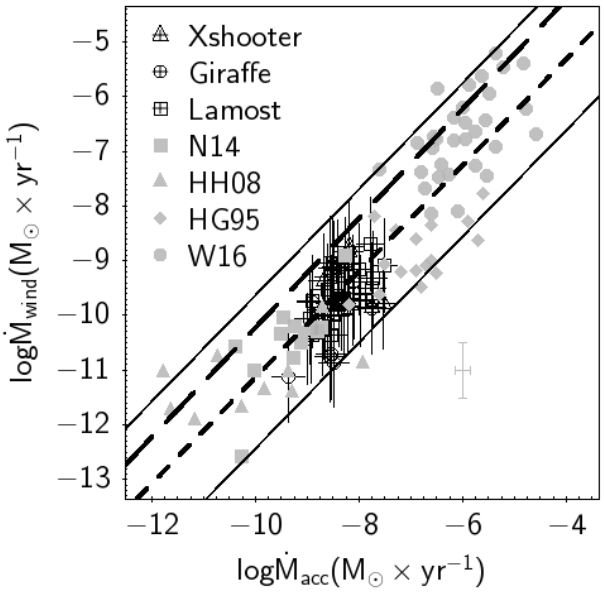

Figure 3.6: Accretion and mass-loss rates for our sample of CTTS (black crosses) and other studies (gray symbols). Complementary data shown in gray correspond to low mass accretors in Taurus from Herczeg and Hillenbrand (2008), (triangles) active CTTS systems from Gullbring et al. (1998); Hartigan et al. (1995) (diamonds) and selected CTTS from Natta et al. (2014) (squares) and Watson et al. (2016) (circles). The long-dashed line indicates the upper limit given by APSW models of Matt et al. (2012), i.e. $\dot{M}_{wind} = \chi \times \dot{M}_{acc}^{\eta}$, with $\eta = 1$, and χ=0.6. The short-dashed line corresponds to the linear regression fit using all the data, which leads to $\eta = (0.97 \pm 0.05)$ and $\chi = 0.04^{+0.05}_{-0.02}$. Upper and lower solid lines represent the 3σ level.

Schatzman (1962) was the first to suggest that open magnetic field lines or the breaking of closed lines could trigger mass loss phenomenons, which could, in the long run, be responsible for taking a large amount of angular momentum from the system. For this reason, the geometry of the magnetic field is an essential element in describing stellar winds. For example, Réville et al. (2015) and Garraffo et al. (2015) found that complexity in the geometry of the magnetic field can dramatically decrease the loss rate of angular momentum to a few orders of magnitude. This is mainly because higher orders of magnetic moments would facilitate the generation of a magnetosphere with many closed lines that would suppress mass loss. Emeriau-Viard and Brun (2017); Folsom et al. (2016) observed that the topology of the magnetic field changes strongly as the star ages because as the radiative core becomes bigger, the dipole components decrease, and the magnetic field becomes more and more complex. Folsom et al. (2016) and Vidotto et al. (2014) found empirical relationships between the large-scale component of the magnetic field strength versus age for pre-main to the main sequence.

Although there are many efforts to measure magnetic fields in T Tauri stars, nowadays, there is no conceptual model that allows us to describe magnetic fields accurately. Some authors approximate the magnetic field topologies, mixing different geometries. For example, Finley and Matt (2017) suggests that combinations of dipolar and quadrupolar fields change the relative orientation of the stellar wind with respect to any planetary or disk magnetic field. In a general view, these components are important in the morphology of the wind. Also, they confirm that the original prescription from Matt et al. (2012), which is the formulation of the present work, uses pure dipolar magnetic fields and remains robust in most cases, even for significantly nondipolar fields.

3.3.2 Model Assumptions

We developed stellar spin multi-parametric models for young low-mass and solar-type stars magnetically linked to a surrounding gaseous accreting disk. Although non-rotational, pre-main-sequence evolutionary models provide the internal structure of stars (i.e., Baraffe et al., 2015). We assume that stars can produce their stellar magnetic fields when they rotate. The magnetic fields are originated through dynamo processes in the convective regions of the stellar interior.

For simplicity, we assume a dipolar field with strength B_* at the equator of the stellar surface and co-rotating with the star. At larger stellar radii, this dipole enables angular

momentum transport with the disk and magnetosphere. We assume values range between 500-3500 G in agreement with previous studies (Johns-Krull, 2007) and recent surveys such as Lavail et al. (2017, 2019). The main assumptions for constructing our grid of rotational models are the following:

- **A solid body approach**: We consider a simple approach in our models, assuming that the stars rotate as a solid body with a core and envelope coupled to each other. We neglect any difference in angular momentum between the stellar surface and its stellar interior. Rotation is thus entirely controlled by the external torques. This approach is sufficient for fully convective stars on their Hayashi tracks, although our simplified treatment should be revised for stars with radiative zones in their interiors using a more realistic treatment, similar to the considered redistribution of angular momentum between the two layers (MacGregor and Brenner, 1991). We do not expect a strong impact on the rotation rates predicted by our models in the CTTS phase (<10 Myr) because the expected time scale for the core-envelope decoupling interaction starts around ∼10-30 Myr (Gallet and Bouvier, 2013, 2015).

- **Accretion rate onto the star**: We assume an exponential decay for the accretion rate as a function of age ($\dot{M}_{acc} = \dot{M}^{in}_{acc}\, e^{-\frac{(t-t_0)}{\tau_a}}$), starting from an initial value $\dot{M}^{in}_{acc}$ at $t_0 = 0.5$ Myr and with a characteristic accretion timescale of $\tau_a = 2.1$ Myr reported by Briceño et al. (2019). Since the exponential relation for the accretor fraction evolution (Briceño et al., 2019) represents a probability that stars in a stellar group have accretion rates above the threshold detection limit, the τ_a obtained from this relation is a statistical proxy for the timescale of the general accretion rate evolution behavior in stellar groups. The accretion process adds angular momentum that is transferred from the disk truncation radius (R_t) toward the stellar surface at a rate of:

$$\tau_{acc} = \dot{M}_{acc}\sqrt{GM_* R_t} \tag{3.4}$$

  R_t denotes the distance at which the magnetic field fully governs the stress in the internal disk. At this location, disk material and the stellar surface share identical rotation. We assumed R_t inside disk corotation, which is computed using the Newton-Raphson method and the equation 15 of Matt and Pudritz (2005b).

- **Stellar winds**: We consider the APSW an important source of angular momentum loss in CTTS (Matt and Pudritz, 2008a). Previous studies have shown that open field regions in the magnetic field lead to the formation of ASPW that efficiently removes substantial amounts of angular momentum from the star (e.g., Hartmann and Stauffer, 1989; Matt et al., 2012; Pantolmos et al., 2020; Pinzón et al., 2021; Uzdensky, 2004). It

is assumed that a fraction χ of the mass in the accretion flow is transferred to a stellar wind, i.e., $\dot{M}_{wind} = \chi \dot{M}_{acc}$, providing an efficient angular momentum loss mechanism. The formulation is inspired by the analytic work of Weber and Davis (1967), in which the net torque from a one-dimensional wind is as follows:

$$\tau_{wind} = -\dot{M}_{wind}\,\Omega_*\,r_A^2 \tag{3.5}$$

where $\dot{M}_{wind}$ is the integrated wind mass-loss rate, Ω_* is the angular velocity of the star, and r_A is the Alfvén radius. In our one-dimensional approach, we used the semi-analytical results obtained from numerical MHD simulations of Matt and Pudritz (2008a):

$$\frac{r_A}{R_*} = K\left(\frac{B_*^2 R_*^2}{\dot{M}_{wind} v_{esc}}\right)^m \tag{3.6}$$

where $K \approx 2.11$ and $m \approx 0.223$ are dimensionless constants and $v_{esc} = (2GM_*/R_*)^{1/2}$ is the escape velocity from the star.

- **Star-disk interaction**: Along with angular momentum losses through disk winds, CTTS also spin down due to their magnetic interaction with the Keplerian rotating disk (e.g., Collier Cameron and Campbell, 1993a; Ghosh and Lamb, 1978; Koenigl, 1991). In a scenario of large Reynolds numbers of the star-disk interaction (low diffusion parameter β), the strong coupling between disk matter and stellar magnetic field lines leads to a twisting of the vertical field component B_z and thus to a spin-down torque given by:

$$\tau_{DL} = \frac{B_*^2 R_*^6}{3\beta R_{co}^3}\left[2\Big(\frac{R_{co}}{R_{out}}\Big)^{\frac{3}{2}} - \Big(\frac{R_{co}}{R_{out}}\Big)^3 - 2\Big(\frac{R_{co}}{R_t}\Big)^{\frac{3}{2}} + \Big(\frac{R_{co}}{R_t}\Big)^3\right] \tag{3.7}$$

here $R_{out} = R_{co}\big(1+\beta\gamma_c\big)^{\frac{2}{3}}$ defines the extent of the connected magnetic region. R_{co} is the co-rotation radius, R_t the disk truncation radius, and $\gamma_c = B_\phi/Bz$ characterizes the proportion of magnetic field twisted at the disk's surface at each radial location. We use $\gamma_c = 1$ and $\beta = 10^{-2}$ as fixed parameters in all our simulations (Matt et al., 2010).

Grid of Rotational Models

The evolution of the stellar rotation rate (Ω_*) is computed by solving the following differential equation:

$$\frac{d\Omega_*}{dt} = \frac{\tau_*}{I_*} - \frac{\Omega_*}{I_*}\frac{dI_*}{dt} \tag{3.8}$$

where τ_* is the sum of the individual torques due to the accretion, winds, and star–disk interaction as described above, and $I_* = k^2 M_* R_*^2$ is the stellar moment of inertia and k^2 is the gyration radius obtained from the stellar evolutionary models of Baraffe et al. (2015). We note that the accretion rate is incorporated into the calculation of dI_*/dt and used to update M_*.

Using the fourth-order Runge-Kutta method with adaptive step size, we find the solution to the equation (3.8). At each time step of the simulation, we compute the next time step, ensuring changes over the Ω_* solution remain lower than 1% per step.

We use the set of parameters [M_*, B_*, χ, P_{rot}^{in}, $\dot{M}_{acc}^{in}$] based on the values of Table 3.3. We use all possible combinations of the parameters, without repetitions, and within the value ranges and steps to build a grid with 2.232×10^6 individual models. Simulations start at 0.5 Myr and end at 15 Myr, the age at which there are some long-lived CTTS. Nevertheless, statistically, the typical age when the gas component of the disk has been dissipated is around 5 Myr (Carpenter et al., 2006; Hernández et al., 2008). Given a simulation, both the angular velocity (stellar period) and the mass accretion rate evolve with time.

3.3.3 $v\sin(i)$ synthetic distributions

The rotation rates given by our grid of models are related to the projected rotational velocities through the previous knowledge of spin-axis orientation. By assuming that the spin-axes of objects are randomly oriented, and utilizing the inclination average method proposed by Chandrasekhar and Münch (1950), the projected rotational velocity can be expressed as $v\sin(i) = \frac{\pi}{4} R_* \Omega_*$, where R_* is the stellar radius and Ω_* is the angular velocity of the star.

In Figure 3.7, we show individual evolutionary tracks of $v\sin(i)$ for specific cases of the parameter set. While in Figure 3.8, we display the complete grid of models for masses of 0.3, 0.5, 0.8, and $1.0 M_\odot$. In each panel, the color scale represents the number of models enclosed in each hexagonal bin pixel of the $v\sin(i)$ versus age diagram. We have included the 90^{th} percentile and the median per pixel indicated with grey and black lines, respectively.

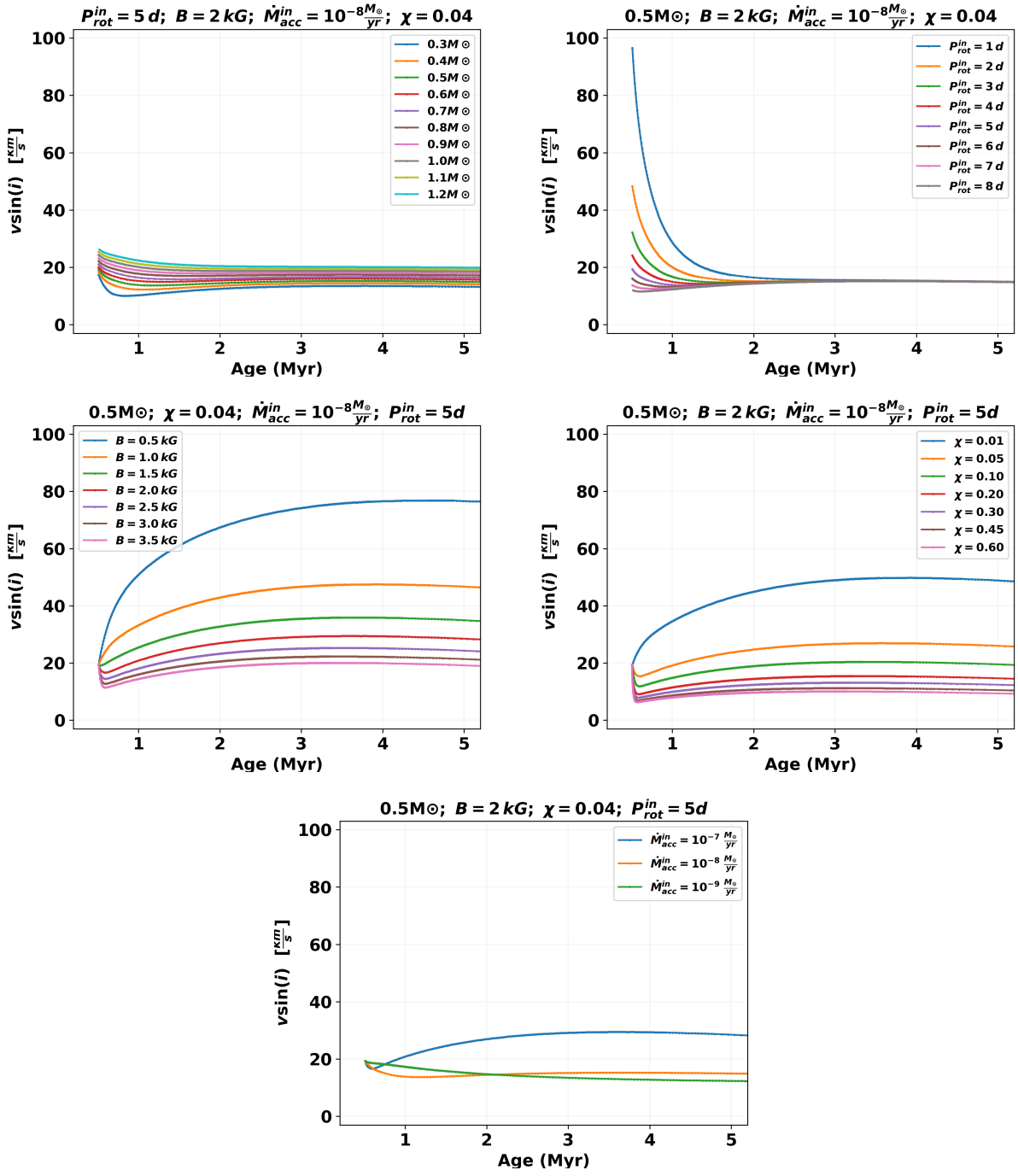

Figure 3.7: Spin evolutionary tracks represented as $v\sin(i) = \frac{\pi}{4}v_{rot}$ as a function of age for individual cases. The title of each panel shows the fixed parameters. Meanwhile, the legend colors represent different cases for a respective variable in the models.

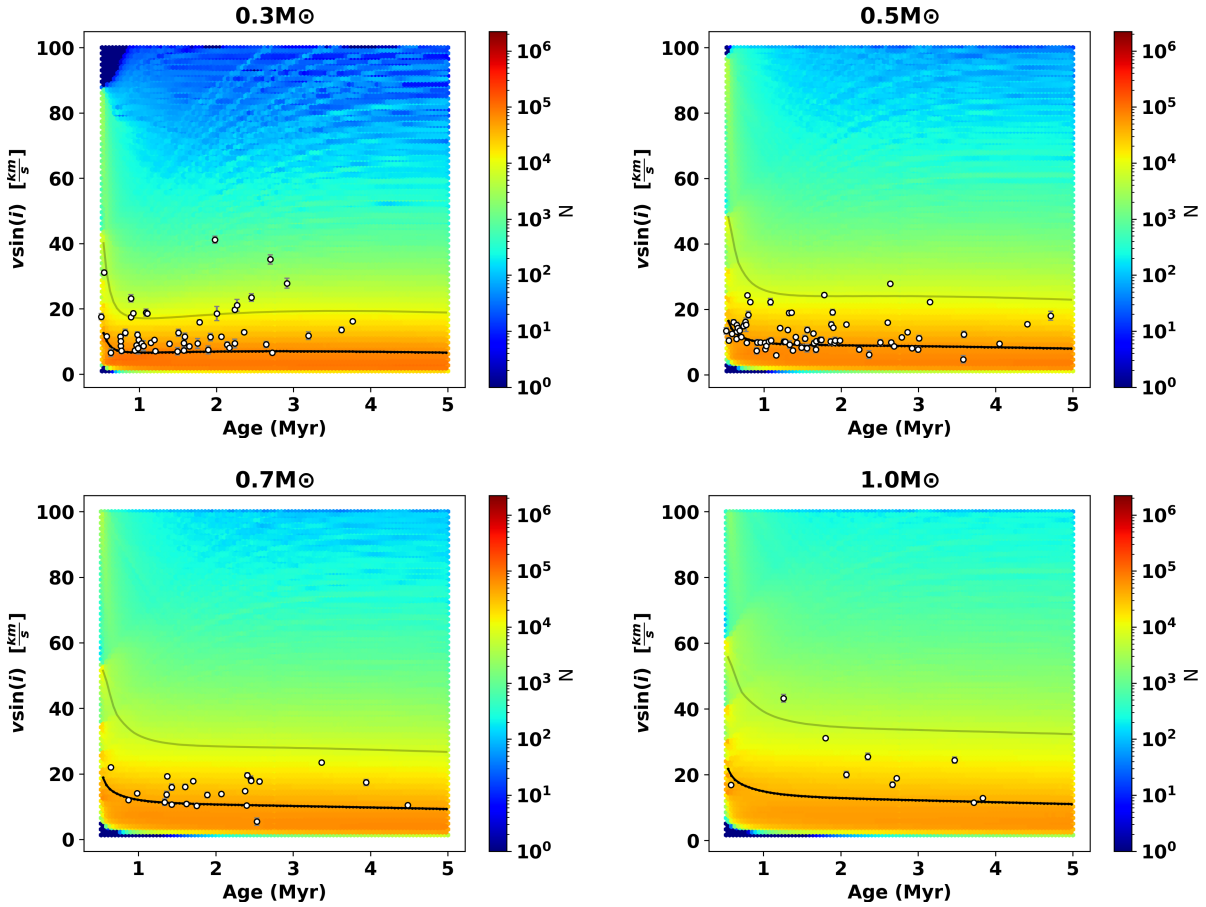

Figure 3.8: Grid of models illustrated as a density plot of $v\sin(i) = \frac{\pi}{4}v_{rot}$ as a function of the age, in different values of mass. The black line shows the grid's median $v\sin(i)$, while the gray line contains 90% of the models below it. The color scale represents the number of models per hex bin pixel. The white dots represent the $v\sin(i)$ and age for the CTTS sample.

Table 3.3: Input parameters of the models, their ranges, and steps.

Parameters	Min	Max	Step
P_{rot}^{in} (days)	1	8	1
$\dot{M}_{acc}^{in}$ ($M_\odot$ yr^{-1})	10^{-10}	10^{-7}	$10^{-0.2}$
M_* ($M_\odot$)	0.3	1.2	0.1
B_* (G)	500	3500	100
χ	0.01	0.60	0.01

The panels in Figure 3.8 show a decreasing trend of the median of $v\sin(i)$ with age. Despite the wide range of initial conditions considered in Table 3.1, most solutions lie on the slow rotator regime with rotation below 10% of the break-up limit as expected for CTTS. Synthetic velocities increase with stellar mass, as confirmed by the gradual growth of the 90^{th} percentile of the $v\sin(i)$ distributions, plotted with a gray line at each panel of Figure 3.8. We also note that rotational equilibrium is reached very rapidly, particularly for low-mass stars (<1 Myr). For comparison purposes, we have added the rotation rates measured for our sample of CTTS. With a few exceptions, especially for $0.3M_\odot$, the bulk of $v\sin(i)$ values remains below the 90^{th} percentile of our simulations, reaching a rotational locked state by the end of the Hayashi track (<3 Myr) in agreement with previous studies.

3.3.4 Spin-torque equilibrium

The total torque on the system is the sum of the accretion, winds, and star-disk interaction torques:

$$\tau_* = \tau_{acc} + \tau_{wind} + \tau_{DL} \tag{3.9}$$

Values of $\tau_* = 0$ are also known as the torque equilibrium state. In the APSW scenario, stellar rotation evolves rapidly (<1 Myr) toward an equilibrium state in which angular momentum transferred toward the star by the disk accretion is balanced with that transferred outward via winds and magnetic star-disk interaction (Matt and Pudritz, 2005a; Matt et al., 2012). For bonafide samples of CTTS with reliable masses, ages, accretion, and rotation rates, the determination of this equilibrium state permits indirectly inferring the response of the wind to different magnetic strengths and topologies and allows for searching statistical trends between the branching ratio and the stellar magnetic field.

Panel A of Figure 3.9 reveals that the torque equilibrium state, on average, is reached at

1.5 Myr. On the other side, panels B and C of Figure 3.9 also indicate that an equilibrium state can be achieved with higher values of B_* and χ at ages earlier than 1.5 Myr. The majority of the models are placed on the equilibrium zone, especially stars older than 1.5 Myrs, to ensure that equilibrium is rapidly reached, a fact consistent with previous studies (Armitage and Clarke, 1996; Matt et al., 2012; Yi, 1994).

Interestingly, stellar winds can achieve equilibrium spin rates during the Hayashi track when magnetic field strengths and branching ratios are large. In §3.4, we discuss this result based on statistical techniques in depth.

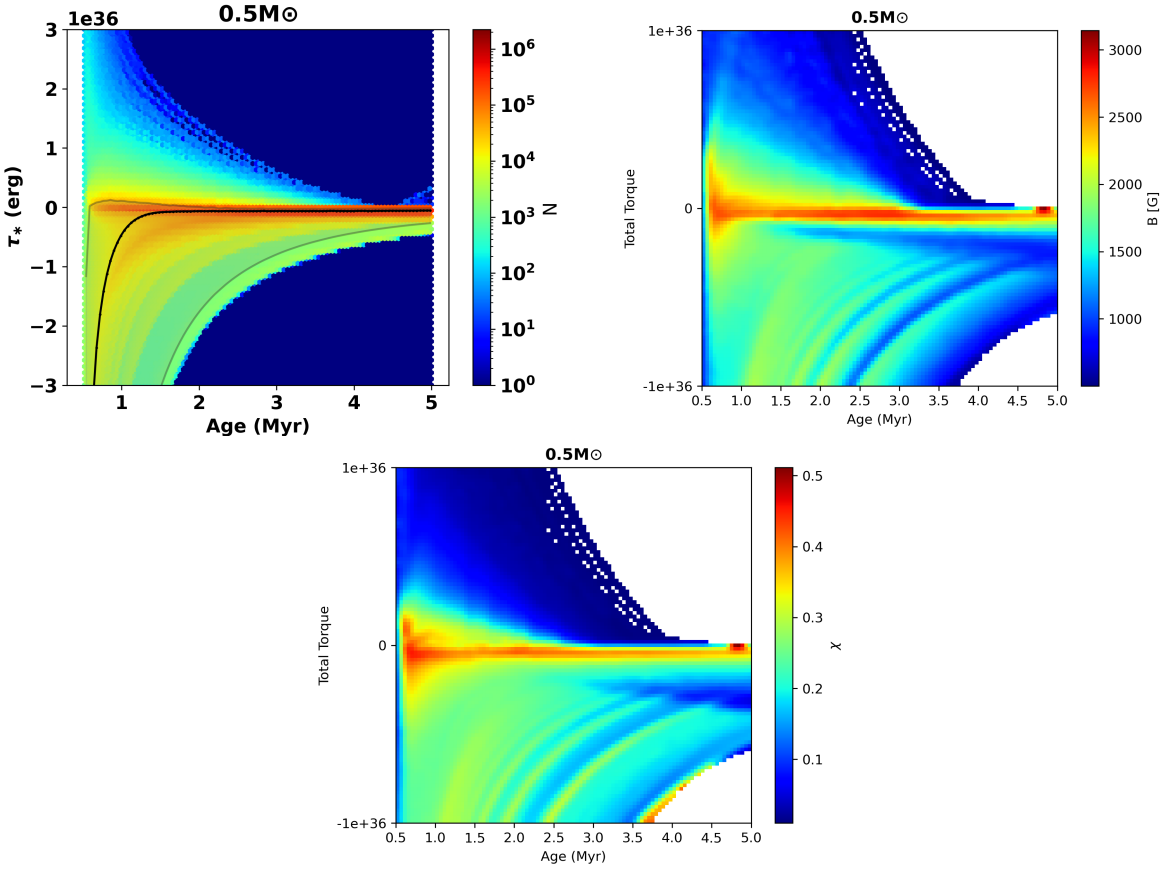

Figure 3.9: Rotational grid for the case 0.5 $M_\odot$ obtained using the set of input parameters in Table 3.3. (1) The distribution of the total torque applied onto the stars as a function of age. The color bar represents the number of models per bin. The median of the models is represented as the black line. The grey zone contains 90% of the models. (2) Distribution of magnetic stellar field strengths versus age. The color bar illustrates the median value per bin. (3) Distribution of branching ratio versus age. Similarly to (2), the color bar represents the median values per bin.

3.3.5 Observations and models comparison

With the aim of conducting careful comparisons between observations and models, we implement Bayesian techniques. We use our sample of CTTS (§3.2.1), together with the models described in §3.3.2, to explore the interplay between stellar magnetic field strength and the branching ratio χ in young accreting systems during the first Myr of their stellar evolution. To perform the comparison, we use the observed rotation rates compiled in Table 3.1 and the rotation rates provided by the models, varying the parameters in the ranges shown in Table 3.3. Below we describe the use of the Bayesian technique in more detail.

Stellar magnetic field and wind mass-loss rate evolution: forward modeling

We carry out a statistical study to understand the changes in the physical parameters related to the evolution of the rotation velocities of young stars. In order to perform an analysis as robust as possible, we split our sample of CTTS described in §3.2.1 into four age bins as follows: bin 1: 0-1 Myr (62 stars), bin 2: 1-2 Myr (68 stars), bin 3: 2-3 Myr (40 stars), and bin 4: 3-13 Myr (30 stars). We use the compiled $v\sin(i)$ measurements (see §3.2.2) to build the corresponding distribution of rotational velocities for each age bin. These distributions are shown in Figure 3.10.

Then, we reproduce the observed $v\sin(i)$ histograms for each age bin using the Approximate Bayesian Computation (ABC) method, a statistical approach that compares models with observed data (e.g., Manzo-Martínez et al., 2020; Marjoram et al., 2015). This is achieved by randomly selecting $v\sin(i)$ values from the grid of models generated in Sec 3.2. For each $v\sin(i)$ distribution of Figure 10, we keep and stack the values that fall within the range of the observations and discard those which fall out of this range. We continue selecting theoretical $v\sin(i)$ values randomly until we complete one realization, meaning that the observed histogram is exactly reproduced (e.g. Turner and Van Zandt, 2012). From this realization, we obtain the posterior distributions of theoretical parameters (e.g., χ, B_*) of the model. We perform 100 realizations to build a statistically robust distribution of parameters at each age bin.

In the ABC analysis, we use $M_* = 0.5 M_\odot$ since it is the median stellar mass from the sample of stars used in each bin. We decided to use a representative value of stellar mass for this analysis since the mass range of the CTTS sample is relatively narrow (e.g., an interquartile range of $\sim$0.2 $M_\odot$), and we do not have enough CTTS to additionally split them into several mass bins. We also have included the observed distribution of mass accretion

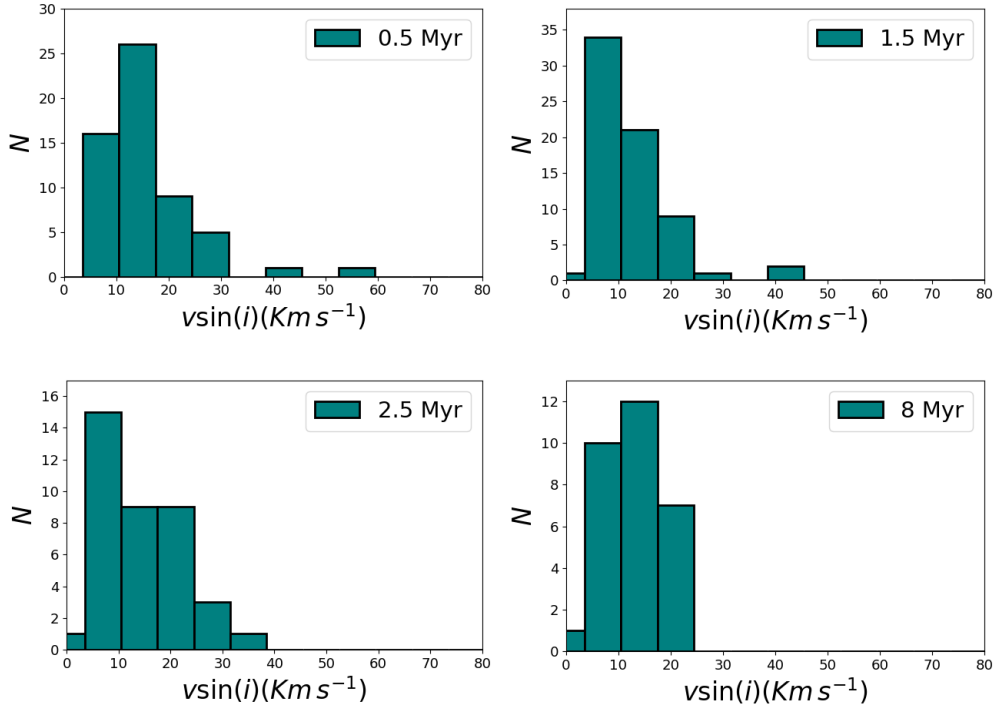

Figure 3.10: Rotational velocity distributions for the age bins described in §3.3.5.

rates discussed in §3.3.1 as a constraint. For this purpose, we separate the sample of stars with accretion measurements into the same age bins defined in this section and use the corresponding $\dot{M}_{acc}$ distribution at each age bin as a prior distribution. Figure 3.11 shows the distributions of mass accretion rates for each bin. It can be seen that, as the age increases, the distributions move towards lower values of accretion, as expected (e.g. Hartmann et al., 2016, see §3.3.1 for more discussion). The randomly selected $\dot{M}_{acc}$ values used in the ABC analysis follow the corresponding cumulative distribution of accretion rates for each age bin. Finally, we obtained the posterior distribution of χ and B_* (see Figure 3.12). Using the 100 realizations of the ABC techniques, we construct the histograms using the mean and the standard deviation for each bin of χ and B_*, respectively.

Figure 3.12 shows the resulting distribution for: (1) B_* (left column) and (2) $\log(\chi)$ (right column) obtained from our Bayesian analysis. In these plots, the age increases downwards. For the stellar magnetic field, the distribution at bin 1 shows that median value is $\sim$ 2100 G, and the median in bins 2, 3, and 4 moves toward lower values. This suggest that B_* decreases as the stars evolve during the pre-main sequence. Similarly, for the branching ratio, the distribution in bin 1 shows a median value at $\chi = 0.15$, and the median values of the 2 and 3 distributions move to lower branching ratios than the first bin. At bin 4, the peak appears slightly shifted toward larger χ values ($\chi \sim 0.04$) with respect to bin 3. These results

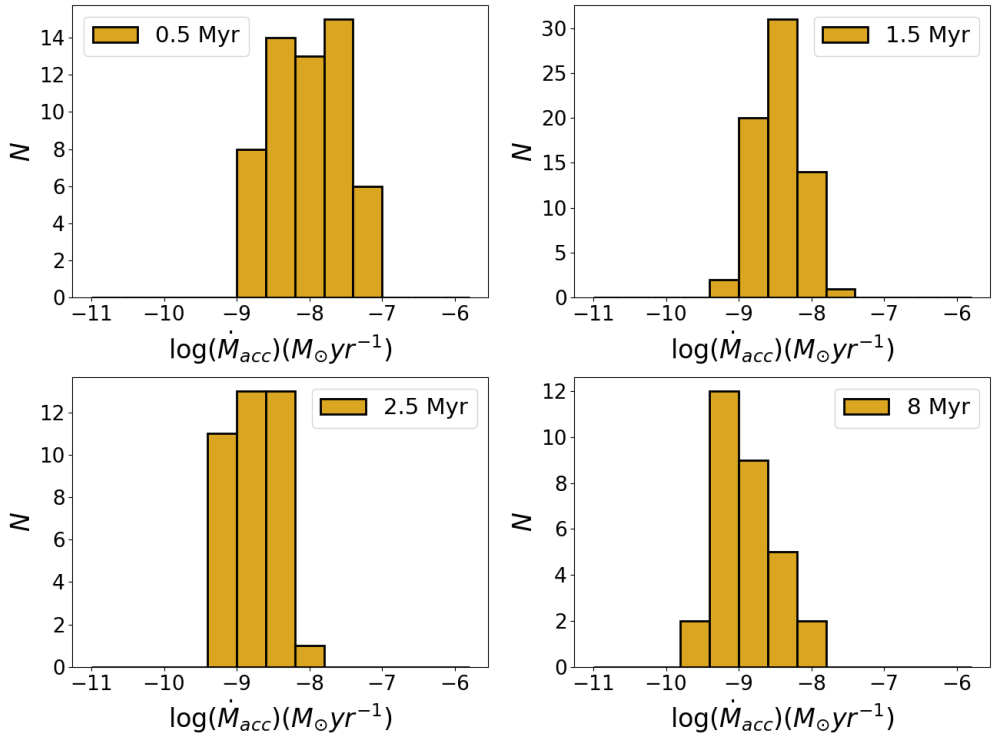

Figure 3.11: Mass accretion rate distributions for the age bins defined in the Bayesian analysis.

are shown more clearly in Figure 3.13, in which we plot the cumulative distributions of the data from Figure 3.12.

The histograms in Figure 3.12 show a gradual decrease in the branching ratio and magnetic field strength for the first three age bins. The slight increase in the branching ratio (χ) from bin 3 to bin 4 is unexpected. It must be noticed that the oldest bin has an age spread of 3-13 Myr and is the smallest sample of the different bins. If the sample in bin 4 is not a representative distribution for $v\sin(i)$ in this age interval, the results for χ from the ABC method could be biased towards values that describe this incomplete sample.

In order to test the robustness of our results with the ABC technique, particularly the impact of low numbers in the sample used in bin 4, we performed an additional Bayesian test using synthetic prior distributions for $v\sin(i)$. We generated random Gaussian distributions for each age bin, using the corresponding median value and the median absolute deviation (MAD) of the observed $v\sin(i)$ histograms shown in Figure 3.10. We demonstrate in Appendix **??** that the general trends seen in Figure 3.12 hold, and they are independent of the number of stars in each bin. Further details of this test can be found in Appendix **??**. Although our results suggest that the observed increase of B_* and χ toward bin 4 (Figure 3.12)

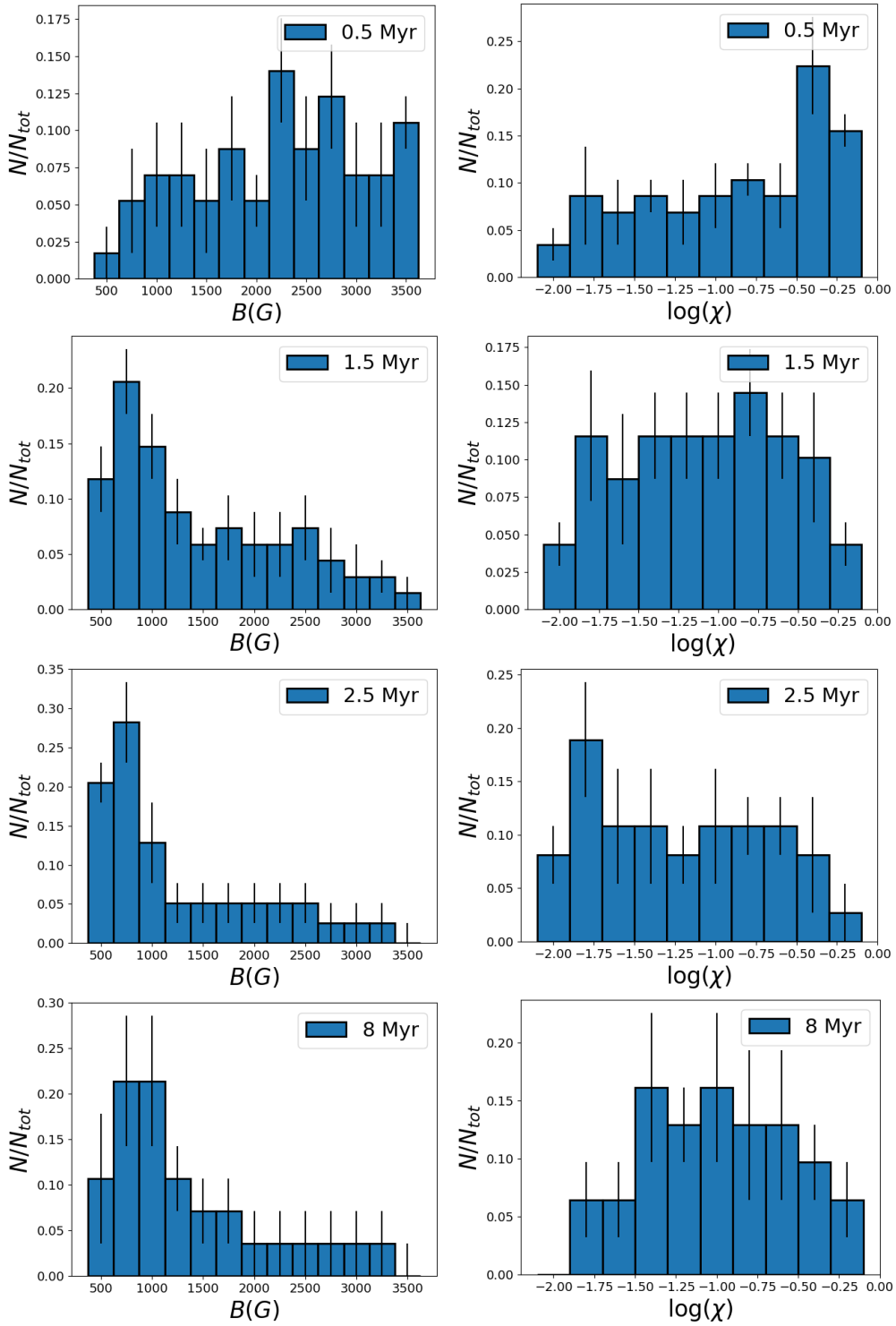

Figure 3.12: Distributions of B_* and $\log(\chi)$ in each age bin as a result of Bayesian analysis.

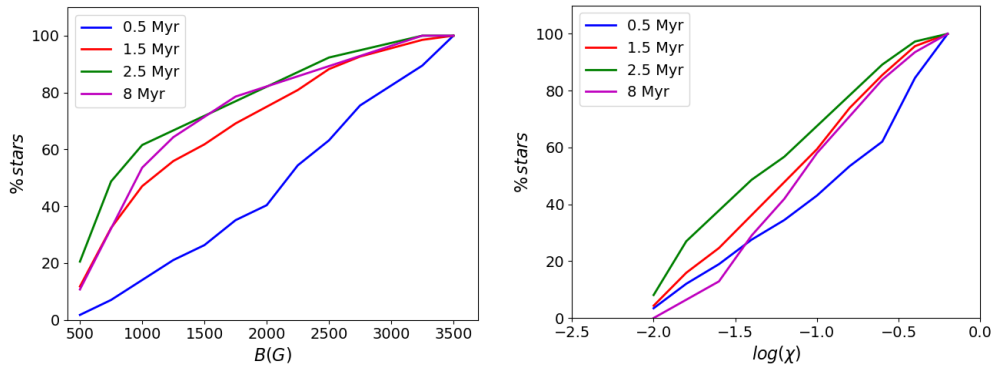

Figure 3.13: Cumulative distributions for B_* (upper panel) and $\log(\chi)$ (lower panel), for bin 1 (blue), bin 2 (red), bin 3 (green), and bin 4 (magenta).

is not a statistical fluctuation caused by low numbers, this result should be taken carefully since: (1) The sample of CTTS in the last bin could not be as representative as in the younger bins. In particular, given the variable nature of TTS, slow accretors or CTTS approaching the end of their accretion phase (Briceño et al., 2019; Thanathibodee et al., 2022) could not be included in the last bins; (2) A wide age range (3-13 Myr) is considered in the last bin, in which the stars significantly change their properties during the pre-main sequence evolution. However, torque equilibrium in the system is reached earlier than 3 Myr, and models beyond this age do not change significantly (see figure 3.8); (3) We assume that the parameters γ_c and β are constant. These parameters are related to the magnetic connection between the star and the disk, which might change, together with the complexity of the magnetic field, during the evolution of the star; (4) The models ignore the changes in the inner stellar structure, particularly, the core-envelope decoupling is not considered in the models, which might impact the angular momentum evolution at bin 4. Some of these effects are not so important for very young low-mass stars, however, solar-type stars are expected to develop a radiative core at the end of the Hayashi track (Iben, 1965). Exploring these effects' impact is out of this paper's scope.

We applied a Kolmogorov-Smirnov (K-S) test, which is used to determine if two samples are drawn from the same distribution, to the B_* and $\log(\chi)$ posterior distributions obtained from the ABC analysis. The p values are shown in Table 3.4. For bins 1 and 2, we find the low p values of 0.05% and 5%, for B_* and $\log(\chi)$, respectively, suggest a clear evolution of both parameters, as discussed above. In contrast, for B_*, the high p value between bin 3 and bin 4 shows that there is barely an evolution, which suggests that most of the stars have reached a state in which the strength of their magnetic field has decreased to lower values. For $\log(\chi)$, the difference between bins 3 and 4 seems more clear; the possible explanations for these differences are also discussed above.

Table 3.4: K-S test and p values .

Bin pairs	parameter	K-S	p-value
1-2	B_*	0.35	0.0005
	$\log(\chi)$	0.23	0.05
2-3	B_*	0.16	0.45
	$\log(\chi)$	0.13	0.73
3-4	B_*	0.16	0.68
	$\log(\chi)$	0.24	0.20

As the main result of this subsection, we found the median of B_* and $\log(\chi)$ decreases as the age of the bins increases, which suggests that for the sample of CTTS studied in this work, both parameters are evolving during the first Myr. It must be noticed that additional measurements of the more evolved CTTS are needed to confirm the trend behavior toward bin 4.

3.4 Discussion

3.4.1 Binarity

We make a quality astrometric selection of the CTTS using the Re-normalized unit weighted error (RUWE) reported by *Gaia* DR3. For the selection, we use RUWE values less than 1.4, suggested by Lindegren et al. (2020b). However, Stassun and Torres (2021) and Kounkel et al. (2021) confirmed that RUWE values from 1.0 to 1.4 may contain unresolved binary systems.

One of the main consequences of having binary stars in our sample will be the inconsistency of the physical parameters (e.g., Rotation rates, masses, ages, etc.). In that sense, we have cleared our sample of possible close companions systems using the spectroscopic binaries reported by (Kounkel et al., 2019) and visual binaries reported by Tokovinin et al. (2020). Also, we did not find discrepancies in rotation rates for CTTS groups by mass and age that could indicate the presence of binaries. As a double-check test, we inspected each LC available in TESS (§3.3.1), and as a result, we did not detect signatures of eclipsing binaries in the sample.

The RUWE and the LCs inspection can not reject all multiple systems in our sample, particularly unresolved systems. However, we expect that binary systems do not dominate our sample and, thus, do not affect our results.

3.4.2 Clues about the branching ratio

Several studies have explored the branching ratio parameter from a numerical perspective to explain the slow rotations in CTTS. At the same time, only some efforts have focused on the observational viewpoint. For example, Hartmann and Stauffer (1989); Matt and Pudritz (2005); Matt et al. (2012) have suggested that if there is a stellar wind with a sustained mass-loss rate of about 0.1 of the accretion rate, the wind can carry away enough angular momentum to achieve a stellar-spin equilibrium. Matt and Pudritz (2008a) suggested a hard upper limit of $\chi \leq 0.6$. Cranmer (2008), by his part, predicts a maximum of 0.014. Gallet et al. (2019) studied two cases where they argued that a branching ratio $\chi = 0.01$ would favor the stellar wind theory. However, simulations would require stronger dipolar magnetic fields to reproduce the rotation rates, while $\chi = 0.1$ requires weaker dipolar fields that are commonly observed. Ireland et al. (2020) suggest that $\chi > 0.3$ is required to achieve spin-equilibrium in their simulated cases. Particularly, for the BP Tau star, they predict a $\chi \approx 0.25$ to achieve an equilibrium between the wind and accretion torques. Pantolmos et al. (2020) predict that winds should eject more than 0.1 of the mass-accretion rate to counteract the stellar spin-up due to accretion. Gehrig et al. (2022) reproduce the observed rotational period of most young stars with values less than 0.05. Independently of their numerical approaches and strategies to describe the star-disk interactions and winds, nowadays, no consensus has been reached. Observational analyses of Hartigan et al. (1995) have found that χ can reach up to 0.2, but most values are below 0.02 in all ages between 1 and 10 Myr. Measurements provided by this work could help to contribute to a general perspective of the expected χ in CTTS.

We have 37 stars with available χ measurements that simultaneously hold an estimation of age (Table 3.1). These stars were utilized in Figure 3.14 to investigate the relationship between χ and age (left panel). As seen in the histogram (right panel), branching ratio values tend to be below 0.1, and the most likely values are around $0.04 - 0.05$. Even though few data are displayed in Figure 3.14, within the uncertainties, our data suggest that strong stellar wind with a mass loss rate greater than 0.1 of the accretion rate is possible at earlier ages (< 3 Myr).

The ABC analysis in §3.3.5 plus measurements reported here could suggest a possible trend for the branching ratio with age. In the future, supplementary surveys of accretion and mass-loss rates in CTTS (e.g., Kounkel et al., 2023) will improve the sampling and allow us

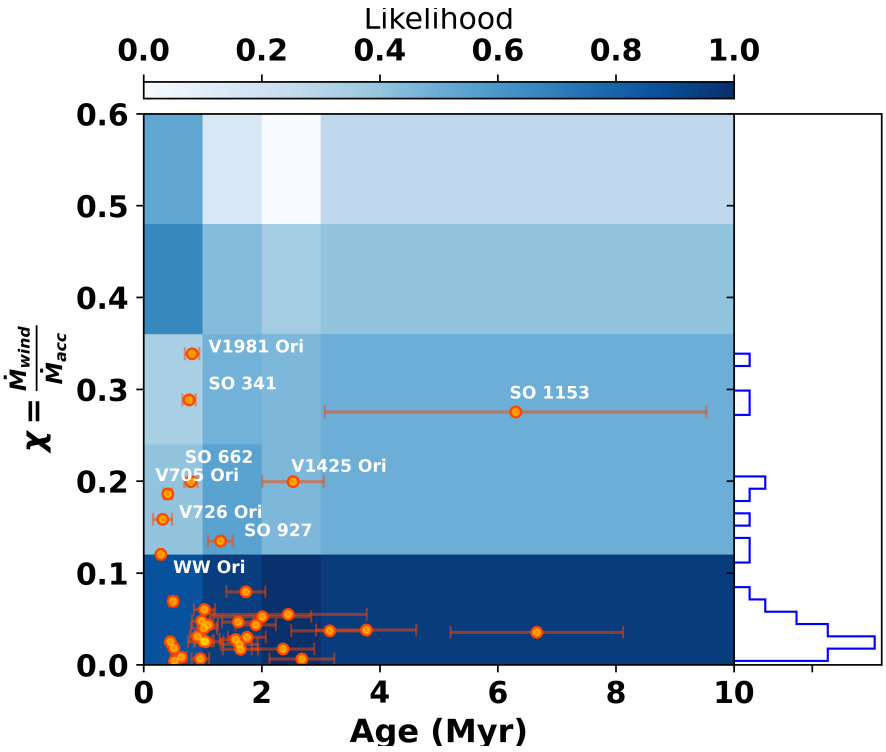

Figure 3.14: Branching ratio for measured Classical T Tauri stars versus age (left panel). The background map illustrates the density of the posterior distribution of χ given by the ABC analysis. We display their name for those stars with $\chi > 0.1$. The distribution of the branching ratio represented with the histogram on the right side exhibits a pronounced peak at $\chi = 0.04$ as expected from data in Figure 3.6.

to understand better the nature and strength of the APSW mechanism at the early stages of the stars.

3.5 Summary and Conclusions

In this work, we developed one-dimensional numerical models of the spin evolution of CTTS, which allowed us to build a comprehensive grid of specific cases for CTTS. We build approximately two million simulations, varying physical parameters such as magnetic field, wind, accretion, initial rotation periods, and mass.
Our models allow for the first time to study how the magnetic field strength (B_*) and branching ratio (χ) change in relation to rotation rates and ages. The results are broadly consistent with the APSW picture and predict a steady evolution of B_* and χ during the CTTS phase. Below we list the results of this work:

- Ninety percent of our model's grid is compliant with $v \sin(i)$ rotation rates below $50\,\mathrm{km}\,s^{-1}$.
- Using the observed rotation and accretion rates as prior distributions, we did a Bayesian analysis that suggests a decreasing trend of χ and B_* intensities with age.
- The models indicate that strong dipolar magnetic field components and higher branching ratios would achieve an effective equilibrium state of torque at the first stages of the evolution in CTTS (< 1.5 Myr). However, at least for the branching ratio, measurements and posterior distributions of ABC analysis prove that $\chi > 0.1$ values, although they are possible, $\chi < 0.1$ are more likely.
- Models predict a branching ratio decreasing with age, in particular, during the first 2 Myr when a pronounced peak for χ=0.04 is observed. This result is in agreement with our measurements using a diverse sample of CTTS (Figure 3.6) suggesting that small χ values up to 10% of the APSW upper limit are capable of extracting enough angular momentum from the CTTS system.

4 TESSExtractor: A Web Application for Quick Visualization and Period Estimation of TESS Light Curves from Full-frame Images.

The content presented in this section is part of the manuscript in preparation. This manuscript will present the web application TESSExtractor, which is already available online.

Abstract: We present a user-friendly web application that allows users to extract, visualize, and interact with the TESS light curves from Full-frame images (FFIs). The service works for any star identifier cataloged in the SIMBAD database or using the stellar coordinates. TESSExtractor is optimized for searching rotation periods and performs photometry using a circular aperture centered on the object of interest, with a sky annulus for background subtraction. The application also utilizes cotrending basis vectors (CBVs) provided by TESS to correct photometry for possible systematic effects. The TESSExtractor's website provides an intuitive interface that is easy to use for scientific and educational purposes and is publicly available at https://www.tessextractor.app. This tool simplifies the analysis of TESS light curves and provides valuable insight for researchers seeking to extract and analyze TESS data for various applications, including stellar rotation and transit detection studies. This work is evidence that TESS is revolutionizing our understanding of time-domain astrophysics by enabling new detections in a wide range of phenomena to the scope of any person in an easy-to-use web application.

4.1 Extracting the light curves

4.1.1 TESS Cutouts

TESS obtains images, known as full-frame Images (FFIs), of each sector at a 30-minutes cadence for the first two years of TESS operation. Nowadays, TESS counts with a better cadence of 10 and 3.33 minutes for the second extended mission. Approximately one million stars per FFI are brighter than $T_{mag} < 16$ mag. Being a challenge to extract the photometry for the complete catalog of stars at once. `TESScut` service (Brasseur et al., 2019) is a powerful tool that allows us to make small cuts of the FFI, also called cutouts, around a target of interest, reducing the time consumption of processing big sequences of images as the FFIs.

We download the TESS cutouts for the target of interest using the *TESScut* service via `astropy` (Astropy Collaboration et al., 2013a, 2018, 2022). Using by default, an image of 10×10 pixel is extracted from the FFI, where the object is centered.

To support the visual inspection of the target in the TESS cutout image and verify if neighboring sources contaminate the science source, we simultaneously download a Digital Sky Survey (DSS2 IR) image with the same field of view as the TESS cutout[1], see Figure 4.1. The DSS2 IR filter band is ideal for making a comparison with the TESS cutout because it is relatively similar to the TESS filter band, covering the wavelength range $(6950 - 9000\mathring{A})$

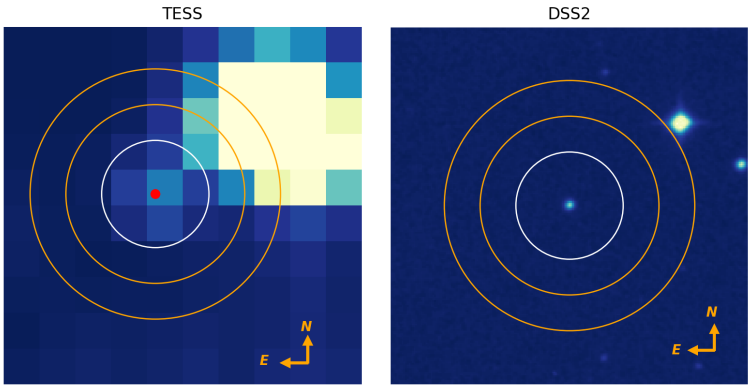

Figure 4.1: TESS and DSS2 IR cutout for the target TIC 72921546. Both plots with the same Field of view (210 x 210 sq arcsec) correspond to a TESS image of 10x10 pixels. The white circle shows the photometric aperture, and the orange circle shows the sky annulus.

4.1.2 Crowding ratio (CR)

Given the relatively large TESS pixel size of 21 arcsecs, the TESS data is highly susceptible to crowding, blending, and source confusion. Some light curves may be contaminated by

[1]The DSS2 area is (210 arcsec)^2 or (10$\times$ 10 pixels) TESS cutout

point sources inside the selected photometric aperture. To estimate the impact of this effect, we computed the ratio as follows:

$$CR = \frac{f_{in}}{f_*} \times 100 \ [\%] \tag{4.1}$$

where f_{in} is the flux of the target and f_* is the total flux of Gaia sources that fall within the aperture radius, excluding the target. The fluxes are based on the G filter of Gaia-DR3 (Gaia Collaboration et al., 2018). We suggest that those targets with CR> 25% be taken with caution. Probably, the LCs in these cases are contaminated by nearby sources, lowering the reliability of data.

4.1.3 Aperture selection and photometry

After downloading the TESS cutout, our pipeline utilizes the `Photutils` package in Python (Bradley et al., 2019) to perform simple aperture photometry (SAP). The aperture for the target is determined based on its TESS magnitude (T_{mag}) as cataloged in Stassun (2019, TIC v8.0). Table 4.1 lists the aperture and annulus radii options.

Table 4.1: Aperture and annulus radius used in `photutils`.

T_{mag}	Aperture (px)	Annulus (px)
≤ 9	3.0	4.0-5.0
$> 9, \leq 11$	2.5	3.5-4.5
$> 11, \leq 13$	2.0	3.0-4.0
> 13	1.5	2.5-3.5

The user also has the option to adjust the aperture size from 1.0 to 2.5 pixels and the sky annulus from 2.5 to 10 pixels in the left panel called photometry settings.

The background subtraction of the photometry is made using the mode value of the sky annulus.

To avoid anomalies in the photometry (e.g., Cosmic rays, Popcorn noise, and Fireworks)[2], we remove from the raw all data points with bad TESS quality flags. Also, to prefilter the contamination from scattering light patterns on the TESS detector, we reject all data points with a strong variability above the percentile 95% of the sky annulus flux.

The transformation of RAW flux to magnitude for the LCs is computed as follows:

$$m = -2.5 \log F_* + ZP \tag{4.2}$$

[2]TESS Data release notes: https://archive.stsci.edu/tess/tess_drn.html

where F_* is the flux after subtracting the background. ZP is the zero point of the TESS filter band.

Despite the FFIs cadence changes from the prime missions to the extended missions of TESS. On average, we assume a ZP value of 20.4402281476 (REF).

Following the error propagation theory, the uncertainty of m is computed as:

$$\delta m = 1.09 \frac{\delta F}{F_*} \tag{4.3}$$

Where δF is the uncertainty in the counts, this data set is obtained from the TESS cutout.

In most cases, the median magnitude of the star is not similar to the T_{mag} reported for the star in Stassun (2019, TIC v8.0). Then, we make an aperture correction of the LC magnitude using the m time series, its median value ($\overline{m}$), and T_{mag}. Following the next two-part function, we calibrate the LC magnitude to the TESS magnitude of the point source.

$$m = \begin{cases} m - |T_{mag} - \overline{m}|, & \overline{m} > T_{mag}, \\ m + |T_{mag} - \overline{m}|, & \overline{m} < T_{mag} \end{cases}$$

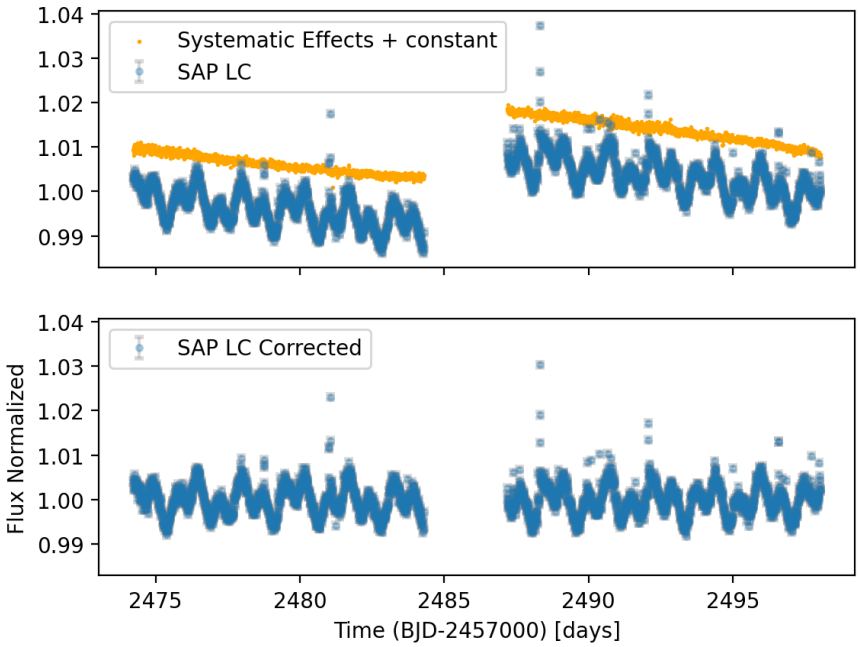

Figure 4.2: Systematic correction for the TESS LC TIC 60874953. In the top panel, we plot the best fit of the first four CBVs to the normalized LC. In the below panel, we plot the normalized LC after the systematic trend correction.

4.1.4 Systematic Effects Correction

For the correction of the LCs, first, we normalize the LC in flux and then use the co-trending basis vectors (CBVs), a set of orthonormal vectors that describe the dominant sources of variability shared among multiple stars in the TESS cameras, extrinsic of the stellar variability, the typical effects go from CCD's issues to the scattering in cameras due to the earth brightness or moonlight. There are 16 CBVs from 1 to 16, decreasing in importance. We use the first four CBVs to minimize the possibility of intrinsic astrophysical variability results removed from LC by the correction.

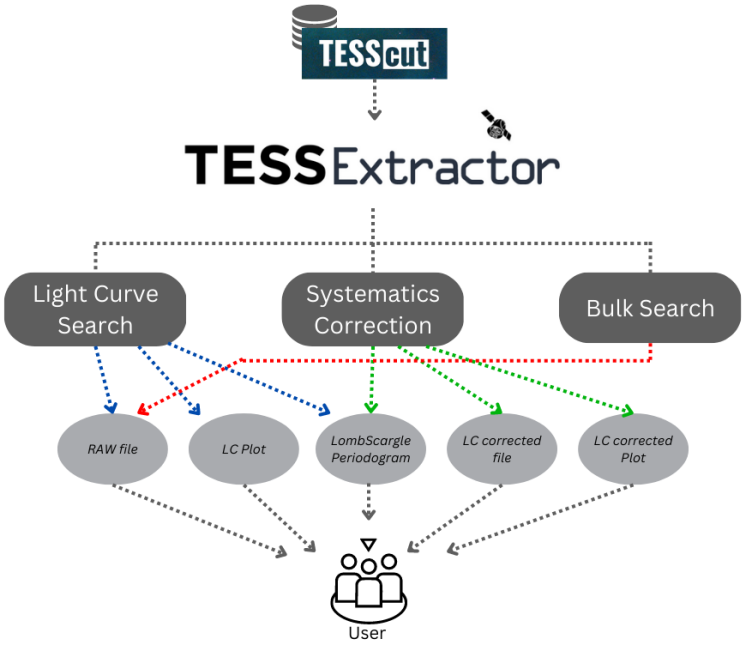

Figure 4.3: Flowchart diagram of the TESSExtractor web application, showing modules as rectangular boxes and ellipses as data products. The dashed lines between the diagram's parts symbolize the steps in the application.

To correct the normalized LC of systematics effects, we built the representative systematics vector as the linear combination of the CBVs, and then we get the flux corrected by systematics represented as:

$$F_{corr} = F_* - F_{sys} \equiv F_* - \sum_{i=1}^{N} a_i \times CBV_i \tag{4.4}$$

Where F_* is the normalized flux. The index (i) goes from 1 to 4, and a_i is the scaling coefficient, given by the least-squares solution as $a_i = (A^T A)^{-1} A^T F_*$, where A is the normal matrix with CBVs components as columns. The correction is made until χ^2 is minimized or the process reaches 100 tests. See Figure 4.2. The chi squared is obtained as $\chi^2 =$

$\sum_j (F_{*,j} - F_{sys,j})^2/(F_{*,j})$, where j index run over the data points of the LC.

4.1.5 Deployment, Accessibility, and User Modes

TESSExtractor was developed in Python and designed in the streamlit framework, an open-source library to build a web application[3]. The application is deployed in the Salesforce cloud service, using a 24/7 dedicated Linux machine with a network bandwidth of 2TB per month. This is available at `https://www.tessextractor.app` and allows users to search from single targets to a small list of stars in the experimental bulk search mode.

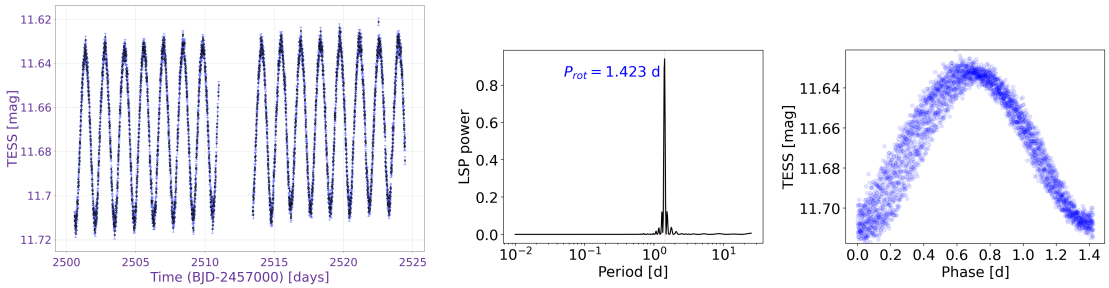

Figure 4.4: Primarily data product of TESSExtractor for TIC 58229237, LC, periodogram, and phase-folded LC.

The app has three user modes, each one with a specific task. The first is the *Light Curve Search*, a lightweight service for processing SAP of the FFIs of individual targets. It counts with a search bar where the user inputs the name or coordinates of the target, clicks on the search button, and the app begins to download FFIs cutouts, process the LCs, and display the data products (LC, periodogram, phase folded LC, and CSV datafile). The second mode, called *Systematics Correction*, does the same steps as the first mode. It corrects the SAP LCs by systematic trends. The data products are similar to the first mode. The third service, the *Bulk Search*, is released in an experimental mode. Currently, it allows users to upload a small list of targets and, in the end, provide the CSV files for all the targets per TESS sector. For more details about the operability, user modes, and data products, see Figure 4.3.

4.1.6 Data products

LC, Periodogram, and Phase LC plots

The main product of our application is the LC, obtained following the procedure of section §4.1.3. To enable users to explore and analyze this data more deeply, we use Plotly

[3] https://streamlit.io/

(Plotly Technologies Inc., 2015) to display an interactive scatter plot of the TESS magnitude (equation 4.2) as a function of the time. We also incorporate error bars estimated with the equation 4.3. Our interactive visualization offers advanced features such as zooming, panning, and hover-over tool, which can help users to handle data easily. Also, the plot can be downloaded in png format to share with others.

Once LC is processed, a Lomb-Scargle periodogram (Lomb, 1976; Scargle, 1982) is processed to estimate the rotational period. We use a resolution of 500 steps in logarithmic scale within the interval $0.01 < P_{rot} < 25$ days. The best period is selected based on the highest peak of the periodogram. Simultaneously, a phase-folded LC is processed. Using the task `FoldAt` of PyAstronomy (Czesla et al., 2019a), the LC is folded to the found period in the periodogram. An example of each data product can be seen in Figure 4.4.

File Format

In addition to the visual and interactive products, we have the data files containing the info to generate plots. In the modes *Light Curve Search* and *Systematics Correction*, the final data product can be accessed in the format of a CSV file at the TESSExtractor portal. The user can download this file using the bottom "Download data". Each file has three columns called "Time [BJD], T_{mag}, $T_{mag}err$" in the first mode and "Time [BJD], FLUX_CORRECTED, FLUX_ERR" in the second mode, respectively. The LC filename follows the structure:

{target name}_s_{sector}.csv

{target name}_s_{sector}_corr.csv

To optimize the cloud resources, the cache is refreshed every 3 minutes, and the final data product is kept on the website for this time or until the user does another search.

4.2 Periods Comparison

Kounkel and Covey (2019) performed a homogeneous search of young stars in the galactic disk, identifying thousands of clusters within 1 kpc, estimating the ages of the individual groups, and providing a comprehensive catalog of clusters and their potential members.

Using TESSExtractor for the catalog reported by Kounkel and Covey (2019), we built an extensive library of young stars with rotation periods, collecting LCs and periods for 127,023 sources. This sample includes stars with ages ranging from 1 to 100 Myr.

(Kounkel et al., 2022) processed LCs for our study sample, using the `eleanor` pipeline, also they estimated Lomb-Scargle periods. To compare the periods found in this work, we cross-matched both catalogs. In total, we have 43,273 sources in common. See panel A's period comparison in Figure 4.6.

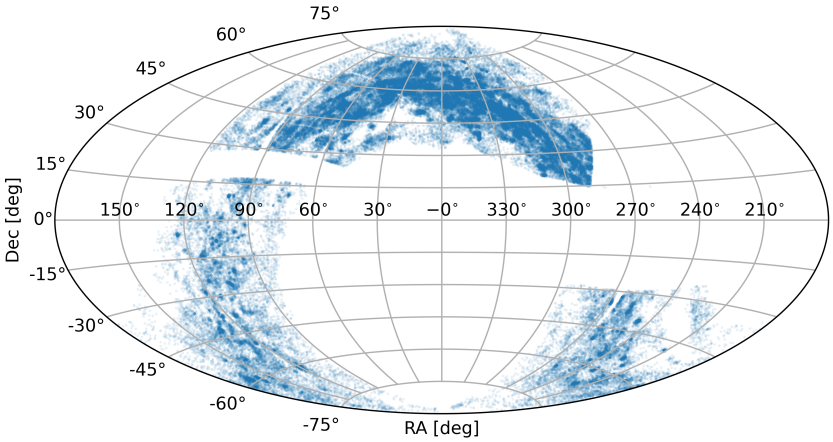

Figure 4.5: TESSExtractor sources.

4.3 Applicability: Selected projects

Here, we present some selected projects that use TESSextractor as one of the main tools for obtaining their results:

Machine learning morphological classification of TESS light curves of T Tauri stars (Rodríguez-Feliciano et al., 2023). We present a variability and morphological classification study of TESS light curves for T Tauri star candidates in the Orion, IC 348, γ Velorum, Upper Scorpius, Corona Australis, and Perseus OB2 regions. We use features that depend on time, periodicity, and magnitude distribution. A catalog of 3672 T Tauri star candidates and their possible period estimations, predicted morphological classes and visually revised ones are presented. The 11 morphological classes generally relate to physical properties such as stellar rotation, multiplicity, variable extinction from protoplanetary disks, and accretion.

A TESS survey of flare activity and stellar rotation of Young Stellar Objects in the Taurus Region (Batista et al. in preparation). As part of a Ph.D. project, we perform a flare census in a sample of previously confirmed T Tauri stars located in the Taurus Star-Forming Region. We used TESS observation with a cadence of 2 minutes and developed the FLare ANalizer tool (FLAN) to detect and characterize the Flares with a duration larger than 10 minutes (5 points in the light curve). We obtained several trends of the total energy of the flare and stellar properties, such as effective temperature, age, and FUV emission.

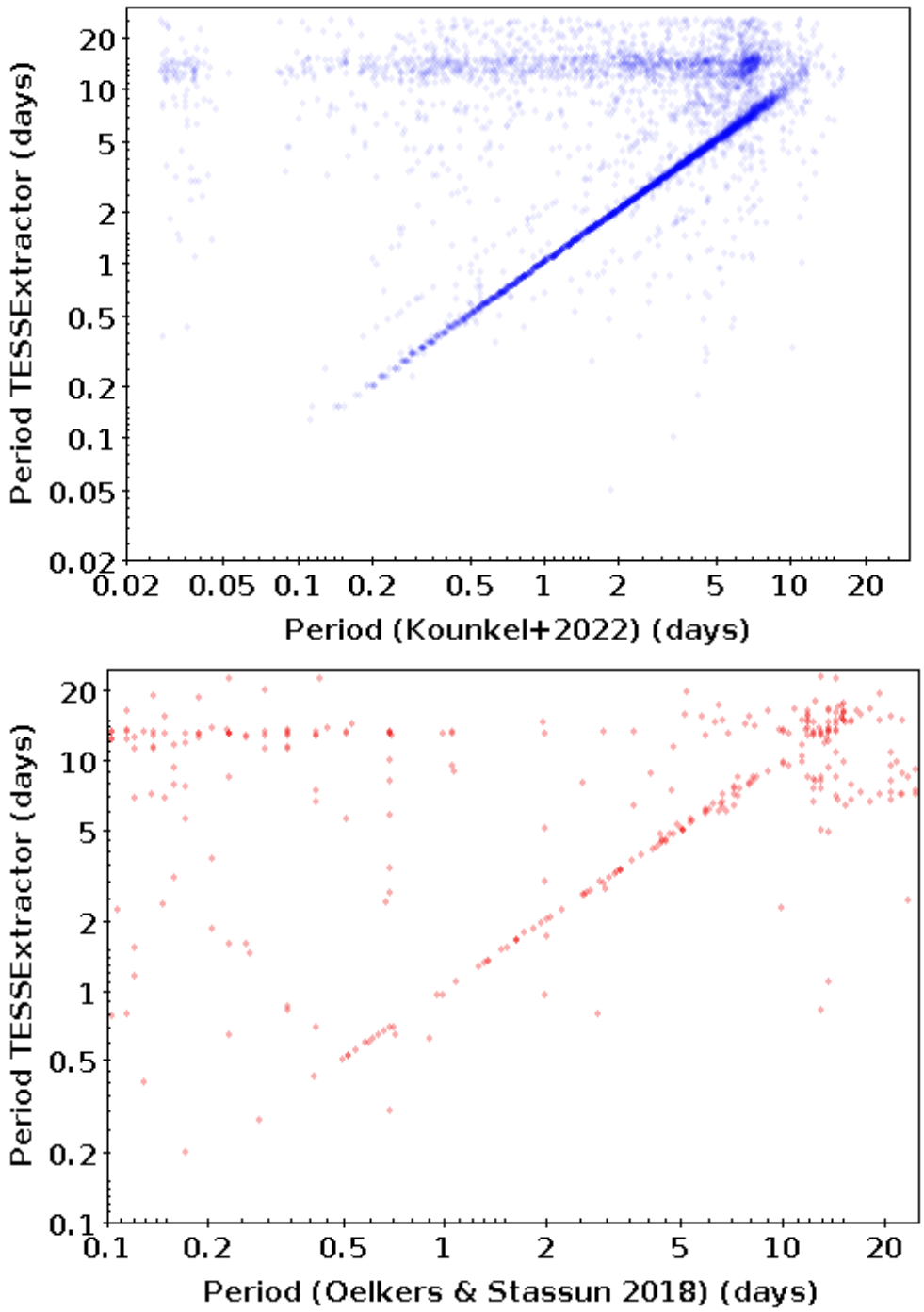

Figure 4.6: Periods comparison between TESSExtractor and other pipelines.

Close eclipsing binaries in the Orion Star Forming Complex (Hernandez et al in preparation). Based on the analysis of TESS light curves, we have detected and characterized seven Young Close Eclipsing Binaries (YCEB) in the Orion Star Forming Complex. These systems have separations smaller than 0.1 AU and orbital periods close to or equal to the rotational period of the primary. The binary models were computed independently

using the tools STARRY and PHysics Of Eclipsing BinariEs (PHOEBE). We find that these systems have eccentricities close to zero, suggesting that tidal effects have circularized their orbits. The binary Brun 691 is particularly interesting among the analyzed systems because it exhibits a detectable decrease in the transit depth in a very short time ($\sim$2 years). Our orbital models indicate that a radius reduction of the companion can cause this decrease. The orbital parameters obtained for our whole YCEB sample support the scenario in which tidal interaction in a few Myrs circularized the orbits and synchronized the rotational and orbital periods of the systems.

5 Conclusions and Future Work

5.1 Conclusions

In this work, we study evolutionary trends in the rotation of T Tauri stars in the Orion Star-Forming Complex to predict evolution scenarios of angular momentum and develop models to infer the physical parameters of Classical T Tauri stars. Here, we list the main results obtained from this analysis:

- $v \sin(i)$ and Age Relationship: We found an empirical trend in stellar rotation ($v \sin(i)$) with age, revealing a transitional phase at 5-6 million years (Myr). This observation aligns with the disk lifetime utilized in angular momentum evolutionary models and the timescale for disk dissipation, underscoring the pivotal role of disks in the evolution of angular momentum.

- The analysis of $v \sin(i)$ distributions emphasizes that Classical T Tauri Stars (CTTS) exhibit slow rotation, indicative of the disk-braking effect's role in regulating angular momentum. CTTS with $v \sin(i)$ exceeding 28 km s^{-1} were inferred to be likely binary systems.

- Transition from CTTS to WTTS (Intermediate Phase): Stars approaching the end of their accretion phase (CWTTS) show statistical properties similar to Weak-Lined T Tauri Stars (WTTS), indicating that the disk-braking effect might less influence this subset.

- Slow Rotators Domain: The stellar rotation simulations of stars bearing accreting disk corroborated observational evidence, with the majority of the model grid producing slow rotation rates ($v \sin(i) < 50$ km s^{-1}), consistent with the majority of slow rotators among CTTS populations.

- Magnetic field and branching ratio prediction for the observed distributions of CTTS trends: The Bayesian analysis for the grid of models, incorporating observed rotation and accretion rates in the study, indicates a systematic decrease in magnetic field

strength (B_*) and branching ratio (χ) as long CTTS evolve. This suggests that slow rotators result from higher values of these parameters at the early stages of evolution until the disk is dissipated.

- Early Equilibrium State: The models suggest that strong dipolar magnetic field components and higher branching ratios could establish an effective equilibrium torque early in CTTS evolution ($\sim$1.5 Myrs). However, our measurements reveal that χ values below 0.1 were more probable, emphasizing the influence of lower χ values.

- Evidence of the Branching ratio temporal evolution via measurements: The measurements unveiled an age-dependent behavior of the branching ratio, particularly during the first 2 million years of CTTS evolution, with a prominent peak around $\chi = 0.04$, and it plays a crucial role in angular momentum extraction from CTTS systems.

- We developed a set of tools available to the community: One is designed to estimate the projected rotational velocity using high-resolution spectral lines, called vsini by the Fourier method. Another tool is the web application called TESSExtractor, which downloads, extracts, and processes the photometry from the RAW data provided by the TESS space telescope. This application is ideal for analyzing the stellar variability of the objects in optical-near infrared wavelength and estimating the rotational period (https://github.com/javiserna).

5.2 Significant Contributions

A significant portion of my dedicated efforts during the pursuit of my doctoral project was directed toward active participation in collaborative groups, including ARYSO, YSOs of SDSS-IV, and ULLYSES. These collaborations afforded me the valuable opportunity to acquire hands-on experience in the analysis of photometric and spectroscopic data, as well as to promote my programming skills to an advanced level. In the following sections, my contribution to each of these initiatives will be discussed, and their connection to the overarching goals of my thesis project will be discussed:

Rodriguez-Feliciano et al. 2023 (Second author)

In collaboration with Dr. Jesús Hernández from UNAM and MSc. Bayron Rodriguez and Dr. Alejandro Garcia Varela from Universidad de los Andes, Bogota, Colombia, I processed a set of $\sim$3000 TESS light curves from star-forming regions such as Orion, Taurus, Upper Scorpius, Perseus OB2, Corona Australis, IC 348, and Gamma Velorum. These light curves were visually classified into several morphological classes. This sample was utilized as a

training sample to develop Machine-learning models and classify new TESS light curves of young stars. This work was published in the paper Rodríguez-Feliciano et al. (2023).

Pinzón et al. 2021 (Third author)

I measured the rotational velocity ($v \sin(i)$) for 72 T Tauri stars and 5 Herbig Ae/Be stars using the spectra of FIES, an instrument of the Nordic Optical Telescope, and HECTOCHELLE, an instrument associated with the MMT observatory. These measurements are in agreement with the spin models of Herbig Ae/Be. This work was published in the paper Pinzón et al. (2021).

Thanathibodee et al. 2023 (Third author)

In collaboration with Dr. Thanawuth Thanathibodee, currently a postdoc at Boston University, I used my tool that uses the Fourier method to measure the rotational velocity ($v \sin(i)$) for 18 T Tauri stars using the MIKE spectra observed in the Magellan Clay telescope at the Las Campanas Observatory. These measurements were used to estimate the corotation radius of disk stars. This research suggests that most of the low-accretors are in a stable regime of mass accretion (Thanathibodee et al., 2023).

Thanathibodee et al. 2020 (Fourth author)

In collaboration with Thanawuth Thanathibodee of the University of Michigan, I measured the rotational velocity ($v \sin(i)$) for the protoplanet host star PDS70 using a set of HARPS spectra compiled by the project of low accretors (PI: T. Thanathibodee). In addition to the TESS period and the host-star radius, we estimated the inclination of the protoplanetary disk (Thanathibodee et al., 2020).

Hinton et al. 2022 (Fourth author)

In collaboration with Dr. Parker Hinton and Dr. Kevin France from the University of Colorado, Boulder, USA, in the project Far-ultraviolet Flares on Accreting Protostars: Weak and Classical T Tauri Stellar Pair Analysis, I performed the TESS light curves for 6 T Tauri stars and found various optical flares, which were analyzed to explore the flare statistics (i.e., frequency, the energy released, the time elapsed), and we explored for a correlation with Far-ultraviolet flares using data from Hubble space telescope. This work resulted in one publication (Hinton et al., 2022).

Espalliat et al. 2022 (Seventh author)

In the ODYSSEUS collaboration (Outflows and Disks around Young Stars: Synergies for the Exploration of ULLYSES Spectra)), I use multiple sectors of TESS for the star CVSO 109 to get a robust estimation of the rotational period. I use two methods: the Lomb-Scargle periodogram and the Autocorrelation function. My contribution was useful in estimating the inclination angle of the protoplanetary disks using the vsini, period, and radius relations. This work was published in the paper (Espaillat et al., 2022).

5.2.1 Additional Contributions

Thanks to my active involvement in working groups within SDSS-IV and my participation in discussions within the APOGEE-2 Young Star Objects working group. I have had the privilege of co-authoring the following collaborative papers: I) Hsu et al. 2023, submitted in ApJ, II) Cañas et al. (2023), III) Kounkel et al. (2023), IV) Daher et al. (2022), V) Herczeg et al. (2023), VI) 18th Data Release of SDSS (Almeida et al., 2023), VII) 17th Data Release of SDSS (Abdurro'uf et al., 2022), VIII) Wanderley et al. (2023), IX) Román-Zúñiga et al. (2023), X) Campbell et al. (2022), XI) Pittman et al. (2022), XII) Hernández et al. (2023), and XIII) Kounkel et al. (2021).

5.3 Proceedings

5.3.1 Cool Stars 22

During the Cool Star 22 conference placed in Toulouse, France, I presented a scientific poster with the results of Serna et al. (2021) and shared the first version of the tessextractor with the public.

References

Abdurro'uf, Katherine Accetta, Conny Aerts, Víctor Silva Aguirre, Romina Ahumada, Nikhil Ajgaonkar, N. Filiz Ak, Shadab Alam, Carlos Allende Prieto, Andrés Almeida, Friedrich Anders, Scott F. Anderson, Brett H. Andrews, Borja Anguiano, Erik Aquino-Ortíz, Alfonso Aragón-Salamanca, Maria Argudo-Fernández, Metin Ata, Marie Aubert, Vladimir Avila-Reese, Carles Badenes, Rodolfo H. Barbá, Kat Barger, Jorge K. Barrera-Ballesteros, Rachael L. Beaton, Timothy C. Beers, Francesco Belfiore, Chad F. Bender, Mariangela Bernardi, Matthew A. Bershady, Florian Beutler, Christian Moni Bidin, Jonathan C. Bird, Dmitry Bizyaev, Guillermo A. Blanc, Michael R. Blanton, Nicholas Fraser Boardman, Adam S. Bolton, Médéric Boquien, Jura Borissova, Jo Bovy, W. N. Brandt, Jordan Brown, Joel R. Brownstein, Marcella Brusa, Johannes Buchner, Kevin Bundy, Joseph N. Burchett, Martin Bureau, Adam Burgasser, Tuesday K. Cabang, Stephanie Campbell, Michele Cappellari, Joleen K. Carlberg, Fábio Carneiro Wanderley, Ricardo Carrera, Jennifer Cash, Yan-Ping Chen, Wei-Huai Chen, Brian Cherinka, Cristina Chiappini, Peter Doohyun Choi, S. Drew Chojnowski, Haeun Chung, Nicolas Clerc, Roger E. Cohen, Julia M. Comerford, Johan Comparat, Luiz da Costa, Kevin Covey, Jeffrey D. Crane, Irene Cruz-Gonzalez, Connor Culhane, Katia Cunha, Y. Sophia Dai, Guillermo Damke, Jeremy Darling, James W. Davidson Jr., Roger Davies, Kyle Dawson, Nathan De Lee, Aleksandar M. Diamond-Stanic, Mariana Cano-Díaz, Helena Domínguez Sánchez, John Donor, Chris Duckworth, Tom Dwelly, Daniel J. Eisenstein, Yvonne P. Elsworth, Eric Emsellem, Mike Eracleous, Stephanie Escoffier, Xiaohui Fan, Emily Farr, Shuai Feng, José G. Fernández-Trincado, Diane Feuillet, Andreas Filipp, Sean P Fillingham, Peter M. Frinchaboy, Sebastien Fromenteau, Lluís Galbany, Rafael A. García, D. A. García-Hernández, Junqiang Ge, Doug Geisler, Joseph Gelfand, Tobias Géron, Benjamin J. Gibson, Julian Goddy, Diego Godoy-Rivera, Kathleen Grabowski, Paul J. Green, Michael Greener, Catherine J. Grier, Emily Griffith, Hong Guo, Julien Guy, Massinissa Hadjara, Paul Harding, Sten Hasselquist, Christian R. Hayes, Fred Hearty, Jesús Hernández, Lewis Hill, David W. Hogg, Jon A. Holtzman, Danny Horta, Bau-Ching Hsieh, Chin-Hao Hsu, Yun-Hsin Hsu, Daniel Huber, Marc Huertas-Company, Brian Hutchinson, Ho Seong Hwang, Héctor J. Ibarra-Medel, Jacob Ider Chitham, Gabriele S. Ilha, Julie Imig, Will Jaekle, Tharindu Jayasinghe, Xi-

han Ji, Jennifer A. Johnson, Amy Jones, Henrik Jönsson, Ivan Katkov, Dr. Arman Khalatyan, Karen Kinemuchi, Shobhit Kisku, Johan H. Knapen, Jean-Paul Kneib, Juna A. Kollmeier, Miranda Kong, Marina Kounkel, Kathryn Kreckel, Dhanesh Krishnarao, Ivan Lacerna, Richard R. Lane, Rachel Langgin, Ramon Lavender, David R. Law, Daniel Lazarz, Henry W. Leung, Ho-Hin Leung, Hannah M. Lewis, Cheng Li, Ran Li, Jianhui Lian, Fu-Heng Liang, Lihwai Lin, Yen-Ting Lin, Sicheng Lin, Chris Lintott, Dan Long, Penélope Longa-Peña, Carlos López-Cobá, Shengdong Lu, Britt F. Lundgren, Yuanze Luo, J. Ted Mackereth, Axel de la Macorra, Suvrath Mahadevan, Steven R. Majewski, Arturo Manchado, Travis Mandeville, Claudia Maraston, Berta Margalef-Bentabol, Thomas Masseron, Karen L. Masters, Savita Mathur, Richard M. McDermid, Myles Mckay, Andrea Merloni, Michael Merrifield, Szabolcs Meszaros, Andrea Miglio, Francesco Di Mille, Dante Minniti, Rebecca Minsley, Antonela Monachesi, Jeongin Moon, Benoit Mosser, John Mulchaey, Demitri Muna, Ricardo R. Muñoz, Adam D. Myers, Natalie Myers, Seshadri Nadathur, Preethi Nair, Kirpal Nandra, Justus Neumann, Jeffrey A. Newman, David L. Nidever, Farnik Nikakhtar, Christian Nitschelm, Julia E. O'Connell, Luis Garma-Oehmichen, Gabriel Luan Souza de Oliveira, Richard Olney, Daniel Oravetz, Mario Ortigoza-Urdaneta, Yeisson Osorio, Justin Otter, Zachary J. Pace, Nelson Padilla, Kaike Pan, Hsi-An Pan, Taniya Parikh, James Parker, Sebastien Peirani, Karla Peña Ramírez, Samantha Penny, Will J. Percival, Ismael Perez-Fournon, Marc Pinsonneault, Frédérick Poidevin, Vijith Jacob Poovelil, Adrian M. Price-Whelan, Anna Bárbara de Andrade Queiroz, M. Jordan Raddick, Amy Ray, Sandro Barboza Rembold, Nicole Riddle, Rogemar A. Riffel, Rogério Riffel, Hans-Walter Rix, Annie C. Robin, Aldo Rodríguez-Puebla, Alexandre Roman-Lopes, Carlos Román-Zúñiga, Benjamin Rose, Ashley J. Ross, Graziano Rossi, Kate H. R. Rubin, Mara Salvato, Sebástian F. Sánchez, José R. Sánchez-Gallego, Robyn Sanderson, Felipe Antonio Santana Rojas, Edgar Sarceno, Regina Sarmiento, Conor Sayres, Elizaveta Sazonova, Adam L. Schaefer, Ricardo Schiavon, David J Schlegel, Donald P. Schneider, Mathias Schultheis, Axel Schwope, Aldo Serenelli, Javier Serna, Zhengyi Shao, Griffin Shapiro, Anubhav Sharma, Yue Shen, Matthew Shetrone, Yiping Shu, Joshua D. Simon, M. F. Skrutskie, Rebecca Smethurst, Verne Smith, Jennifer Sobeck, Taylor Spoo, Dani Sprague, David V. Stark, Keivan G. Stassun, Matthias Steinmetz, Dennis Stello, Alexander Stone-Martinez, Thaisa Storchi-Bergmann, Guy S. Stringfellow, Amelia Stutz, Yung-Chau Su, Manuchehr Taghizadeh-Popp, Michael S. Talbot, Jamie Tayar, Eduardo Telles, Johanna Teske, Ani Thakar, Christopher Theissen, Andrew Tkachenko, Daniel Thomas, Rita Tojeiro, Hector Hernandez Toledo, Nicholas W. Troup, Jonathan R. Trump, James Trussler, Jacqueline Turner, Sarah Tuttle, Eduardo Unda-Sanzana, José Antonio Vázquez-Mata, Marica Valentini, Octavio Valenzuela, Jaime Vargas-González, Mariana Vargas-Magaña, Pablo Vera Alfaro, Sandro Villanova, Fiorenzo Vincenzo, David Wake,

Jack T. Warfield, Jessica Diane Washington, Benjamin Alan Weaver, Anne-Marie Weijmans, David H. Weinberg, Achim Weiss, Kyle B. Westfall, Vivienne Wild, Matthew C. Wilde, John C. Wilson, Robert F. Wilson, Mikayla Wilson, Julien Wolf, W. M. Wood-Vasey, Renbin Yan, Olga Zamora, Gail Zasowski, Kai Zhang, Cheng Zhao, Zheng Zheng, Zheng Zheng, and Kai Zhu. The seventeenth data release of the sloan digital sky surveys: Complete release of manga, mastar, and apogee-2 data. *The Astrophysical Journal Supplement Series*, 259(2):35, mar 2022. doi: 10.3847/1538-4365/ac4414. URL https://dx.doi.org/10.3847/1538-4365/ac4414.

Silvia H. P. Alencar and Gibor Basri. Profiles of Strong Permitted Lines in Classical T Tauri Stars. AJ, 119(4):1881–1900, April 2000. doi: 10.1086/301300.

Andrés Almeida, Scott F. Anderson, Maria Argudo-Fernández, Carles Badenes, Kat Barger, Jorge K. Barrera-Ballesteros, Chad F. Bender, Erika Benitez, Felipe Besser, Jonathan C. Bird, Dmitry Bizyaev, Michael R. Blanton, John Bochanski, Jo Bovy, William Nielsen Brandt, Joel R. Brownstein, Johannes Buchner, Esra Bulbul, Joseph N. Burchett, Mariana Cano Díaz, Joleen K. Carlberg, Andrew R. Casey, Vedant Chandra, Brian Cherinka, Cristina Chiappini, Abigail A. Coker, Johan Comparat, Charlie Conroy, Gabriella Contardo, Arlin Cortes, Kevin Covey, Jeffrey D. Crane, Katia Cunha, Collin Dabbieri, James W. Davidson, Megan C. Davis, Anna Barbara de Andrade Queiroz, Nathan De Lee, José Eduardo Méndez Delgado, Sebastian Demasi, Francesco Di Mille, John Donor, Peter Dow, Tom Dwelly, Mike Eracleous, Jamey Eriksen, Xiaohui Fan, Emily Farr, Sara Frederick, Logan Fries, Peter Frinchaboy, Boris T. Gänsicke, Junqiang Ge, Consuelo González Ávila, Katie Grabowski, Catherine Grier, Guillaume Guiglion, Pramod Gupta, Patrick Hall, Keith Hawkins, Christian R. Hayes, J. J. Hermes, Lorena Hernández-García, David W. Hogg, Jon A. Holtzman, Hector Javier Ibarra-Medel, Alexander Ji, Paula Jofre, Jennifer A. Johnson, Amy M. Jones, Karen Kinemuchi, Matthias Kluge, Anton Koekemoer, Juna A. Kollmeier, Marina Kounkel, Dhanesh Krishnarao, Mirko Krumpe, Ivan Lacerna, Paulo Jakson Assuncao Lago, Chervin Laporte, Chao Liu, Ang Liu, Xin Liu, Alexandre Roman Lopes, Matin Macktoobian, Steven R. Majewski, Viktor Malanushenko, Dan Maoz, Thomas Masseron, Karen L. Masters, Gal Matijevic, Aidan McBride, Ilija Medan, Andrea Merloni, Sean Morrison, Natalie Myers, Szabolcs Mészáros, C. Alenka Negrete, David L. Nidever, Christian Nitschelm, Daniel Oravetz, Audrey Oravetz, Kaike Pan, Yingjie Peng, Marc H. Pinsonneault, Rick Pogge, Dan Qiu, Solange V. Ramirez, Hans-Walter Rix, Daniela Fernández Rosso, Jessie Runnoe, Mara Salvato, Sebastian F. Sanchez, Felipe A. Santana, Andrew Saydjari, Conor Sayres, Kevin C. Schlaufman, Donald P. Schneider, Axel Schwope, Javier Serna, Yue Shen, Jennifer Sobeck, Ying-Yi Song, Diogo Souto, Taylor Spoo, Keivan G. Stassun, Matthias Steinmetz, Ilya Straumit, Guy Stringfel-

low, José Sánchez-Gallego, Manuchehr Taghizadeh-Popp, Jamie Tayar, Ani Thakar, Patricia B. Tissera, Andrew Tkachenko, Hector Hernandez Toledo, Benny Trakhtenbrot, José G. Fernández-Trincado, Nicholas Troup, Jonathan R. Trump, Sarah Tuttle, Natalie Ulloa, Jose Antonio Vazquez-Mata, Pablo Vera Alfaro, Sandro Villanova, Stefanie Wachter, Anne-Marie Weijmans, Adam Wheeler, John Wilson, Leigh Wojno, Julien Wolf, Xiang-Xiang Xue, Jason E. Ybarra, Eleonora Zari, and Gail Zasowski. The eighteenth data release of the sloan digital sky surveys: Targeting and first spectra from sdss-v. *The Astrophysical Journal Supplement Series*, 267(2):44, aug 2023. doi: 10.3847/1538-4365/acda98. URL https://dx.doi.org/10.3847/1538-4365/acda98.

L. Amard, A. Palacios, C. Charbonnel, F. Gallet, and J. Bouvier. Rotating models of young solar-type stars. Exploring braking laws and angular momentum transport processes. A&A, 587:A105, March 2016. doi: 10.1051/0004-6361/201527349.

L. Amard, A. Palacios, C. Charbonnel, F. Gallet, C. Georgy, N. Lagarde, and L. Siess. First grids of low-mass stellar models and isochrones with self-consistent treatment of rotation. From 0.2 to 1.5 M at seven metallicities from PMS to TAMS. A&A, 631:A77, November 2019. doi: 10.1051/0004-6361/201935160.

G. M. Anderson. Error propagation by the Monte Carlo method in geochemical calculations. Geochim. Cosmochim. Acta, 40(12):1533–1538, December 1976. doi: 10.1016/0016-7037(76)90092-2.

M Ansdell, E Gaidos, C Hedges, M Tazzari, A L Kraus, M C Wyatt, G M Kennedy, J P Williams, A W Mann, I Angelo, G Dûchene, E E Mamajek, J Carpenter, T L Esplin, and A C Rizzuto. Are inner disc misalignments common? ALMA reveals an isotropic outer disc inclination distribution for young dipper stars. *Monthly Notices of the Royal Astronomical Society*, 492(1):572–588, 12 2019. ISSN 0035-8711. doi: 10.1093/mnras/stz3361. URL https://doi.org/10.1093/mnras/stz3361.

P. J. Armitage and C. J. Clarke. Magnetic braking of T Tauri stars. MNRAS, 280(2):458–468, May 1996. doi: 10.1093/mnras/280.2.458.

S. A. Artemenko, K. N. Grankin, and P. P. Petrov. Rotation effects in classical T Tauri stars. *Astronomy Letters*, 38(12):783–792, December 2012. doi: 10.1134/S1063773712110011.

Astropy Collaboration, T. P. Robitaille, E. J. Tollerud, P. Greenfield, M. Droettboom, E. Bray, T. Aldcroft, M. Davis, A. Ginsburg, A. M. Price-Whelan, W. E. Kerzendorf, A. Conley, N. Crighton, K. Barbary, D. Muna, H. Ferguson, F. Grollier, M. M. Parikh, P. H. Nair, H. M. Unther, C. Deil, J. Woillez, S. Conseil, R. Kramer, J. E. H. Turner,

L. Singer, R. Fox, B. A. Weaver, V. Zabalza, Z. I. Edwards, K. Azalee Bostroem, D. J. Burke, A. R. Casey, S. M. Crawford, N. Dencheva, J. Ely, T. Jenness, K. Labrie, P. L. Lim, F. Pierfederici, A. Pontzen, A. Ptak, B. Refsdal, M. Servillat, and O. Streicher. Astropy: A community Python package for astronomy. A&A, 558:A33, October 2013a. doi: 10.1051/0004-6361/201322068.

Astropy Collaboration, Thomas P. Robitaille, Erik J. Tollerud, Perry Greenfield, Michael Droettboom, Erik Bray, Tom Aldcroft, Matt Davis, Adam Ginsburg, Adrian M. Price-Whelan, Wolfgang E. Kerzendorf, Alexander Conley, Neil Crighton, Kyle Barbary, Demitri Muna, Henry Ferguson, Frédéric Grollier, Madhura M. Parikh, Prasanth H. Nair, Hans M. Unther, Christoph Deil, Julien Woillez, Simon Conseil, Roban Kramer, James E. H. Turner, Leo Singer, Ryan Fox, Benjamin A. Weaver, Victor Zabalza, Zachary I. Edwards, K. Azalee Bostroem, D. J. Burke, Andrew R. Casey, Steven M. Crawford, Nadia Dencheva, Justin Ely, Tim Jenness, Kathleen Labrie, Pey Lian Lim, Francesco Pierfederici, Andrew Pontzen, Andy Ptak, Brian Refsdal, Mathieu Servillat, and Ole Streicher. Astropy: A community Python package for astronomy. A&A, 558:A33, Oct 2013b. doi: 10.1051/0004-6361/201322068.

Astropy Collaboration, A. M. Price-Whelan, B. M. Sipőcz, H. M. Günther, P. L. Lim, S. M. Crawford, S. Conseil, D. L. Shupe, M. W. Craig, N. Dencheva, A. Ginsburg, J. T. Vand erPlas, L. D. Bradley, D. Pérez-Suárez, M. de Val-Borro, T. L. Aldcroft, K. L. Cruz, T. P. Robitaille, E. J. Tollerud, C. Ardelean, T. Babej, Y. P. Bach, M. Bachetti, A. V. Bakanov, S. P. Bamford, G. Barentsen, P. Barmby, A. Baumbach, K. L. Berry, F. Biscani, M. Boquien, K. A. Bostroem, L. G. Bouma, G. B. Brammer, E. M. Bray, H. Breytenbach, H. Buddelmeijer, D. J. Burke, G. Calderone, J. L. Cano Rodríguez, M. Cara, J. V. M. Cardoso, S. Cheedella, Y. Copin, L. Corrales, D. Crichton, D. D'Avella, C. Deil, É. Depagne, J. P. Dietrich, A. Donath, M. Droettboom, N. Earl, T. Erben, S. Fabbro, L. A. Ferreira, T. Finethy, R. T. Fox, L. H. Garrison, S. L. J. Gibbons, D. A. Goldstein, R. Gommers, J. P. Greco, P. Greenfield, A. M. Groener, F. Grollier, A. Hagen, P. Hirst, D. Homeier, A. J. Horton, G. Hosseinzadeh, L. Hu, J. S. Hunkeler, Ž. Ivezić, A. Jain, T. Jenness, G. Kanarek, S. Kendrew, N. S. Kern, W. E. Kerzendorf, A. Khvalko, J. King, D. Kirkby, A. M. Kulkarni, A. Kumar, A. Lee, D. Lenz, S. P. Littlefair, Z. Ma, D. M. Macleod, M. Mastropietro, C. McCully, S. Montagnac, B. M. Morris, M. Mueller, S. J. Mumford, D. Muna, N. A. Murphy, S. Nelson, G. H. Nguyen, J. P. Ninan, M. Nöthe, S. Ogaz, S. Oh, J. K. Parejko, N. Parley, S. Pascual, R. Patil, A. A. Patil, A. L. Plunkett, J. X. Prochaska, T. Rastogi, V. Reddy Janga, J. Sabater, P. Sakurikar, M. Seifert, L. E. Sherbert, H. Sherwood-Taylor, A. Y. Shih, J. Sick, M. T. Silbiger, S. Singanamalla, L. P. Singer, P. H. Sladen, K. A. Sooley, S. Sornarajah, O. Streicher, P. Teuben, S. W. Thomas, G. R. Tremblay, J. E. H.

Turner, V. Terrón, M. H. van Kerkwijk, A. de la Vega, L. L. Watkins, B. A. Weaver, J. B. Whitmore, J. Woillez, V. Zabalza, and Astropy Contributors. The Astropy Project: Building an Open-science Project and Status of the v2.0 Core Package. AJ, 156(3):123, September 2018. doi: 10.3847/1538-3881/aabc4f.

Astropy Collaboration, Adrian M. Price-Whelan, Pey Lian Lim, Nicholas Earl, Nathaniel Starkman, Larry Bradley, David L. Shupe, Aarya A. Patil, Lia Corrales, C. E. Brasseur, Maximilian N"othe, Axel Donath, Erik Tollerud, Brett M. Morris, Adam Ginsburg, Eero Vaher, Benjamin A. Weaver, James Tocknell, William Jamieson, Marten H. van Kerkwijk, Thomas P. Robitaille, Bruce Merry, Matteo Bachetti, H. Moritz G"unther, Thomas L. Aldcroft, Jaime A. Alvarado-Montes, Anne M. Archibald, Attila B'odi, Shreyas Bapat, Geert Barentsen, Juanjo Baz'an, Manish Biswas, M'ed'eric Boquien, D. J. Burke, Daria Cara, Mihai Cara, Kyle E. Conroy, Simon Conseil, Matthew W. Craig, Robert M. Cross, Kelle L. Cruz, Francesco D'Eugenio, Nadia Dencheva, Hadrien A. R. Devillepoix, J"org P. Dietrich, Arthur Davis Eigenbrot, Thomas Erben, Leonardo Ferreira, Daniel Foreman-Mackey, Ryan Fox, Nabil Freij, Suyog Garg, Robel Geda, Lauren Glattly, Yash Gondhalekar, Karl D. Gordon, David Grant, Perry Greenfield, Austen M. Groener, Steve Guest, Sebastian Gurovich, Rasmus Handberg, Akeem Hart, Zac Hatfield-Dodds, Derek Homeier, Griffin Hosseinzadeh, Tim Jenness, Craig K. Jones, Prajwel Joseph, J. Bryce Kalmbach, Emir Karamehmetoglu, Mikolaj Kaluszy'nski, Michael S. P. Kelley, Nicholas Kern, Wolfgang E. Kerzendorf, Eric W. Koch, Shankar Kulumani, Antony Lee, Chun Ly, Zhiyuan Ma, Conor MacBride, Jakob M. Maljaars, Demitri Muna, N. A. Murphy, Henrik Norman, Richard O'Steen, Kyle A. Oman, Camilla Pacifici, Sergio Pascual, J. Pascual-Granado, Rohit R. Patil, Gabriel I. Perren, Timothy E. Pickering, Tanuj Rastogi, Benjamin R. Roulston, Daniel F. Ryan, Eli S. Rykoff, Jose Sabater, Parikshit Sakurikar, Jes'us Salgado, Aniket Sanghi, Nicholas Saunders, Volodymyr Savchenko, Ludwig Schwardt, Michael Seifert-Eckert, Albert Y. Shih, Anany Shrey Jain, Gyanendra Shukla, Jonathan Sick, Chris Simpson, Sudheesh Singanamalla, Leo P. Singer, Jaladh Singhal, Manodeep Sinha, Brigitta M. SipHocz, Lee R. Spitler, David Stansby, Ole Streicher, Jani Sumak, John D. Swinbank, Dan S. Taranu, Nikita Tewary, Grant R. Tremblay, Miguel de Val-Borro, Samuel J. Van Kooten, Zlatan Vasovi'c, Shresth Verma, Jos'e Vin'icius de Miranda Cardoso, Peter K. G. Williams, Tom J. Wilson, Benjamin Winkel, W. M. Wood-Vasey, Rui Xue, Peter Yoachim, Chen Zhang, Andrea Zonca, and Astropy Project Contributors. The Astropy Project: Sustaining and Growing a Community-oriented Open-source Project and the Latest Major Release (v5.0) of the Core Package. *apj*, 935(2):167, August 2022. doi: 10.3847/1538-4357/ac7c74.

R. V. Baluev. Assessing the statistical significance of periodogram peaks. *Monthly Notices of the Royal Astronomical Society*, 385(3):1279–1285, 03 2008. ISSN 0035-8711. doi:

10.1111/j.1365-2966.2008.12689.x. URL https://doi.org/10.1111/j.1365-2966.2008.12689.x.

Andrea Banzatti, Ilaria Pascucci, Suzan Edwards, Min Fang, Uma Gorti, and Mario Flock. Kinematic Links and the Coevolution of MHD Winds, Jets, and Inner Disks from a High-resolution Optical [O I] Survey. ApJ, 870(2):76, January 2019. doi: 10.3847/1538-4357/aaf1aa.

I. Baraffe, G. Chabrier, F. Allard, and P. H. Hauschildt. Evolutionary models for solar metallicity low-mass stars: mass-magnitude relationships and color-magnitude diagrams. A&A, 337:403–412, September 1998.

Isabelle Baraffe, Derek Homeier, France Allard, and Gilles Chabrier. New evolutionary models for pre-main sequence and main sequence low-mass stars down to the hydrogen-burning limit. *A&A*, 577:A42, 2015. doi: 10.1051/0004-6361/201425481. URL https://doi.org/10.1051/0004-6361/201425481.

J. R. Barnes, A. Collier Cameron, J.-F. Donati, D. J. James, S. C. Marsden, and P. Petit. The dependence of differential rotation on temperature and rotation. *Monthly Notices of the Royal Astronomical Society: Letters*, 357(1):L1–L5, 02 2005. ISSN 1745-3925. doi: 10.1111/j.1745-3933.2005.08587.x. URL https://doi.org/10.1111/j.1745-3933.2005.08587.x.

A. Bayo, D. Barrado, N. Huélamo, M. Morales-Calderón, C. Melo, J. Stauffer, and B. Stelzer. Spectroscopy of very low-mass stars and brown dwarfs in the Lambda Orionis star-forming region. II. Rotation, activity and other properties of spectroscopically confirmed members of Collinder 69. A&A, 547:A80, November 2012. doi: 10.1051/0004-6361/201219374.

K. Biazzo, C. H. F. Melo, L. Pasquini, S. Randich, J. Bouvier, and X. Delfosse. Evidence of early disk-locking among low-mass members of the orion nebula cluster ***. *A&A*, 508(3):1301–1312, 2009. doi: 10.1051/0004-6361/200913125. URL https://doi.org/10.1051/0004-6361/200913125.

Thompson S. Le Blanc, Kevin R. Covey, and Keivan G. Stassun. SPECTRAL ENERGY DISTRIBUTIONS OF YOUNG STARS IN IC 348: THE ROLE OF DISKS IN ANGULAR MOMENTUM EVOLUTION OF YOUNG, LOW-MASS STARS. *The Astronomical Journal*, 142(2):55, jul 2011. doi: 10.1088/0004-6256/142/2/55. URL https://doi.org/10.1088%2F0004-6256%2F142%2F2%2F55.

J. Bouvier. Observational studies of stellar rotation. *EAS Publications Series*, 62:143–168, 2013. doi: 10.1051/eas/1362005. URL https://doi.org/10.1051/eas/1362005.

J. Bouvier, S. Cabrit, M. Fernandez, E. L. Martin, and J. M. Matthews. COYOTES I : the photometric variability and rotational evolution of T Tauri stars. A&A, 272:176–206, May 1993.

J. Bouvier, S. P. Matt, S. Mohanty, A. Scholz, K. G. Stassun, and C. Zanni. Angular Momentum Evolution of Young Low-Mass Stars and Brown Dwarfs: Observations and Theory. In Henrik Beuther, Ralf S. Klessen, Cornelis P. Dullemond, and Thomas Henning, editors, *Protostars and Planets VI*, page 433, January 2014. doi: 10.2458/azu_uapress_9780816531240-ch019.

J. Bouvier, A. C. Lanzafame, L. Venuti, A. Klutsch, R. Jeffries, A. Frasca, E. Moraux, K. Biazzo, S. Messina, G. Micela, S. Randich, J. Stauffer, A. M. Cody, E. Flaccomio, G. Gilmore, A. Bayo, T. Bensby, A. Bragaglia, G. Carraro, A. Casey, M. T. Costado, F. Damiani, E. Delgado Mena, P. Donati, E. Franciosini, A. Hourihane, S. Koposov, C. Lardo, J. Lewis, L. Magrini, L. Monaco, L. Morbidelli, L. Prisinzano, G. Sacco, L. Sbordone, S. G. Sousa, A. Vallenari, C. C. Worley, S. Zaggia, and T. Zwitter. The Gaia-ESO Survey: A lithium-rotation connection at 5 Myr? A&A, 590:A78, May 2016. doi: 10.1051/0004-6361/201628336.

Larry Bradley, Brigitta Sipőcz, Thomas Robitaille, Erik Tollerud, Zè Vinícius, Christoph Deil, Kyle Barbary, Hans Moritz Günther, Mihai Cara, Ivo Busko, Simon Conseil, Michael Droettboom, Azalee Bostroem, E. M. Bray, Lars Andersen Bratholm, Tom Wilson, Matt Craig, Geert Barentsen, Sergio Pascual, Axel Donath, Johnny Greco, Gabriel Perren, P. L. Lim, and Wolfgang Kerzendorf. astropy/photutils: v0.6, January 2019. URL https://doi.org/10.5281/zenodo.2533376.

C. E. Brasseur, Carlita Phillip, Scott W. Fleming, S. E. Mullally, and Richard L. White. Astrocut: Tools for creating cutouts of TESS images, May 2019.

C Briceño. The Dispersed Young Population in Orion. *Handb. Star Form. Reg. Vol. I North. Sky ASP Monogr. Publ. Vol. 4. Ed. by Bo Reipurth, p.838*, 4:838, 2008. URL http://adsabs.harvard.edu/abs/2008hsf1.book..838B.

César Briceño, Nuria Calvet, Jesús Hernández, A. Katherina Vivas, Cecilia Mateu, Juan José Downes, Jaqueline Loerincs, Alice Pérez-Blanco, Perry Berlind, Catherine Espaillat, Lori Allen, Lee Hartmann, Mario Mateo, and John I. Bailey III. The CIDA variability survey of orion OB1. II. demographics of the young, low-mass stellar populations. *The Astronomical Journal*, 157(2):85, jan 2019. doi: 10.3847/1538-3881/aaf79b. URL https://doi.org/10.3847%2F1538-3881%2Faaf79b.

Peter J. Brown, Alice Breeveld, Peter W. A. Roming, and Michael Siegel. Interpreting Flux from Broadband Photometry. AJ, 152(4):102, October 2016. doi: 10.3847/0004-6256/152/4/102.

Sylvie Cabrit, Suzan Edwards, Stephen E. Strom, and Karen M. Strom. Forbidden-Line Emission and Infrared Excesses in T Tauri Stars: Evidence for Accretion-driven Mass Loss? ApJ, 354:687, May 1990. doi: 10.1086/168725.

Hunter Campbell, Elliott Khilfeh, Kevin R. Covey, Marina Kounkel, Richard Ballantyne, Sabrina Corey, Carlos G. Román-Zúñiga, Jesús Hernández, Ezequiel Manzo Martínez, Karla Peña Ramírez, Alexandre Roman-Lopes, Keivan G. Stassun, Guy S. Stringfellow, Jura Borissova, S. Drew Chojnowski, Valeria Ramírez-Preciado, Jinyoung Serena Kim, Javier Serna, Amelia M. Stutz, Ricardo López-Valdivia, Genaro Suárez, Jason E. Ybarra, Penélope Longa-Peña, and José G. Fernández-Trincado. Pre-main-sequence brackett emitters in the apogee dr17 catalog: Line strengths and physical properties of accretion columns. *The Astrophysical Journal*, 942(1):22, dec 2022. doi: 10.3847/1538-4357/aca324. URL https://dx.doi.org/10.3847/1538-4357/aca324.

Lyra Cao and Marc H. Pinsonneault. Star-spots and magnetism: testing the activity paradigm in the Pleiades and M67. MNRAS, 517(2):2165–2189, December 2022. doi: 10.1093/mnras/stac270610.48550/arXiv.2209.10549.

John M. Carpenter, Lynne A. Hillenbrand, and M. F. Skrutskie. Near-Infrared Photometric Variability of Stars toward the Orion A Molecular Cloud. *Astron. J.*, 121(6):3160–3190, jun 2001. ISSN 00046256. doi: 10.1086/321086. URL http://stacks.iop.org/1538-3881/121/i=6/a=3160.

John M. Carpenter, Eric E. Mamajek, Lynne A. Hillenbrand, and Michael R. Meyer. Evidence for mass-dependent circumstellar disk evolution in the 5 myr old upper scorpius OB association. *The Astrophysical Journal*, 651(1):L49–L52, oct 2006. doi: 10.1086/509121. URL https://doi.org/10.1086%2F509121.

J. A. Carroll. The Spectroscopic Determination of Stellar Rotation and its Effect on Line Profiles. *Mon. Not. R. Astron. Soc.*, 93(7):478–507, may 1933. ISSN 0035-8711. doi: 10.1093/mnras/93.7.478. URL https://academic.oup.com/mnras/article-lookup/doi/10.1093/mnras/93.7.478.

Caleb I. Cañas, Chad F. Bender, Suvrath Mahadevan, Dmitry Bizyaev, Nathan De Lee, Scott W. Fleming, Fred Hearty, Steven R. Majewski, Christian Nitschelm, Donald P. Schneider, Javier Serna, Keivan G. Stassun, Gumundur Stefánsson, Guy S. Stringfellow,

and John C. Wilson. Characterization of low-mass companions to kepler objects of interest observed with apogee-n. *The Astrophysical Journal Supplement Series*, 265(2):50, apr 2023. doi: 10.3847/1538-4365/acbcbe. URL https://dx.doi.org/10.3847/1538-4365/acbcbe.

S. Chandrasekhar and G. Münch. On the Integral Equation Governing the Distribution of the True and the Apparent Rotational Velocities of Stars. ApJ, 111:142, January 1950. doi: 10.1086/145245.

Ann Marie Cody and Lynne A. Hillenbrand. PRECISION PHOTOMETRIC MONITORING OF VERY LOW MASS σ ORIONIS CLUSTER MEMBERS: VARIABILITY AND ROTATION AT A FEW Myr. *Astrophys. J. Suppl. Ser.*, 191(2):389–422, dec 2010. ISSN 0067-0049. doi: 10.1088/0067-0049/191/2/389. URL http://stacks.iop.org/0067-0049/191/i=2/a=389?key=crossref.bd5a05b1f1ba776167ee780827c6a669.

Ann Marie Cody and Lynne A. Hillenbrand. The Many-faceted Light Curves of Young Disk-bearing Stars in Upper Sco – Oph Observed by K2 Campaign 2. AJ, 156(2):71, August 2018. doi: 10.3847/1538-3881/aacead.

Ann Marie Cody, John Stauffer, Annie Baglin, Giuseppina Micela, Luisa M. Rebull, Ettore Flaccomio, María Morales-Calderón, Suzanne Aigrain, Jèrôme Bouvier, Lynne A. Hillenbrand, Robert Gutermuth, Inseok Song, Neal Turner, Silvia H. P. Alencar, Konstanze Zwintz, Peter Plavchan, John Carpenter, Krzysztof Findeisen, Sean Carey, Susan Terebey, Lee Hartmann, Nuria Calvet, Paula Teixeira, Frederick J. Vrba, Scott Wolk, Kevin Covey, Katja Poppenhaeger, Hans Moritz Günther, Jan Forbrich, Barbara Whitney, Laura Affer, William Herbst, Joseph Hora, David Barrado, Jon Holtzman, Franck Marchis, Kenneth Wood, Marcelo Medeiros Guimarães, Jorge Lillo Box, Ed Gillen, Amy McQuillan, Catherine Espaillat, Lori Allen, Paola D'Alessio, and Fabio Favata. CSI 2264: Simultaneous Optical and Infrared Light Curves of Young Disk-bearing Stars in NGC 2264 with CoRoT and Spitzer—Evidence for Multiple Origins of Variability. AJ, 147(4):82, April 2014. doi: 10.1088/0004-6256/147/4/82.

A. Collier Cameron and C. G. Campbell. Rotational evolution of magnetic T Tauri stars with accretion discs. A&A, 274:309, July 1993a.

A. Collier Cameron and C. G. Campbell. Rotational evolution of magnetic T Tauri stars with accretion discs. A&A, 274:309, July 1993b.

Michiel Cottaar, Kevin R. Covey, Michael R. Meyer, David L. Nidever, Keivan G. Stassun, Jonathan B. Foster, Jonathan C. Tan, S. Drew Chojnowski, Nicola da Rio, Kevin M. Flaherty, Peter M. Frinchaboy, Michael Skrutskie, Steven R. Majewski, John C. Wilson, and

Gail Zasowski. IN-SYNC i: HOMOGENEOUS STELLAR PARAMETERS FROM HIGH-RESOLUTION APOGEE SPECTRA FOR THOUSANDS OF PRE-MAIN SEQUENCE STARS. *The Astrophysical Journal*, 794(2):125, oct 2014. doi: 10.1088/0004-637x/794/2/125. URL https://doi.org/10.1088%2F0004-637x%2F794%2F2%2F125.

J'Neil Cottle, Kevin R. Covey, Genaro Suárez, Carlos Román-Zúñiga, Edward Schlafly, Juan Jose Downes, Jason E. Ybarra, Jesus Hernandez, Keivan Stassun, Guy S. Stringfellow, Konstantin Getman, Eric Feigelson, Jura Borissova, J. Serena Kim, A. Roman-Lopes, Nicola Da Rio, Nathan De Lee, Peter M. Frinchaboy, Marina Kounkel, Steven R. Majewski, Ronald E. Mennickent, David L. Nidever, Christian Nitschelm, Kaike Pan, Matthew Shetrone, Gail Zasowski, Ken Chambers, Eugene Magnier, and Jeff Valenti. The APOGEE-2 Survey of the Orion Star-forming Complex. I. Target Selection and Validation with Early Observations. *Astrophys. J. Suppl. Ser.*, 236(2):27, may 2018. ISSN 1538-4365. doi: 10.3847/1538-4365/aabada. URL http://stacks.iop.org/0067-0049/236/i=2/a=27?key=crossref.5ea6e9e92eb672ecdccd362b1a22842b.

Kevin R. Covey, Thomas P. Greene, Greg W. Doppmann, and Charles J. Lada. The angular momentum content and evolution of class i and flat-spectrum protostars*. *The Astronomical Journal*, 129(6):2765, jun 2005. doi: 10.1086/429736. URL https://dx.doi.org/10.1086/429736.

Steven R. Cranmer. Turbulence-driven polar winds from t tauri stars energized by magnetospheric accretion. *The Astrophysical Journal*, 689(1):316–334, dec 2008. doi: 10.1086/592566. URL https://doi.org/10.1086/592566.

R. M. Cutri, M. F. Skrutskie, S. van Dyk, C. A. Beichman, J. M. Carpenter, T. Chester, L. Cambresy, T. Evans, J. Fowler, J. Gizis, E. Howard, J. Huchra, T. Jarrett, E. L. Kopan, J. D. Kirkpatrick, R. M. Light, K. A. Marsh, H. McCallon, S. Schneider, R. Stiening, M. Sykes, M. Weinberg, W. A. Wheaton, S. Wheelock, and N. Zacarias. VizieR Online Data Catalog: 2MASS All-Sky Catalog of Point Sources (Cutri+ 2003). *VizieR Online Data Catalog*, art. II/246, June 2003.

Stefan Czesla, Sebastian Schröter, Christian P. Schneider, Klaus F. Huber, Fabian Pfeifer, Daniel T. Andreasen, and Mathias Zechmeister. PyA: Python astronomy-related packages. Astrophysics Source Code Library, record ascl:1906.010, June 2019a.

Stefan Czesla, Sebastian Schröter, Christian P. Schneider, Klaus F. Huber, Fabian Pfeifer, Daniel T. Andreasen, and Mathias Zechmeister. PyA: Python astronomy-related packages, Jun 2019b.

Christine Mazzola Daher, Carles Badenes, Jamie Tayar, Marc Pinsonneault, Sergey E Koposov, Kaitlin Kratter, Maxwell Moe, Borja Anguiano, Diego Godoy-Rivera, Steven Majewski, Joleen K Carlberg, Matthew G Walker, Rachel Buttry, Don Dixon, Javier Serna, Keivan G Stassun, Nathan De Lee, Jesús Hernández, Christian Nitschelm, Guy S Stringfellow, and Nicholas W Troup. Stellar multiplicity and stellar rotation: insights from APOGEE. *Monthly Notices of the Royal Astronomical Society*, 512(2):2051–2061, 03 2022. ISSN 0035-8711. doi: 10.1093/mnras/stac590. URL https://doi.org/10.1093/mnras/stac590.

Claire L. Davies, Scott G. Gregory, and Jane S. Greaves. Accretion discs as regulators of stellar angular momentum evolution in the ONC and Taurus–Auriga. *Mon. Not. R. Astron. Soc.*, 444(2):1157–1176, oct 2014. ISSN 0035-8711. doi: 10.1093/mnras/stu1488. URL https://academic.oup.com/mnras/article/444/2/1157/992637.

J. F. Donati and J. D. Landstreet. Magnetic Fields of Nondegenerate Stars. ARA&A, 47(1): 333–370, September 2009. doi: 10.1146/annurev-astro-082708-101833.

Aaron Dotter. MESA Isochrones and Stellar Tracks (MIST) 0: Methods for the Construction of Stellar Isochrones. ApJS, 222(1):8, January 2016. doi: 10.3847/0067-0049/222/1/8.

Suzan Edwards, William Fischer, John Kwan, Lynne Hillenbrand, and A. K. Dupree. He I λ10830 as a Probe of Winds in Accreting Young Stars. ApJ, 599(1):L41–L44, December 2003. doi: 10.1086/381077.

Constance Emeriau-Viard and Allan Sacha Brun. Origin and evolution of magnetic field in PMS stars: Influence of rotation and structural changes. *The Astrophysical Journal*, 846(1):8, aug 2017. doi: 10.3847/1538-4357/aa7b33. URL https://doi.org/10.3847/1538-4357/aa7b33.

Barbara Ercolano, Giovanni Picogna, Kristina Monsch, Jeremy J. Drake, and Thomas Preibisch. The dispersal of protoplanetary discs - II: photoevaporation models with observationally derived irradiating spectra. MNRAS, 508(2):1675–1685, December 2021. doi: 10.1093/mnras/stab259010.48550/arXiv.2109.04113.

C. C. Espaillat, C. E. Robinson, M. M. Romanova, T. Thanathibodee, J. Wendeborn, N. Calvet, M. Reynolds, and J. Muzerolle. Measuring the density structure of an accretion hot spot. Nature, 597(7874):41–44, September 2021. doi: 10.1038/s41586-021-03751-5.

C. C. Espaillat, G. J. Herczeg, T. Thanathibodee, C. Pittman, N. Calvet, N. Arulanantham, K. France, Javier Serna, J. Hernández, Á. Kóspál, F. M. Walter, A. Frasca, W. J. Fischer, C. M. Johns-Krull, P. C. Schneider, C. Robinson, Suzan Edwards, P. Ábrahám, Min Fang,

J. Erkal, C. F. Manara, J. M. Alcalá, E. Alecian, R. D. Alexander, J. Alonso-Santiago, Simone Antoniucci, David R. Ardila, Andrea Banzatti, M. Benisty, Edwin A. Bergin, Katia Biazzo, César Briceño, Justyn Campbell-White, L. Ilsedore Cleeves, Deirdre Coffey, Jochen Eislöffel, Stefano Facchini, D. Fedele, Eleonora Fiorellino, Dirk Froebrich, Manuele Gangi, Teresa Giannini, K. Grankin, Hans Moritz Günther, Zhen Guo, Lee Hartmann, Lynne A. Hillenbrand, P. C. Hinton, Joel H. Kastner, Chris Koen, K. Maucó, I. Mendigutía, B. Nisini, Neelam Panwar, D. A. Principe, Massimo Robberto, A. Sicilia-Aguilar, Jeff A. Valenti, J. Wendeborn, Jonathan P. Williams, Ziyan Xu, and R. K. Yadav. The odysseus survey. motivation and first results: Accretion, ejection, and disk irradiation of cvso 109. *The Astronomical Journal*, 163(3):114, feb 2022. doi: 10.3847/1538-3881/ac479d. URL https://dx.doi.org/10.3847/1538-3881/ac479d.

D. Fedele, M. E. van den Ancker, Th. Henning, R. Jayawardhana, and J. M. Oliveira. Timescale of mass accretion in pre-main-sequence stars. A&A, 510:A72, February 2010. doi: 10.1051/0004-6361/200912810.

Adam J. Finley and Sean P. Matt. The effect of combined magnetic geometries on thermally driven winds. i. interaction of dipolar and quadrupolar fields. *The Astrophysical Journal*, 845(1):46, aug 2017. doi: 10.3847/1538-4357/aa7fb9. URL https://doi.org/10.3847/1538-4357/aa7fb9.

E. L. Fitzpatrick, Derck Massa, Karl D. Gordon, Ralph Bohlin, and Geoffrey C. Clayton. An Analysis of the Shapes of Interstellar Extinction Curves. VII. Milky Way Spectrophotometric Optical-through-ultraviolet Extinction and Its R-dependence. ApJ, 886(2):108, December 2019. doi: 10.3847/1538-4357/ab4c3a.

C. P. Folsom, P. Petit, J. Bouvier, A. Lèbre, L. Amard, A. Palacios, J. Morin, J.-F. Donati, S. V. Jeffers, S. C. Marsden, and A. A. Vidotto. The evolution of surface magnetic fields in young solar-type stars – I. The first 250 Myr. *Monthly Notices of the Royal Astronomical Society*, 457(1):580–607, 01 2016. ISSN 0035-8711. doi: 10.1093/mnras/stv2924. URL https://doi.org/10.1093/mnras/stv2924.

A. Frasca, E. Covino, L. Spezzi, J. M. Alcalá, E. Marilli, G. F"urész, and D. Gandolfi. Rem near-ir and optical photometric monitoring of pre-main sequence stars in orion ****** - rotation periods and starspot parameters. *A&A*, 508(3):1313–1330, 2009. doi: 10.1051/0004-6361/200913327. URL https://doi.org/10.1051/0004-6361/200913327.

Gaia Collaboration, Brown, A. G. A., Vallenari, A., Prusti, T., de Bruijne, J. H. J., Babusiaux, C., Bailer-Jones, C. A. L., Biermann, M., Evans, D. W., Eyer, L., Jansen, F., Jordi, C., Klioner, S. A., Lammers, U., Lindegren, L., Luri, X., Mignard, F., Panem, C., Pourbaix,

D., Randich, S., Sartoretti, P., Siddiqui, H. I., Soubiran, C., van Leeuwen, F., Walton, N. A., Arenou, F., Bastian, U., Cropper, M., Drimmel, R., Katz, D., Lattanzi, M. G., Bakker, J., Cacciari, C., Castañeda, J., Chaoul, L., Cheek, N., De Angeli, F., Fabricius, C., Guerra, R., Holl, B., Masana, E., Messineo, R., Mowlavi, N., Nienartowicz, K., Panuzzo, P., Portell, J., Riello, M., Seabroke, G. M., Tanga, P., Thévenin, F., Gracia-Abril, G., Comoretto, G., Garcia-Reinaldos, M., Teyssier, D., Altmann, M., Andrae, R., Audard, M., Bellas-Velidis, I., Benson, K., Berthier, J., Blomme, R., Burgess, P., Busso, G., Carry, B., Cellino, A., Clementini, G., Clotet, M., Creevey, O., Davidson, M., De Ridder, J., Delchambre, L., Dell´Oro, A., Ducourant, C., Fernández-Hernández, J., Fouesneau, M., Frémat, Y., Galluccio, L., García-Torres, M., González-Núñez, J., González-Vidal, J. J., Gosset, E., Guy, L. P., Halbwachs, J.-L., Hambly, N. C., Harrison, D. L., Hernández, J., Hestroffer, D., Hodgkin, S. T., Hutton, A., Jasniewicz, G., Jean-Antoine-Piccolo, A., Jordan, S., Korn, A. J., Krone-Martins, A., Lanzafame, A. C., Lebzelter, T., Löffler, W., Manteiga, M., Marrese, P. M., Martín-Fleitas, J. M., Moitinho, A., Mora, A., Muinonen, K., Osinde, J., Pancino, E., Pauwels, T., Petit, J.-M., Recio-Blanco, A., Richards, P. J., Rimoldini, L., Robin, A. C., Sarro, L. M., Siopis, C., Smith, M., Sozzetti, A., Süveges, M., Torra, J., van Reeven, W., Abbas, U., Abreu Aramburu, A., Accart, S., Aerts, C., Altavilla, G., Álvarez, M. A., Alvarez, R., Alves, J., Anderson, R. I., Andrei, A. H., Anglada Varela, E., Antiche, E., Antoja, T., Arcay, B., Astraatmadja, T. L., Bach, N., Baker, S. G., Balaguer-Núñez, L., Balm, P., Barache, C., Barata, C., Barbato, D., Barblan, F., Barklem, P. S., Barrado, D., Barros, M., Barstow, M. A., Bartholomé Muñoz, S., Bassilana, J.-L., Becciani, U., Bellazzini, M., Berihuete, A., Bertone, S., Bianchi, L., Bienaymé, O., Blanco-Cuaresma, S., Boch, T., Boeche, C., Bombrun, A., Borrachero, R., Bossini, D., Bouquillon, S., Bourda, G., Bragaglia, A., Bramante, L., Breddels, M. A., Bressan, A., Brouillet, N., Brüsemeister, T., Brugaletta, E., Bucciarelli, B., Burlacu, A., Busonero, D., Butkevich, A. G., Buzzi, R., Caffau, E., Cancelliere, R., Cannizzaro, G., Cantat-Gaudin, T., Carballo, R., Carlucci, T., Carrasco, J. M., Casamiquela, L., Castellani, M., Castro-Ginard, A., Charlot, P., Chemin, L., Chiavassa, A., Cocozza, G., Costigan, G., Cowell, S., Crifo, F., Crosta, M., Crowley, C., Cuypers+, J., Dafonte, C., Damerdji, Y., Dapergolas, A., David, P., David, M., de Laverny, P., De Luise, F., De March, R., de Martino, D., de Souza, R., de Torres, A., Debosscher, J., del Pozo, E., Delbo, M., Delgado, A., Delgado, H. E., Di Matteo, P., Diakite, S., Diener, C., Distefano, E., Dolding, C., Drazinos, P., Durán, J., Edvardsson, B., Enke, H., Eriksson, K., Esquej, P., Eynard Bontemps, G., Fabre, C., Fabrizio, M., Faigler, S., Falcão, A. J., Farràs Casas, M., Federici, L., Fedorets, G., Fernique, P., Figueras, F., Filippi, F., Findeisen, K., Fonti, A., Fraile, E., Fraser, M., Frézouls, B., Gai, M., Galleti, S., Garabato, D., García-Sedano, F., Garofalo, A., Garralda, N., Gavel, A., Gavras, P., Gerssen, J., Geyer, R., Giacobbe, P., Gilmore, G., Girona, S., Giuffrida, G., Glass, F., Gomes, M., Granvik,

M., Gueguen, A., Guerrier, A., Guiraud, J., Gutiérrez-Sánchez, R., Haigron, R., Hatzidimitriou, D., Hauser, M., Haywood, M., Heiter, U., Helmi, A., Heu, J., Hilger, T., Hobbs, D., Hofmann, W., Holland, G., Huckle, H. E., Hypki, A., Icardi, V., Janßen, K., Jevardat de Fombelle, G., Jonker, P. G., Juhász, Á. L., Julbe, F., Karampelas, A., Kewley, A., Klar, J., Kochoska, A., Kohley, R., Kolenberg, K., Kontizas, M., Kontizas, E., Koposov, S. E., Kordopatis, G., Kostrzewa-Rutkowska, Z., Koubsky, P., Lambert, S., Lanza, A. F., Lasne, Y., Lavigne, J.-B., Le Fustec, Y., Le Poncin-Lafitte, C., Lebreton, Y., Leccia, S., Leclerc, N., Lecoeur-Taibi, I., Lenhardt, H., Leroux, F., Liao, S., Licata, E., Lindstrøm, H. E. P., Lister, T. A., Livanou, E., Lobel, A., López, M., Managau, S., Mann, R. G., Mantelet, G., Marchal, O., Marchant, J. M., Marconi, M., Marinoni, S., Marschalkó, G., Marshall, D. J., Martino, M., Marton, G., Mary, N., Massari, D., Matijevic, G., Mazeh, T., McMillan, P. J., Messina, S., Michalik, D., Millar, N. R., Molina, D., Molinaro, R., Molnár, L., Montegriffo, P., Mor, R., Morbidelli, R., Morel, T., Morris, D., Mulone, A. F., Muraveva, T., Musella, I., Nelemans, G., Nicastro, L., Noval, L., O´Mullane, W., Ordénovic, C., Ordóñez-Blanco, D., Osborne, P., Pagani, C., Pagano, I., Pailler, F., Palacin, H., Palaversa, L., Panahi, A., Pawlak, M., Piersimoni, A. M., Pineau, F.-X., Plachy, E., Plum, G., Poggio, E., Poujoulet, E., Prsa, A., Pulone, L., Racero, E., Ragaini, S., Rambaux, N., Ramos-Lerate, M., Regibo, S., Reylé, C., Riclet, F., Ripepi, V., Riva, A., Rivard, A., Rixon, G., Roegiers, T., Roelens, M., Romero-Gómez, M., Rowell, N., Royer, F., Ruiz-Dern, L., Sadowski, G., Sagristà Sellés, T., Sahlmann, J., Salgado, J., Salguero, E., Sanna, N., Santana-Ros, T., Sarasso, M., Savietto, H., Schultheis, M., Sciacca, E., Segol, M., Segovia, J. C., Ségransan, D., Shih, I-C., Siltala, L., Silva, A. F., Smart, R. L., Smith, K. W., Solano, E., Solitro, F., Sordo, R., Soria Nieto, S., Souchay, J., Spagna, A., Spoto, F., Stampa, U., Steele, I. A., Steidelmüller, H., Stephenson, C. A., Stoev, H., Suess, F. F., Surdej, J., Szabados, L., Szegedi-Elek, E., Tapiador, D., Taris, F., Tauran, G., Taylor, M. B., Teixeira, R., Terrett, D., Teyssandier, P., Thuillot, W., Titarenko, A., Torra Clotet, F., Turon, C., Ulla, A., Utrilla, E., Uzzi, S., Vaillant, M., Valentini, G., Valette, V., van Elteren, A., Van Hemelryck, E., van Leeuwen, M., Vaschetto, M., Vecchiato, A., Veljanoski, J., Viala, Y., Vicente, D., Vogt, S., von Essen, C., Voss, H., Votruba, V., Voutsinas, S., Walmsley, G., Weiler, M., Wertz, O., Wevers, T., Wyrzykowski, L., Yoldas, A., Zerjal, M., Ziaeepour, H., Zorec, J., Zschocke, S., Zucker, S., Zurbach, C., and Zwitter, T. Gaia data release 2 - summary of the contents and survey properties. *A&A*, 616:A1, 2018. doi: 10.1051/0004-6361/201833051. URL https://doi.org/10.1051/0004-6361/201833051.

Gaia Collaboration, A. G. A. Brown, A. Vallenari, T. Prusti, J. H. J. de Bruijne, C. Babusiaux, and M. Biermann. Gaia Early Data Release 3: Summary of the contents and survey properties. *arXiv e-prints*, art. arXiv:2012.01533, December 2020.

Gaia Collaboration, A. Vallenari, A. G. A. Brown, T. Prusti, J. H. J. de Bruijne, F. Arenou, C. Babusiaux, M. Biermann, O. L. Creevey, C. Ducourant, D. W. Evans, L. Eyer, R. Guerra, A. Hutton, C. Jordi, S. A. Klioner, U. L. Lammers, L. Lindegren, X. Luri, F. Mignard, C. Panem, D. Pourbaix, S. Randich, P. Sartoretti, C. Soubiran, P. Tanga, N. A. Walton, C. A. L. Bailer-Jones, U. Bastian, R. Drimmel, F. Jansen, D. Katz, M. G. Lattanzi, F. van Leeuwen, J. Bakker, C. Cacciari, J. Castañeda, F. De Angeli, C. Fabricius, M. Fouesneau, Y. Frémat, L. Galluccio, A. Guerrier, U. Heiter, E. Masana, R. Messineo, N. Mowlavi, C. Nicolas, K. Nienartowicz, F. Pailler, P. Panuzzo, F. Riclet, W. Roux, G. M. Seabroke, R. Sordoørcit, F. Thévenin, G. Gracia-Abril, J. Portell, D. Teyssier, M. Altmann, R. Andrae, M. Audard, I. Bellas-Velidis, K. Benson, J. Berthier, R. Blomme, P. W. Burgess, D. Busonero, G. Busso, H. Cánovas, B. Carry, A. Cellino, N. Cheek, G. Clementini, Y. Damerdji, M. Davidson, P. de Teodoro, M. Nuñez Campos, L. Delchambre, A. Dell'Oro, P. Esquej, J. Fernández-Hernández, E. Fraile, D. Garabato, P. García-Lario, E. Gosset, R. Haigron, J. L. Halbwachs, N. C. Hambly, D. L. Harrison, J. Hernández, D. Hestroffer, S. T. Hodgkin, B. Holl, K. Janßen, G. Jevardat de Fombelle, S. Jordan, A. Krone-Martins, A. C. Lanzafame, W. Löffler, O. Marchal, P. M. Marrese, A. Moitinho, K. Muinonen, P. Osborne, E. Pancino, T. Pauwels, A. Recio-Blanco, C. Reylé, M. Riello, L. Rimoldini, T. Roegiers, J. Rybizki, L. M. Sarro, C. Siopis, M. Smith, A. Sozzetti, E. Utrilla, M. van Leeuwen, U. Abbas, P. Ábrahám, A. Abreu Aramburu, C. Aerts, J. J. Aguado, M. Ajaj, F. Aldea-Montero, G. Altavilla, M. A. Álvarez, J. Alves, F. Anders, R. I. Anderson, E. Anglada Varela, T. Antoja, D. Baines, S. G. Baker, L. Balaguer-Núñez, E. Balbinot, Z. Balog, C. Barache, D. Barbato, M. Barros, M. A. Barstow, S. Bartolomé, J. L. Bassilana, N. Bauchet, U. Becciani, M. Bellazzini, A. Berihuete, M. Bernet, S. Bertone, L. Bianchi, A. Binnenfeld, S. Blanco-Cuaresma, A. Blazere, T. Boch, A. Bombrun, D. Bossini, S. Bouquillon, A. Bragaglia, L. Bramante, E. Breedt, A. Bressan, N. Brouillet, E. Brugaletta, B. Bucciarelli, A. Burlacu, A. G. Butkevich, R. Buzzi, E. Caffau, R. Cancelliere, T. Cantat-Gaudin, R. Carballo, T. Carlucci, M. I. Carnerero, J. M. Carrasco, L. Casamiquela, M. Castellani, A. Castro-Ginard, L. Chaoul, P. Charlot, L. Chemin, V. Chiaramida, A. Chiavassa, N. Chornay, G. Comoretto, G. Contursi, W. J. Cooper, T. Cornez, S. Cowell, F. Crifo, M. Cropper, M. Crosta, C. Crowley, C. Dafonte, A. Dapergolas, M. David, P. David, P. de Laverny, F. De Luise, R. De March, J. De Ridder, R. de Souza, A. de Torres, E. F. del Peloso, E. del Pozo, M. Delbo, A. Delgado, J. B. Delisle, C. Demouchy, T. E. Dharmawardena, P. Di Matteo, S. Diakite, C. Diener, E. Distefano, C. Dolding, B. Edvardsson, H. Enke, C. Fabre, M. Fabrizio, S. Faigler, G. Fedorets, P. Fernique, A. Fienga, F. Figueras, Y. Fournier, C. Fouron, F. Fragkoudi, M. Gai, A. Garcia-Gutierrez, M. Garcia-Reinaldos, M. García-Torres, A. Garofalo, A. Gavel, P. Gavras, E. Gerlach, R. Geyer, P. Giacobbe, G. Gilmore,

S. Girona, G. Giuffrida, R. Gomel, A. Gomez, J. González-Núñez, I. González-Santamaría, J. J. González-Vidal, M. Granvik, P. Guillout, J. Guiraud, R. Gutiérrez-Sánchez, L. P. Guy, D. Hatzidimitriou, M. Hauser, M. Haywood, A. Helmer, A. Helmi, M. H. Sarmiento, S. L. Hidalgo, T. Hilger, N. Hładczuk, D. Hobbs, G. Holland, H. E. Huckle, K. Jardine, G. Jasniewicz, A. Jean-Antoine Piccolo, Ó. Jiménez-Arranz, A. Jorissen, J. Juaristi Campillo, F. Julbe, L. Karbevska, P. Kervella, S. Khanna, M. Kontizas, G. Kordopatis, A. J. Korn, Á Kóspál, Z. Kostrzewa-Rutkowska, K. Kruszyńska, M. Kun, P. Laizeau, S. Lambert, A. F. Lanza, Y. Lasne, J. F. Le Campion, Y. Lebreton, T. Lebzelter, S. Leccia, N. Leclerc, I. Lecoeur-Taibi, S. Liao, E. L. Licata, H. E. P. Lindstrøm, T. A. Lister, E. Livanou, A. Lobel, A. Lorca, C. Loup, P. Madrero Pardo, A. Magdaleno Romeo, S. Managau, R. G. Mann, M. Manteiga, J. M. Marchant, M. Marconi, J. Marcos, M. M. S. Marcos Santos, D. Marín Pina, S. Marinoni, F. Marocco, D. J. Marshall, L. Martin Polo, J. M. Martín-Fleitas, G. Marton, N. Mary, A. Masip, D. Massari, A. Mastrobuono-Battisti, T. Mazeh, P. J. McMillan, S. Messina, D. Michalik, N. R. Millar, A. Mints, D. Molina, R. Molinaro, L. Molnár, G. Monari, M. Monguió, P. Montegriffo, A. Montero, R. Mor, A. Mora, R. Morbidelli, T. Morel, D. Morris, T. Muraveva, C. P. Murphy, I. Musella, Z. Nagy, L. Noval, F. Ocaña, A. Ogden, C. Ordenovic, J. O. Osinde, C. Pagani, I. Pagano, L. Palaversa, P. A. Palicio, L. Pallas-Quintela, A. Panahi, S. Payne-Wardenaar, X. Peñalosa Esteller, A. Penttilä, B. Pichon, A. M. Piersimoni, F. X. Pineau, E. Plachy, G. Plum, E. Poggio, A. Prša, L. Pulone, E. Racero, S. Ragaini, M. Rainer, C. M. Raiteri, N. Rambaux, P. Ramos, M. Ramos-Lerate, P. Re Fiorentin, S. Regibo, P. J. Richards, C. Rios Diaz, V. Ripepi, A. Riva, H. W. Rix, G. Rixon, N. Robichon, A. C. Robin, C. Robin, M. Roelens, H. R. O. Rogues, L. Rohrbasser, M. Romero-Gómez, N. Rowell, F. Royer, D. Ruz Mieres, K. A. Rybicki, G. Sadowski, A. Sáez Núñez, A. Sagristà Sellés, J. Sahlmann, E. Salguero, N. Samaras, V. Sanchez Gimenez, N. Sanna, R. Santoveña, M. Sarasso, M. Schultheis, E. Sciacca, M. Segol, J. C. Segovia, D. Ségransan, D. Semeux, S. Shahaf, H. I. Siddiqui, A. Siebert, L. Siltala, A. Silvelo, E. Slezak, I. Slezak, R. L. Smart, O. N. Snaith, E. Solano, F. Solitro, D. Souami, J. Souchay, A. Spagna, L. Spina, F. Spoto, I. A. Steele, H. Steidelmüller, C. A. Stephenson, M. Süveges, J. Surdej, L. Szabados, E. Szegedi-Elek, F. Taris, M. B. Taylo, R. Teixeira, L. Tolomei, N. Tonello, F. Torra, J. Torra, G. Torralba Elipe, M. Trabucchi, A. T. Tsounis, C. Turon, A. Ulla, N. Unger, M. V. Vaillant, E. van Dillen, W. van Reeven, O. Vanel, A. Vecchiato, Y. Viala, D. Vicente, S. Voutsinas, M. Weiler, T. Wevers, L. Wyrzykowski, A. Yoldas, P. Yvard, H. Zhao, J. Zorec, S. Zucker, and T. Zwitter. Gaia Data Release 3: Summary of the content and survey properties. *arXiv e-prints*, art. arXiv:2208.00211, July 2022.

F. Gallet and J. Bouvier. Improved angular momentum evolution model for solar-like stars. *Astron. Astrophys.*, 556:A36, aug 2013. ISSN 0004-6361. doi: 10.1051/0004-6361/

201321302. URL http://www.aanda.org/10.1051/0004-6361/201321302.

F. Gallet and J. Bouvier. Improved angular momentum evolution model for solar-like stars - ii. exploring the mass dependence. *A&A*, 577:A98, 2015. doi: 10.1051/0004-6361/201525660. URL https://doi.org/10.1051/0004-6361/201525660.

F. Gallet, C. Zanni, and L. Amard. Rotational evolution of solar-type protostars during the star-disk interaction phase. A&A, 632:A6, December 2019. doi: 10.1051/0004-6361/201935432.

Ana E. García Pérez, Carlos Allende Prieto, Jon A. Holtzman, Matthew Shetrone, Szabolcs Mészáros, Dmitry Bizyaev, Ricardo Carrera, Katia Cunha, D. A. García-Hernández, Jennifer A. Johnson, Steven R. Majewski, David L. Nidever, Ricardo P. Schiavon, Neville Shane, Verne V. Smith, Jennifer Sobeck, Nicholas Troup, Olga Zamora, David H. Weinberg, Jo Bovy, Daniel J. Eisenstein, Diane Feuillet, Peter M. Frinchaboy, Michael R. Hayden, Fred R. Hearty, Duy C. Nguyen, Robert W. O'Connell, Marc H. Pinsonneault, John C. Wilson, and Gail Zasowski. ASPCAP: The APOGEE Stellar Parameter and Chemical Abundances Pipeline. AJ, 151(6):144, June 2016. doi: 10.3847/0004-6256/151/6/144.

Cecilia Garraffo, Jeremy J. Drake, and Ofer Cohen. MAGNETIC COMPLEXITY AS AN EXPLANATION FOR BIMODAL ROTATION POPULATIONS AMONG YOUNG STARS. *The Astrophysical Journal*, 807(1):L6, jun 2015. doi: 10.1088/2041-8205/807/1/l6. URL https://doi.org/10.1088/2041-8205/807/1/l6.

Lukas Gehrig, Daniel Steiner, Eduard Vorobyov, and Manuel Güdel. Time-dependent, long-term hydrodynamic simulations of the inner protoplanetary disk II: The importance of stellar rotation. *arXiv e-prints*, art. arXiv:2208.08852, August 2022.

P. Ghosh and F. K. Lamb. Disk accretion by magnetic neutron stars. ApJ, 223:L83–L87, July 1978. doi: 10.1086/182734.

P. Ghosh and F. K. Lamb. Accretion by rotating magnetic neutron stars. III. Accretion torques and period changes in pulsating X-ray sources. ApJ, 234:296–316, November 1979. doi: 10.1086/157498.

Steven H. Gilhool, Cullen H. Blake, Ryan C. Terrien, Chad Bender, Suvrath Mahadevan, and Rohit Deshpande. The Rotation of M Dwarfs Observed by the Apache Point Galactic Evolution Experiment. AJ, 155(1):38, January 2018. doi: 10.3847/1538-3881/aa9c7c.

Diego Godoy-Rivera, Marc H. Pinsonneault, and Luisa M. Rebull. Stellar Rotation in the Gaia Era: Revised Open Clusters Sequences. *arXiv e-prints*, art. arXiv:2101.01183, January 2021.

A. Gonneau, M. Lyubenova, A. Lançon, S. C. Trager, R. F. Peletier, A. Arentsen, Y. P. Chen, P. R. T. Coelho, M. Dries, J. Falcón-Barroso, P. Prugniel, P. Sánchez-Blázquez, A. Vazdekis, and K. Verro. The X-shooter Spectral Library (XSL): Data release 2. A&A, 634:A133, February 2020. doi: 10.1051/0004-6361/201936825.

Josefa E. Großschedl, João Alves, Stefan Meingast, Christine Ackerl, Joana Ascenso, Hervé Bouy, Andreas Burkert, Jan Forbrich, Verena Fürnkranz, Alyssa Goodman, Álvaro Hacar, Gabor Herbst-Kiss, Charles J. Lada, Irati Larreina, Kieran Leschinski, Marco Lombardi, André Moitinho, Daniel Mortimer, and Eleonora Zari. 3D shape of Orion A from Gaia DR2. A&A, 619:A106, November 2018. doi: 10.1051/0004-6361/201833901.

Erik Gullbring, Lee Hartmann, Cesar Briceño, and Nuria Calvet. Disk Accretion Rates for T Tauri Stars. ApJ, 492(1):323–341, January 1998. doi: 10.1086/305032.

Patrick Hartigan, Suzan Edwards, and Louma Ghandour. Disk Accretion and Mass Loss from Young Stars. ApJ, 452:736, October 1995. doi: 10.1086/176344.

J. D. Hartman, G. Á. Bakos, G. Kovács, and R. W. Noyes. A large sample of photometric rotation periods for FGK Pleiades stars. *Monthly Notices of the Royal Astronomical Society*, 408(1):475–489, 08 2010. ISSN 0035-8711. doi: 10.1111/j.1365-2966.2010.17147.x. URL https://doi.org/10.1111/j.1365-2966.2010.17147.x.

L. Hartmann and J. R. Stauffer. Additional Measurements of Pre-Main-Sequence Stellar Rotation. AJ, 97:873, March 1989. doi: 10.1086/115033.

L. Hartmann, E. Avrett, and S. Edwards. Wave-driven winds from cool stars. II - Models for T Tauri stars. ApJ, 261:279–292, October 1982. doi: 10.1086/160339.

Lee Hartmann, Gregory Herczeg, and Nuria Calvet. Accretion onto pre-main-sequence stars. *Annual Review of Astronomy and Astrophysics*, 54(1):135–180, 2016. doi: 10.1146/annurev-astro-081915-023347. URL https://doi.org/10.1146/annurev-astro-081915-023347.

W. Herbst, C. A. L. Bailer-Jones, R. Mundt, K. Meisenheimer, and R. Wackermann. Stellar rotation and variability in the orion nebula cluster ***. *A&A*, 396(2):513–532, 2002. doi: 10.1051/0004-6361:20021362. URL https://doi.org/10.1051/0004-6361:20021362.

Gregory J. Herczeg and Lynne A. Hillenbrand. UV Excess Measures of Accretion onto Young Very Low Mass Stars and Brown Dwarfs. ApJ, 681(1):594–625, July 2008. doi: 10.1086/586728.

Gregory J. Herczeg, Yuguang Chen, Jean-Francois Donati, Andrea K. Dupree, Frederick M. Walter, Lynne A. Hillenbrand, Christopher M. Johns-Krull, Carlo F. Manara, Hans Moritz Guenther, Min Fang, P. Christian Schneider, Jeff A. Valenti, Silvia H. P. Alencar, Laura Venuti, Juan Manuel Alcala, Antonio Frasca, Nicole Arulanantham, Jeffrey L. Linsky, Jerome Bouvier, Nancy S. Brickhouse, Nuria Calvet, Catherine C. Espaillat, Justyn Campbell-White, John M. Carpenter, Seok-Jun Chang, Kelle L. Cruz, S. E. Dahm, Jochen Eisloeffel, Suzan Edwards, William J. Fischer, Zhen Guo, Thomas Henning, Tao Ji, Jesse Jose, Joel H. Kastner, Ralf Launhardt, David A. Principe, Conner E. Robinson, Javier Serna, Michal Siwak, Michael F. Sterzik, and Shinsuke Takasao. Twenty-Five Years of Accretion onto the Classical T Tauri Star TW Hya. *arXiv e-prints*, art. arXiv:2308.14590, August 2023. doi: 10.48550/arXiv.2308.14590.

J. Hernandez, C. Briceño, N. Calvet, L. Hartmann, P. Berlind, and K. Luhman. SPTCLASS: SPecTral CLASSificator code, May 2017.

Jesús Hernández, Nuria Calvet, César Briceño, Lee Hartmann, and Perry Berlind. Spectral Analysis and Classification of Herbig Ae/Be Stars. AJ, 127(3):1682–1701, March 2004. doi: 10.1086/381908.

Jesus Hernandez, L. Hartmann, T. Megeath, R. Gutermuth, J. Muzerolle, N. Calvet, A. K. Vivas, C. Briceno, L. Allen, J. Stauffer, E. Young, and G. Fazio. ASpitzer space TelescopeStudy of disks in the young orionis cluster. *The Astrophysical Journal*, 662(2):1067–1081, jun 2007. doi: 10.1086/513735. URL https://doi.org/10.1086%2F513735.

Jesús Hernández, Lee Hartmann, Nuria Calvet, R. D. Jeffries, R. Gutermuth, J. Muzerolle, and J. Stauffer. A Spitzer View of Protoplanetary Disks in the γ Velorum Cluster. ApJ, 686(2):1195–1208, October 2008. doi: 10.1086/591224.

Jesús Hernández, Nuria Calvet, Alice Perez, Cesar Briceño, Lorenzo Olguin, Maria E. Contreras, Lee Hartmann, Lori Allen, Catherine Espaillat, and Ramírez Hernan. A SPECTROSCOPIC CENSUS IN YOUNG STELLAR REGIONS: THE ORIONIS CLUSTER. *The Astrophysical Journal*, 794(1):36, sep 2014. doi: 10.1088/0004-637x/794/1/36. URL https://doi.org/10.1088%2F0004-637x%2F794%2F1%2F36.

Jesús Hernández, Luisa F. Zamudio, César Briceño, Nuria Calvet, Zhaohuan Zhu, Haibo Yuan, Xiaowei Liu, Ezequiel Manzo-Martínez, Carlos G. Román-Zúñiga, Javier Serna, Karina Maucó, and Lucía Adame. A lamost spectroscopic study of t tauri stars in the orion ob1a subassociation. *The Astronomical Journal*, 165(5):205, apr 2023. doi: 10.3847/1538-3881/acc467. URL https://dx.doi.org/10.3847/1538-3881/acc467.

P. C. Hinton, Kevin France, Maria Gracia Batista, Javier Serna, Jesús Hernández, Hans Moritz Günther, Adam F. Kowalski, and P. Christian Schneider. Far-ultraviolet flares on accreting protostars: Weak and classical t tauri stellar pair analysis. *The Astrophysical Journal*, 939(2):82, nov 2022. doi: 10.3847/1538-4357/ac8f26. URL https://dx.doi.org/10.3847/1538-4357/ac8f26.

T. O. Husser, S. Wende-von Berg, S. Dreizler, D. Homeier, A. Reiners, T. Barman, and P. H. Hauschildt. A new extensive library of PHOENIX stellar atmospheres and synthetic spectra. A&A, 553:A6, May 2013. doi: 10.1051/0004-6361/201219058.

Jr. Iben, Icko. Stellar Evolution. I. The Approach to the Main Sequence. ApJ, 141:993, April 1965. doi: 10.1086/148193.

Laura Ingleby, Nuria Calvet, Gregory Herczeg, Alex Blaty, Frederick Walter, David Ardila, Richard Alexander, Suzan Edwards, Catherine Espaillat, Scott G. Gregory, Lynne Hillenbrand, and Alexander Brown. ACCRETION RATES FOR t TAURI STARS USING NEARLY SIMULTANEOUS ULTRAVIOLET AND OPTICAL SPECTRA. *The Astrophysical Journal*, 767(2):112, apr 2013. doi: 10.1088/0004-637x/767/2/112. URL https://doi.org/10.1088/0004-637x/767/2/112.

Lewis G. Ireland, Claudio Zanni, Sean P. Matt, and George Pantolmos. Magnetic braking of accreting t tauri stars: Effects of mass accretion rate, rotation, and dipolar field strength. *The Astrophysical Journal*, 906(1):4, dec 2020. doi: 10.3847/1538-4357/abc828. URL https://doi.org/10.3847/1538-4357/abc828.

R. J. Jackson and R. D. Jeffries. The effect of starspots on the radii of low-mass pre-main-sequence stars. MNRAS, 441(3):2111–2123, July 2014. doi: 10.1093/mnras/stu651.

Jackson, R. J., Jeffries, R. D., Randich, S., Bragaglia, A., Carraro, G., Costado, M. T., Flaccomio, E., Lanzafame, A. C., Lardo, C., Monaco, L., Morbidelli, L., Smiljanic, R., and Zaggia, S. The gaia-eso survey: Stellar radii in the young open clusters ngc 2264, ngc 2547, and ngc 2516. *A&A*, 586:A52, 2016. doi: 10.1051/0004-6361/201527507. URL https://doi.org/10.1051/0004-6361/201527507.

Karl Jaehnig, Garrett Somers, and Keivan G. Stassun. Radius Inflation at Low Rossby Number in the Hyades Cluster. ApJ, 879(1):39, July 2019. doi: 10.3847/1538-4357/ab21cf.

T Jayasinghe, C S Kochanek, K Z Stanek, B J Shappee, T W-S Holoien, Toda A Thompson, J L Prieto, Subo Dong, M Pawlak, J V Shields, G Pojmanski, S Otero, C A Britt, and D Will. The ASAS-SN catalogue of variable stars I: The Serendipitous Survey. *Monthly*

Notices of the Royal Astronomical Society, 477(3):3145–3163, 04 2018. ISSN 0035-8711. doi: 10.1093/mnras/sty838. URL https://doi.org/10.1093/mnras/sty838.

T Jayasinghe, K Z Stanek, C S Kochanek, B J Shappee, T W-S Holoien, Todd A Thompson, J L Prieto, Subo Dong, M Pawlak, O Pejcha, J V Shields, G Pojmanski, S Otero, C A Britt, and D Will. The ASAS-SN catalogue of variable stars – II. Uniform classification of 412000 known variables. *Monthly Notices of the Royal Astronomical Society*, 486(2): 1907–1943, 03 2019. ISSN 0035-8711. doi: 10.1093/mnras/stz844. URL https://doi.org/10.1093/mnras/stz844.

Ray Jayawardhana, Jaime Coffey, Alexander Scholz, Alexis Brandeker, and Marten H. van Kerkwijk. Accretion disks around young stars: Lifetimes, disk locking, and variability. *The Astrophysical Journal*, 648(2):1206–1218, sep 2006. doi: 10.1086/506171. URL https://doi.org/10.1086%2F506171.

Christopher M. Johns-Krull. The magnetic fields of classical t tauri stars. *The Astrophysical Journal*, 664(2):975–985, aug 2007. doi: 10.1086/519017. URL https://doi.org/10.1086/519017.

Md Tanveer Karim, Keivan G. Stassun, César Briceño, A. Katherina Vivas, Stefanie Raetz, Cecilia Mateu, Juan José Downes, Nuria Calvet, Jesús Hernández, Ralph Neuhäuser, Markus Mugrauer, Hidenori Takahashi, Kengo Tachihara, Rolf Chini, Gustavo A. Cruz-Dias, Alicia Aarnio, David J. James, and Moritz Hackstein. THE ROTATION PERIOD DISTRIBUTIONS OF 4–10 Myr T TAURI STARS IN ORION OB1: NEW CONSTRAINTS ON PRE-MAIN-SEQUENCE ANGULAR MOMENTUM EVOLUTION. *Astron. J.*, 152(6):198, dec 2016. ISSN 0004-6256. doi: 10.3847/0004-6256/152/6/198. URL http://stacks.iop.org/1538-3881/152/i=6/a=198?key=crossref.021d053a2d6873d4c74412f78b5b73a5.

W. Kausch, S. Noll, A. Smette, Kimeswenger, S., Barden, M., Szyszka, C., Jones, A. M., Sana, H., Horst, H., and Kerber, F. Molecfit: A general tool for telluric absorption correction - ii. quantitative evaluation on eso-vlt/x-shooterspectra. *A&A*, 576:A78, 2015. doi: 10.1051/0004-6361/201423909. URL https://doi.org/10.1051/0004-6361/201423909.

Steven D. Kawaler. Angular momentum in stars - the kraft curve revisited. *Publications of the Astronomical Society of the Pacific*, 99:1322, dec 1987. doi: 10.1086/132120. URL https://doi.org/10.1086/132120.

Steven D. Kawaler. Angular momentum loss in low-mass stars. *Astrophys. J.*, 333:236, oct 1988. ISSN 0004-637X. doi: 10.1086/166740. URL http://adsabs.harvard.edu/doi/10.1086/166740.

Aurora Y. Kesseli, Philip S. Muirhead, Andrew W. Mann, and Greg Mace. Magnetic Inflation and Stellar Mass. II. On the Radii of Single, Rapidly Rotating, Fully Convective M-Dwarf Stars. AJ, 155(6):225, June 2018. doi: 10.3847/1538-3881/aabccb.

Arieh Koenigl. Disk Accretion onto Magnetic T Tauri Stars. ApJ, 370:L39, March 1991. doi: 10.1086/185972.

Marina Kounkel and Kevin Covey. Untangling the galaxy. i. local structure and star formation history of the milky way. *The Astronomical Journal*, 158(3):122, aug 2019. doi: 10.3847/1538-3881/ab339a. URL https://dx.doi.org/10.3847/1538-3881/ab339a.

Marina Kounkel, Lee Hartmann, Laurent Loinard, Gisela N. Ortiz-León, Amy J. Mioduszewski, Luis F. Rodríguez, Sergio A. Dzib, Rosa M. Torres, Gerardo Pech, Phillip A. B. Galli, Juana L. Rivera, Andrew F. Boden, Neal J. Evans II, Cesar Briceño, and John J. Tobin. THE GOULD's BELT DISTANCES SURVEY (GOBELINS). II. DISTANCES AND STRUCTURE TOWARD THE ORION MOLECULAR CLOUDS. *The Astrophysical Journal*, 834(2):142, jan 2017. doi: 10.3847/1538-4357/834/2/142. URL https://doi.org/10.3847%2F1538-4357%2F834%2F2%2F142.

Marina Kounkel, Kevin Covey, Genaro Suárez, Carlos Román-Zúñiga, Jesus Hernandez, Keivan Stassun, Karl O Jaehnig, Eric D. Feigelson, Karla Peña Ramírez, Alexandre Roman-Lopes, Nicola Da Rio, Guy S Stringfellow, J. Serena Kim, Jura Borissova, José G. Fernández-Trincado, Adam Burgasser, D. A. García-Hernández, Olga Zamora, Kaike Pan, and Christian Nitschelm. The APOGEE-2 survey of the orion star-forming complex. II. six-dimensional structure. *The Astronomical Journal*, 156(3):84, aug 2018. doi: 10.3847/1538-3881/aad1f1. URL https://doi.org/10.3847%2F1538-3881%2Faad1f1.

Marina Kounkel, Kevin Covey, Maxwell Moe, Kaitlin M. Kratter, Genaro Suárez, Keivan G. Stassun, Carlos Román-Zúñiga, Jesus Hernand ez, Jinyoung Serena Kim, Karla Peña Ramírez, Alexandre Roman-Lopes, Guy S. Stringfellow, Karl O. Jaehnig, Jura Borissova, Benjamin Tofflemire, Daniel Krolikowski, Aaron Rizzuto, Adam Kraus, Carles Badenes, Penélope Longa-Peña, Yilen Gómez Maqueo Chew, Rodolfo Barba, David L. Nidever, Cody Brown, Nathan De Lee, Kaike Pan, Dmitry Bizyaev, Daniel Oravetz, and Audrey Oravetz. Close Companions around Young Stars. AJ, 157(5):196, May 2019. doi: 10.3847/1538-3881/ab13b1.

Marina Kounkel, Kevin R. Covey, Keivan G. Stassun, Adrian M. Price-Whelan, Jon Holtzman, Drew Chojnowski, Penélope Longa-Peña, Carlos G. Román-Zúñiga, Jesus Hernandez, Javier Serna, Carles Badenes, Nathan De Lee, Steven Majewski, Guy S. Stringfellow, Kaitlin M. Kratter, Maxwell Moe, Peter M. Frinchaboy, Rachael L. Beaton, José G.

Fernández-Trincado, Suvrath Mahadevan, Dante Minniti, Timothy C. Beers, Donald P. Schneider, Rodolfo Barba, Joel R. Brownstein, Domingo Aníbal García-Hernández, Kaike Pan, and Dmitry Bizyaev. Double-lined spectroscopic binaries in the APOGEE DR16 and DR17 data. *The Astronomical Journal*, 162(5):184, oct 2021. doi: 10.3847/1538-3881/ac1798. URL https://doi.org/10.3847/1538-3881/ac1798.

Marina Kounkel, Keivan G. Stassun, Luke G. Bouma, Kevin Covey, Lynne A. Hillenbrand, and Jason Lee Curtis. Untangling the galaxy. iv. empirical constraints on angular momentum evolution and gyrochronology for young stars in the field. *The Astronomical Journal*, 164(4):137, sep 2022. doi: 10.3847/1538-3881/ac866d. URL https://dx.doi.org/10.3847/1538-3881/ac866d.

Marina Kounkel, Keivan G. Stassun, Lynne A. Hillenbrand, Jesús Hernández, Javier Serna, and Jason Lee Curtis. Measurement of the angular momenta of pre-main-sequence stars: Early evolution of slow and fast rotators and empirical constraints on spin-down torque mechanisms. *The Astronomical Journal*, 165(4):182, mar 2023. doi: 10.3847/1538-3881/acc2bd. URL https://dx.doi.org/10.3847/1538-3881/acc2bd.

Marina Kounkel, Eleonora Zari, Kevin Covey, Andrew Tkachenko, Carlos Román Zúñiga, Keivan Stassun, Amelia M. Stutz, Guy Stringfellow, Alexandre Roman-Lopes, Jesús Hernández, Karla Peña Ramírez, Amelia Bayo, Jinyoung Serena Kim, Lyra Cao, Scott J. Wolk, Juna Kollmeier, Ricardo López-Valdivia, and Bárbara Rojas-Ayala. ABYSS I: Targeting strategy for APOGEE & BOSS young star survey in SDSS-V. *arXiv e-prints*, art. arXiv:2301.07186, January 2023. doi: 10.48550/arXiv.2301.07186.

L. V. Kuhi. Mass Loss from T Tauri Stars. ApJ, 140:1409, November 1964. doi: 10.1086/148047.

Michael A. Kuhn, Lynne A. Hillenbrand, Alison Sills, Eric D. Feigelson, and Konstantin V. Getman. Kinematics in Young Star Clusters and Associations with Gaia DR2. ApJ, 870 (1):32, January 2019. doi: 10.3847/1538-4357/aaef8c.

Ryuichi Kurosawa and M. M. Romanova. Spectral variability of classical T Tauri stars accreting in an unstable regime. MNRAS, 431(3):2673–2689, May 2013. doi: 10.1093/mnras/stt365.

N. R. Landin, L. T. S. Mendes, L. P. R. Vaz, and S. H. P. Alencar. Stellar models simulating the disk-locking mechanism and the evolutionary history of the orion nebula cluster and ngc4. *A&A*, 586:A96, 2016. doi: 10.1051/0004-6361/201525851. URL https://doi.org/10.1051/0004-6361/201525851.

A. C. Lanzafame, F. Spada, and E. Distefano. Evidence of radius inflation in stars approaching the slow-rotator sequence. A&A, 597:A63, January 2017. doi: 10.1051/0004-6361/201628833.

A. Lavail, O. Kochukhov, G. A. J. Hussain, E. Alecian, G. J. Herczeg, and C. Johns-Krull. Magnetic fields of intermediate mass T Tauri stars. A&A, 608:A77, December 2017. doi: 10.1051/0004-6361/201731889.

A. Lavail, O. Kochukhov, and G. A. J. Hussain. Characterising the surface magnetic fields of T Tauri stars with high-resolution near-infrared spectroscopy. A&A, 630:A99, October 2019. doi: 10.1051/0004-6361/201935695.

L. Lindegren, U. Bastian, M. Biermann, A. Bombrun, A. de Torres, E. Gerlach, R. Geyer, J. Hernández, T. Hilger, D. Hobbs, S. A. Klioner, U. Lammers, P. J. McMillan, M. Ramos-Lerate, H. Steidelmüller, C. A. Stephenson, and F. van Leeuwen. Gaia Early Data Release 3: Parallax bias versus magnitude, colour, and position. *arXiv e-prints*, art. arXiv:2012.01742, December 2020a.

L. Lindegren, S. A. Klioner, J. Hernández, A. Bombrun, M. Ramos-Lerate, H. Steidelmüller, U. Bastian, M. Biermann, A. de Torres, E. Gerlach, R. Geyer, T. Hilger, D. Hobbs, U. Lammers, P. J. McMillan, C. A. Stephenson, J. Castañeda, M. Davidson, C. Fabricius, G. Gracia-Abril, J. Portell, N. Rowell, D. Teyssier, F. Torra, S. Bartolomé, M. Clotet, N. Garralda, J. J. González-Vidal, J. Torra, U. Abbas, M. Altmann, E. Anglada Varela, L. Balaguer-Núñez, Z. Balog, C. Barache, U. Becciani, M. Bernet, S. Bertone, L. Bianchi, S. Bouquillon, A. G. A. Brown, B. Bucciarelli, D. Busonero, A. G. Butkevich, R. Buzzi, R. Cancelliere, T. Carlucci, P. Charlot, M. R. L. Cioni, M. Crosta, C. Crowley, E. F. del Peloso, E. del Pozo, R. Drimmel, P. Esquej, A. Fienga, E. Fraile, M. Gai, M. Garcia-Reinaldos, R. Guerra, N. C. Hambly, M. Hauser, K. Janßen, S. Jordan, Z. Kostrzewa-Rutkowska, M. G. Lattanzi, S. Liao, E. Licata, T. A. Lister, W. Löffler, J. M. Marchant, A. Masip, F. Mignard, A. Mints, D. Molina, A. Mora, R. Morbidelli, C. P. Murphy, C. Pagani, P. Panuzzo, X. Peñalosa Esteller, E. Poggio, P. Re Fiorentin, A. Riva, A. Sagristà Sellés, V. Sanchez Gimenez, M. Sarasso, E. Sciacca, H. I. Siddiqui, R. L. Smart, D. Souami, A. Spagna, I. A. Steele, F. Taris, E. Utrilla, W. van Reeven, and A. Vecchiato. Gaia Early Data Release 3: The astrometric solution. *arXiv e-prints*, art. arXiv:2012.03380, December 2020b.

L. Lindegren, U. Bastian, M. Biermann, A. Bombrun, A. de Torres, E. Gerlach, R. Geyer, J. Hernández, T. Hilger, D. Hobbs, S. A. Klioner, U. Lammers, P. J. McMillan, M. Ramos-Lerate, H. Steidelmüller, C. A. Stephenson, and F. van Leeuwen. Gaia Early Data Release

3. Parallax bias versus magnitude, colour, and position. A&A, 649:A4, May 2021. doi: 10.1051/0004-6361/202039653.

S. P. Littlefair. Angular momentum evolution of young stars. *Proceedings of the International Astronomical Union*, 9(S302):91–99, 2013. doi: 10.1017/S1743921314001793.

Chao Liu, Jianning Fu, Jianrong Shi, Hong Wu, Zhanwen Han, Li Chen, Subo Dong, Yongheng Zhao, Jian-Jun Chen, Haotong Zhang, Zhong-Rui Bai, Xuefei Chen, Wenyuan Cui, Bing Du, Chih-Hao Hsia, Deng-Kai Jiang, Jinliang Hou, Wen Hou, Haining Li, Jiao Li, Lifang Li, Jiaming Liu, Jifeng Liu, A-Li Luo, Juan-Juan Ren, Hai-Jun Tian, Hao Tian, Jia-Xin Wang, Chao-Jian Wu, Ji-Wei Xie, Hong-Liang Yan, Fan Yang, Jincheng Yu, Bo Zhang, Huawei Zhang, Li-Yun Zhang, Wei Zhang, Gang Zhao, Jing Zhong, Weikai Zong, and Fang Zuo. LAMOST Medium-Resolution Spectroscopic Survey (LAMOST-MRS): Scientific goals and survey plan. *arXiv e-prints*, art. arXiv:2005.07210, May 2020.

N. R. Lomb. Least-Squares Frequency Analysis of Unequally Spaced Data. Ap&SS, 39(2): 447–462, February 1976. doi: 10.1007/BF00648343.

K. L. Luhman and T. L. Esplin. Refining the Census of the Upper Scorpius Association with Gaia. AJ, 160(1):44, July 2020. doi: 10.3847/1538-3881/ab9599.

A-Li Luo, Yong-Heng Zhao, Gang Zhao, Li-Cai Deng, Xiao-Wei Liu, Yi-Peng Jing, Gang Wang, Hao-Tong Zhang, Jian-Rong Shi, Xiang-Qun Cui, Yao-Quan Chu, Guo-Ping Li, Zhong-Rui Bai, Yue Wu, Yan Cai, Shu-Yun Cao, Zi-Huang Cao, Jeffrey L. Carlin, Hai-Yuan Chen, Jian-Jun Chen, Kun-Xin Chen, Li Chen, Xue-Lei Chen, Xiao-Yan Chen, Ying Chen, Norbert Christlieb, Jia-Ru Chu, Chen-Zhou Cui, Yi-Qiao Dong, Bing Du, Dong-Wei Fan, Lei Feng, Jian-Ning Fu, Peng Gao, Xue-Fei Gong, Bo-Zhong Gu, Yan-Xin Guo, Zhan-Wen Han, Bo-Liang He, Jin-Liang Hou, Yong-Hui Hou, Wen Hou, Hong-Zhuan Hu, Ning-Sheng Hu, Zhong-Wen Hu, Zhi-Ying Huo, Lei Jia, Fang-Hua Jiang, Xiang Jiang, Zhi-Bo Jiang, Ge Jin, Xiao Kong, Xu Kong, Ya-Juan Lei, Ai-Hua Li, Chang-Hua Li, Guang-Wei Li, Hai-Ning Li, Jian Li, Qi Li, Shuang Li, Sha-Sha Li, Xin-Nan Li, Yan Li, Yin-Bi Li, Ye-Ping Li, Yuan Liang, Chien-Cheng Lin, Chao Liu, Gen-Rong Liu, Guan-Qun Liu, Zhi-Gang Liu, Wen-Zhi Lu, Yu Luo, Yin-Dun Mao, Heidi Newberg, Ji-Jun Ni, Zhao-Xiang Qi, Yong-Jun Qi, Shi-Yin Shen, Huo-Ming Shi, Jing Song, Yi-Han Song, Ding-Qiang Su, Hong-Jun Su, Zheng-Hong Tang, Qing-Sheng Tao, Yuan Tian, Dan Wang, Da-Qi Wang, Feng-Fei Wang, Guo-Min Wang, Hai Wang, Hong-Chi Wang, Jian Wang, Jia-Ning Wang, Jian-Ling Wang, Jian-Ping Wang, Jun-Xian Wang, Lei Wang, Meng-Xin Wang, Shou-Guan Wang, Shu-Qing Wang, Xia Wang, Ya-Nan Wang, You Wang, Yue-Fei Wang, You-Fen Wang, Peng Wei, Ming-Zhi Wei, Hong Wu, Ke-Fei Wu, Xue-Bing Wu, Yu-Zhong Wu, Xiao-Zheng Xing, Ling-Zhe Xu, Xin-Qi Xu, Yan Xu, Tai-Sheng Yan, De-Hua Yang,

Hai-Feng Yang, Hui-Qin Yang, Ming Yang, Zheng-Qiu Yao, Yong Yu, Hui Yuan, Hai-Bo Yuan, Hai-Long Yuan, Wei-Min Yuan, Chao Zhai, En-Peng Zhang, Hua-Wei Zhang, Jian-Nan Zhang, Li-Pin Zhang, Wei Zhang, Yong Zhang, Yan-Xia Zhang, Zheng-Chao Zhang, Ming Zhao, Fang Zhou, Xu Zhou, Jie Zhu, Yong-Tian Zhu, Si-Cheng Zou, and Fang Zuo. The first data release (DR1) of the LAMOST regular survey. *Research in Astronomy and Astrophysics*, 15(8):1095–1124, jul 2015. doi: 10.1088/1674-4527/15/8/002. URL https://doi.org/10.1088/1674-4527/15/8/002.

K. B. MacGregor and M. Brenner. Rotational Evolution of Solar-Type Stars. I. Main-Sequence Evolution. ApJ, 376:204, July 1991. doi: 10.1086/170269.

Steven R. Majewski, Ricardo P. Schiavon, Peter M. Frinchaboy, Carlos Allende Prieto, Robert Barkhouser, Dmitry Bizyaev, Basil Blank, Sophia Brunner, Adam Burton, Ricardo Carrera, S. Drew Chojnowski, Kátia Cunha, Courtney Epstein, Greg Fitzgerald, Ana E. García Pérez, Fred R. Hearty, Chuck Henderson, Jon A. Holtzman, Jennifer A. Johnson, Charles R. Lam, James E. Lawler, Paul Maseman, Szabolcs Mészáros, Matthew Nelson, Duy Coung Nguyen, David L. Nidever, Marc Pinsonneault, Matthew Shetrone, Stephen Smee, Verne V. Smith, Todd Stolberg, Michael F. Skrutskie, Eric Walker, John C. Wilson, Gail Zasowski, Friedrich Anders, Sarbani Basu, Stephane Beland, Michael R. Blanton, Jo Bovy, Joel R. Brownstein, Joleen Carlberg, William Chaplin, Cristina Chiappini, Daniel J. Eisenstein, Yvonne Elsworth, Diane Feuillet, Scott W. Fleming, Jessica Galbraith-Frew, Rafael A. García, D. Aníbal García-Hernández, Bruce A. Gillespie, Léo Girardi, James E. Gunn, Sten Hasselquist, Michael R. Hayden, Saskia Hekker, Inese Ivans, Karen Kinemuchi, Mark Klaene, Suvrath Mahadevan, Savita Mathur, Benoît Mosser, Demitri Muna, Jeffrey A. Munn, Robert C. Nichol, Robert W. O'Connell, John K. Parejko, A. C. Robin, Helio Rocha-Pinto, Matthias Schultheis, Aldo M. Serenelli, Neville Shane, Victor Silva Aguirre, Jennifer S. Sobeck, Benjamin Thompson, Nicholas W. Troup, David H. Weinberg, and Olga Zamora. The Apache Point Observatory Galactic Evolution Experiment (APOGEE). AJ, 154(3):94, September 2017. doi: 10.3847/1538-3881/aa784d.

Russell B. Makidon, Luisa M. Rebull, Stephen E. Strom, Mark T. Adams, and Brian M. Patten. Periodic Variability of Pre-Main-Sequence Stars in the NGC 2264 OB Association. AJ, 127(4):2228–2245, April 2004. doi: 10.1086/382237.

Ezequiel Manzo-Martínez, Nuria Calvet, Jesús Hernández, Susana Lizano, Ramiro Franco Hernández, Christopher J. Miller, Karina Maucó, César Briceño, and Paola D'Alessio. The Evolution of the Inner Regions of Protoplanetary Disks. ApJ, 893(1):56, April 2020. doi: 10.3847/1538-4357/ab7ead.

Paola Marigo, Léo Girardi, Alessandro Bressan, Philip Rosenfield, Bernhard Aringer, Yang Chen, Marco Dussin, Ambra Nanni, Giada Pastorelli, Thaíse S. Rodrigues, Michele Trabucchi, Sara Bladh, Julianne Dalcanton, Martin A. T. Groenewegen, Josefina Montalbán, and Peter R. Wood. A NEW GENERATION OF PARSEC - COLIBRI STELLAR ISOCHRONES INCLUDING THE TP-AGB PHASE. *Astrophys. J.*, 835(1):77, jan 2017. ISSN 1538-4357. doi: 10.3847/1538-4357/835/1/77. URL http://stacks.iop.org/0004-637X/835/i=1/a=77?key=crossref.68976da918015dcc0c625fe9f2ee0432.

Marilli, E., Frasca, A., Covino, E., Alcalá, J. M., Catalano, S., Fernández, M., Arellano Ferro, A., Rubio-Herrera, E., and Spezzi, L. Rotational periods of solar-mass young stars in orion ***. *A&A*, 463(3):1081–1091, 2007. doi: 10.1051/0004-6361:20066458. URL https://doi.org/10.1051/0004-6361:20066458.

Paul Marjoram, Steven Hamblin, and Brad Foley. Simulation-based bayesian analysis of complex data. In *Proceedings of the Conference on Summer Computer Simulation*, SummerSim '15, page 1–8, San Diego, CA, USA, 2015. Society for Computer Simulation International. ISBN 9781510810594.

Sean Matt and Ralph E. Pudritz. Accretion-powered Stellar Winds as a Solution to the Stellar Angular Momentum Problem. ApJ, 632(2):L135–L138, October 2005a. doi: 10.1086/498066.

Sean Matt and Ralph E. Pudritz. The spin of accreting stars: dependence on magnetic coupling to the disc. MNRAS, 356(1):167–182, January 2005b. doi: 10.1111/j.1365-2966.2004.08431.x.

Sean Matt and Ralph E. Pudritz. Accretion-powered stellar winds as a solution to the stellar angular momentum problem. *The Astrophysical Journal*, 632(2):L135–L138, oct 2005. doi: 10.1086/498066. URL https://doi.org/10.1086%2F498066.

Sean Matt and Ralph E. Pudritz. Accretion-powered Stellar Winds. III. Spin-Equilibrium Solutions. ApJ, 681(1):391–399, July 2008a. doi: 10.1086/587453.

Sean Matt and Ralph E. Pudritz. Accretion-powered Stellar Winds. II. Numerical Solutions for Stellar Wind Torques. ApJ, 678(2):1109–1118, May 2008b. doi: 10.1086/533428.

Sean P. Matt, Giovanni Pinzón, Ramiro de la Reza, and Thomas P. Greene. Spin Evolution of Accreting Young Stars. I. Effect of Magnetic Star-Disk Coupling. ApJ, 714(2):989–1000, May 2010. doi: 10.1088/0004-637X/714/2/989.

Sean P. Matt, Giovanni Pinzón, Thomas P. Greene, and Ralph E. Pudritz. Spin Evolution of Accreting Young Stars. II. Effect of Accretion-powered Stellar Winds. ApJ, 745(1):101, January 2012. doi: 10.1088/0004-637X/745/1/101.

P. F. L. Maxted, R. D. Jeffries, J. M. Oliveira, T. Naylor, and R. J. Jackson. A survey for low-mass spectroscopic binary stars in the young clusters around σ Orionis and λ Orionis. MNRAS, 385(4):2210–2224, April 2008. doi: 10.1111/j.1365-2966.2008.13008.x.

M. Morales-Calderón, J. R. Stauffer, L. A. Hillenbrand, R. Gutermuth, I. Song, L. M. Rebull, P. Plavchan, J. M. Carpenter, B. A. Whitney, K. Covey, C. Alves de Oliveira, E. Winston, M. J. McCaughrean, J. Bouvier, S. Guieu, F. J. Vrba, J. Holtzman, F. Marchis, J. L. Hora, L. H. Wasserman, S. Terebey, T. Megeath, E. Guinan, J. Forbrich, N. Huélamo, P. Riviere-Marichalar, D. Barrado, K. Stapelfeldt, J. Hernández, L. E. Allen, D. R. Ardila, A. Bayo, F. Favata, D. James, M. Werner, and K. Wood. YSOVAR: THE FIRST SENSITIVE, WIDE-AREA, MID-INFRARED PHOTOMETRIC MONITORING OF THE ORION NEBULA CLUSTER. *The Astrophysical Journal*, 733(1):50, may 2011. doi: 10.1088/0004-637x/733/1/50. URL https://doi.org/10.1088%2F0004-637x%2F733%2F1%2F50.

P. Murdin and M. V. Penston. The Lambda Orionis association. MNRAS, 181:657, December 1977. doi: 10.1093/mnras/181.4.657.

A. Natta, L. Testi, J. M. Alcalá, E. Rigliaco, E. Covino, B. Stelzer, and V. D'Elia. X-shooter spectroscopy of young stellar objects. V. Slow winds in T Tauri stars. A&A, 569:A5, September 2014. doi: 10.1051/0004-6361/201424136.

Matthew Newville, Till Stensitzki, Daniel B. Allen, and Antonino Ingargiola. LMFIT: Non-Linear Least-Square Minimization and Curve-Fitting for Python, September 2014. URL https://doi.org/10.5281/zenodo.11813.

Duy Cuong Nguyen, Ray Jayawardhana, Marten H. van Kerkwijk, Alexis Brandeker, Alexander Scholz, and Ivana Damjanov. DISK BRAKING IN YOUNG STARS: PROBING ROTATION IN CHAMAELEON i AND TAURUS-AURIGA. *The Astrophysical Journal*, 695(2):1648–1656, apr 2009. doi: 10.1088/0004-637x/695/2/1648. URL https://doi.org/10.1088%2F0004-637x%2F695%2F2%2F1648.

B A Nicholson, G A J Hussain, J-F Donati, C P Folsom, M Mengel, B D Carter, D Wright, and MaTYSSE collaboration. The surface magnetic activity of the weak-line T Tauri stars TWA 9A and V1095 Sco. *Monthly Notices of the Royal Astronomical Society*, 480 (2):1754–1766, 07 2018. ISSN 0035-8711. doi: 10.1093/mnras/sty1965. URL https://doi.org/10.1093/mnras/sty1965.

Richard Olney, Marina Kounkel, Chad Schillinger, Matthew T. Scoggins, Yichuan Yin, Erin Howard, K. R. Covey, Brian Hutchinson, and Keivan G. Stassun. APOGEE Net: Improving the Derived Spectral Parameters for Young Stars through Deep Learning. AJ, 159(4): 182, April 2020. doi: 10.3847/1538-3881/ab7a97.

G. Pantolmos, C. Zanni, and J. Bouvier. Magnetic torques on t tauri stars: Accreting versus non-accreting systems. *A&A*, 643:A129, 2020. doi: 10.1051/0004-6361/202038569. URL https://doi.org/10.1051/0004-6361/202038569.

Padmakar Parihar, Sergio Messina, Elisa Distefano, N. S. Shantikumar, and Biman J. Medhi. Exploring pre-main-sequence variables of the ONC: the new variables. *Monthly Notices of the Royal Astronomical Society*, 400(2):603–621, 11 2009. ISSN 0035-8711. doi: 10.1111/j.1365-2966.2009.15496.x. URL https://doi.org/10.1111/j.1365-2966.2009.15496.x.

Ilaria Pascucci, Sylvie Cabrit, Suzan Edwards, Uma Gorti, Oliver Gressel, and Takeru Suzuki. The Role of Disk Winds in the Evolution and Dispersal of Protoplanetary Disks. *arXiv e-prints*, art. arXiv:2203.10068, March 2022.

Mark J. Pecaut and Eric E. Mamajek. Intrinsic Colors, Temperatures, and Bolometric Corrections of Pre-main-sequence Stars. ApJS, 208(1):9, September 2013. doi: 10.1088/0067-0049/208/1/9.

Giovanni Pinzón, Jesús Hernández, Javier Serna, Alexandra García, Ezequiel Manzo-Martínez, Alexandre Roman-Lopes, Carlos G. Román-Zúñiga, Maria Gracia Batista, Julio Ramírez-Vélez, Yeisson Osorio, and Ronald Avendaño. Understanding the angular momentum evolution of t tauri and herbig ae/be stars. *The Astronomical Journal*, 162(3):90, aug 2021. doi: 10.3847/1538-3881/ac04ae. URL https://doi.org/10.3847/1538-3881/ac04ae.

Caeley V. Pittman, Catherine C. Espaillat, Connor E. Robinson, Thanawuth Thanathibodee, Nuria Calvet, John Wendeborn, Jesus Hernández, Carlo F. Manara, Fred Walter, Péter Ábrahám, Juan M. Alcalá, Sílvia H. P. Alencar, Nicole Arulanantham, Sylvie Cabrit, Jochen Eislöffel, Eleonora Fiorellino, Kevin France, Manuele Gangi, Konstantin Grankin, Gregory J. Herczeg, Ágnes Kóspál, Ignacio Mendigutía, Javier Serna, and Laura Venuti. Towards a comprehensive view of accretion, inner disks, and extinction in classical t tauri stars: An odysseus study of the orion ob1b association. *The Astronomical Journal*, 164 (5):201, oct 2022. doi: 10.3847/1538-3881/ac898d. URL https://dx.doi.org/10.3847/1538-3881/ac898d.

Plotly Technologies Inc. Collaborative data science, 2015. URL https://plot.ly.

L. M. Rebull. Rotation of young low-mass stars in the orion nebula cluster flanking fields. *The Astronomical Journal*, 121(3):1676–1709, mar 2001. doi: 10.1086/319393. URL https://doi.org/10.1086%2F319393.

L. M. Rebull, J. R. Stauffer, S. T. Megeath, J. L. Hora, and L. Hartmann. A Correlation between Pre–Main-Sequence Stellar Rotation Rates and IRAC Excesses in Orion. *Astrophys. J.*, 646(1):297–303, jul 2006. ISSN 0004-637X. doi: 10.1086/504865. URL http://stacks.iop.org/0004-637X/646/i=1/a=297.

L. M. Rebull, A. M. Cody, K. R. Covey, H. M. Günther, L. A. Hillenbrand, P. Plavchan, K. Poppenhaeger, J. R. Stauffer, S. J. Wolk, R. Gutermuth, M. Morales-Calderón, I. Song, D. Barrado, A. Bayo, D. James, J. L. Hora, F. J. Vrba, C. Alves de Oliveira, J. Bouvier, S. J. Carey, J. M. Carpenter, F. Favata, K. Flaherty, J. Forbrich, J. Hernandez, M. J. McCaughrean, S. T. Megeath, G. Micela, H. A. Smith, S. Terebey, N. Turner, L. Allen, D. Ardila, H. Bouy, and S. Guieu. YOUNG STELLAR OBJECT VARIABILITY (YSOVAR): LONG TIMESCALE VARIATIONS IN THE MID-INFRARED. *The Astronomical Journal*, 148(5):92, oct 2014. doi: 10.1088/0004-6256/148/5/92. URL https://doi.org/10.1088%2F0004-6256%2F148%2F5%2F92.

A. Reiners and J. H. M. M. Schmitt. On the feasibility of the detection of differential rotation in stellar absorption profiles. *Astron. Astrophys.*, 384(1):155–162, mar 2002. ISSN 0004-6361. doi: 10.1051/0004-6361:20011801. URL http://www.aanda.org/10.1051/0004-6361:20011801.

Victor Réville, Allan Sacha Brun, Sean P. Matt, Antoine Strugarek, and Rui F. Pinto. THE EFFECT OF MAGNETIC TOPOLOGY ON THERMALLY DRIVEN WIND: TOWARD a GENERAL FORMULATION OF THE BRAKING LAW. *The Astrophysical Journal*, 798(2):116, jan 2015. doi: 10.1088/0004-637x/798/2/116. URL https://doi.org/10.1088/0004-637x/798/2/116.

Katherine L Rhode, William Herbst, and Robert D Mathieu. Rotational Velocities and Radii of Pre{\textendash}Main-Sequence Stars in the Orion Nebula Cluster. *Astron. J.*, 122(6):3258–3279, dec 2001. doi: 10.1086/324448. URL https://doi.org/10.1086{%}2F324448.

George R. Ricker, Joshua N. Winn, Roland Vanderspek, David W. Latham, Gáspár Á. Bakos, Jacob L. Bean, Zachory K. Berta-Thompson, Timothy M. Brown, Lars Buchhave, Nathaniel R. Butler, R. Paul Butler, William J. Chaplin, David Charbonneau, Jørgen Christensen-Dalsgaard, Mark Clampin, Drake Deming, John Doty, Nathan De Lee, Courtney Dressing, E. W. Dunham, Michael Endl, Francois Fressin, Jian Ge, Thomas Henning, Matthew J. Holman, Andrew W. Howard, Shigeru Ida, Jon Jenkins, Garrett Jerni-

gan, John Asher Johnson, Lisa Kaltenegger, Nobuyuki Kawai, Hans Kjeldsen, Gregory Laughlin, Alan M. Levine, Douglas Lin, Jack J. Lissauer, Phillip MacQueen, Geoffrey Marcy, P. R. McCullough, Timothy D. Morton, Norio Narita, Martin Paegert, Enric Palle, Francesco Pepe, Joshua Pepper, Andreas Quirrenbach, S. A. Rinehart, Dimitar Sasselov, Bun'ei Sato, Sara Seager, Alessandro Sozzetti, Keivan G. Stassun, Peter Sullivan, Andrew Szentgyorgyi, Guillermo Torres, Stephane Udry, and Joel Villasenor. Transiting Exoplanet Survey Satellite (TESS). 9143:556 – 570, 2014. doi: 10.1117/12.2063489. URL https://doi.org/10.1117/12.2063489.

Bayron Rodríguez-Feliciano, Javier Serna, Alejandro García-Varela, Jesús Hernández, and Juan F. Cabrera-García. Machine-learning morphological classification of tess light curves of t tauri stars. *The Astronomical Journal*, 166(5):189, oct 2023. doi: 10.3847/1538-3881/acf865. URL https://dx.doi.org/10.3847/1538-3881/acf865.

Noemi Roggero, Jérôme Bouvier, Luisa M. Rebull, and Ann Marie Cody. The dipper population of Taurus seen with K2. A&A, 651:A44, July 2021. doi: 10.1051/0004-6361/202140646.

Carlos G. Román-Zúñiga, Marina Kounkel, Jesús Hernández, Karla Peña Ramírez, Ricardo López-Valdivia, Kevin R. Covey, Amelia M. Stutz, Alexandre Roman-Lopes, Hunter Campbell, Elliott Khilfeh, Mauricio Tapia, Guy S. Stringfellow, Juan José Downes, Keivan G. Stassun, Dante Minniti, Amelia Bayo, Jinyoung Serena Kim, Genaro Suárez, Jason E. Ybarra, José G. Fernández-Trincado, Penélope Longa-Peña, Valeria Ramírez-Preciado, Javier Serna, Richard R. Lane, D. A. García-Hernández, Rachael L. Beaton, Dmitry Bizyaev, and Kaike Pan. Stellar properties for a comprehensive collection of star-forming regions in the sdss apogee-2 survey*. *The Astronomical Journal*, 165(2):51, jan 2023. doi: 10.3847/1538-3881/aca3a4. URL https://dx.doi.org/10.3847/1538-3881/aca3a4.

F. Royer. Determination of v sin i with Fourier transform techniques. *Memorie della Societa Astronomica Italiana Supplementi*, 8:124, January 2005.

F. Royer, M. Gerbaldi, R. Faraggiana, and A. E. Gómez. Rotational velocities of A-type stars. I. Measurement of v sin i in the southern hemisphere. A&A, 381:105–121, January 2002. doi: 10.1051/0004-6361:20011422.

G. G. Sacco, E. Franciosini, S. Randich, and R. Pallavicini. Flames spectroscopy of low-mass stars in the young clusters and ***. *A&A*, 488(1):167–179, 2008. doi: 10.1051/0004-6361:20079049. URL https://doi.org/10.1051/0004-6361:20079049.

C. Sauty, Z. Meliani, J. J. G. Lima, K. Tsinganos, V. Cayatte, and N. Globus. Nonradial and nonpolytropic astrophysical outflows - ix. modeling t tauri jets with a low mass-

accretion rate. *A&A*, 533:A46, 2011. doi: 10.1051/0004-6361/201116519. URL https://doi.org/10.1051/0004-6361/201116519.

J. D. Scargle. Studies in astronomical time series analysis. II. Statistical aspects of spectral analysis of unevenly spaced data. ApJ, 263:835–853, December 1982. doi: 10.1086/160554.

E. Schatzman. A theory of the role of magnetic activity during star formation. *Annales d'Astrophysique*, 25:18, February 1962.

David W. Scott. On optimal and data-based histograms. *Biometrika*, 66(3):605–610, 12 1979. ISSN 0006-3444. doi: 10.1093/biomet/66.3.605. URL https://doi.org/10.1093/biomet/66.3.605.

Javier Serna, Jesus Hernandez, Marina Kounkel, Ezequiel Manzo-Martínez, Alexandre Roman-Lopes, Carlos G. Román-Zúñiga, Maria Gracia Batista, Giovanni Pinzón, Nuria Calvet, Cesar Briceño, Mauricio Tapia, Genaro Suárez, Karla Peña Ramírez, Keivan G. Stassun, Kevin Covey, J. Vargas-González, and José G. Fernández-Trincado. Stellar Rotation of T Tauri Stars in the Orion Star-forming Complex. ApJ, 923(2):177, December 2021. doi: 10.3847/1538-4357/ac300a.

Frank H. Shu, Susana Lizano, Steven P. Ruden, and Joan Najita. Mass Loss from Rapidly Rotating Magnetic Protostars. ApJ, 328:L19, May 1988. doi: 10.1086/185152.

Aurora Sicilia-Aguilar, Lee W. Hartmann, Andrew H. Szentgyorgyi, Daniel G. Fabricant, Gábor Fűrész, John Roll, Maureen A. Conroy, Nuria Calvet, Susan Tokarz, and Jesús Hernández. Accretion, kinematics, and rotation in the orion nebula cluster: Initial results from hectochelle. *The Astronomical Journal*, 129(1):363–381, jan 2005. doi: 10.1086/426327. URL https://doi.org/10.1086/426327.

M. N. Simon, I. Pascucci, S. Edwards, W. Feng, U. Gorti, D. Hollenbach, E. Rigliaco, and J. T. Keane. Tracing Slow Winds from T Tauri Stars via Low-velocity Forbidden Line Emission. ApJ, 831(2):169, November 2016. doi: 10.3847/0004-637X/831/2/169.

S. Simón-Díaz and A. Herrero. Fourier method of determining the rotational velocities in OB stars. *Astron. Astrophys.*, 468(3):1063–1073, jun 2007. ISSN 0004-6361. doi: 10.1051/0004-6361:20066060. URL http://www.aanda.org/10.1051/0004-6361:20066060.

A Skumanich. Time Scales for CA II Emission Decay, Rotational Braking, and Lithium Depletion. *Astrophys. J.*, 171:565, feb 1972. ISSN 0004-637X. doi: 10.1086/151310. URL http://adsabs.harvard.edu/doi/10.1086/151310.

A. Smette, H. Sana, S. Noll, H. Horst, W. Kausch, S. Kimeswenger, M. Barden, C. Szyszka, A. M. Jones, A. Gallenne, J. Vinther, P. Ballester, and J. Taylor. Molecfit: A general tool for telluric absorption correction. I. Method and application to ESO instruments. A&A, 576:A77, April 2015. doi: 10.1051/0004-6361/201423932.

Garrett Somers and Marc H. Pinsonneault. Older and Colder: The Impact of Starspots on Pre-main-sequence Stellar Evolution. ApJ, 807(2):174, July 2015. doi: 10.1088/0004-637X/807/2/174.

Garrett Somers and Keivan G. Stassun. A Measurement of Radius Inflation in the Pleiades and Its Relation to Rotation and Lithium Depletion. AJ, 153(3):101, March 2017. doi: 10.3847/1538-3881/153/3/101.

Garrett Somers, Lyra Cao, and Marc H. Pinsonneault. The SPOTS Models: A Grid of Theoretical Stellar Evolution Tracks and Isochrones for Testing the Effects of Starspots on Structure and Colors. ApJ, 891(1):29, March 2020. doi: 10.3847/1538-4357/ab722e.

C. Soubiran, T. Cantat-Gaudin, M. Romero-Gómez, L. Casamiquela, C. Jordi, A. Vallenari, T. Antoja, L. Balaguer-Núñez, D. Bossini, A. Bragaglia, R. Carrera, A. Castro-Ginard, F. Figueras, U. Heiter, D. Katz, A. Krone-Martins, J. F. Le Campion, A. Moitinho, and R. Sordo. Open cluster kinematics with Gaia DR2 (Corrigendum). A&A, 623:C2, March 2019. doi: 10.1051/0004-6361/201834020e.

F. Spada and A. C. Lanzafame. Competing effect of wind braking and interior coupling in the rotational evolution of solar-like stars. *A&A*, 636:A76, 2020. doi: 10.1051/0004-6361/201936384. URL https://doi.org/10.1051/0004-6361/201936384.

K. G. Stassun. VizieR Online Data Catalog: TESS Input Catalog - v8.0 (TIC-8) (Stassun+, 2019). *VizieR Online Data Catalog*, art. IV/38, November 2019.

Keivan G. Stassun and Guillermo Torres. Parallax Systematics and Photocenter Motions of Benchmark Eclipsing Binaries in Gaia EDR3. ApJ, 907(2):L33, February 2021. doi: 10.3847/2041-8213/abdaad.

Keivan G. Stassun, Robert D. Mathieu, Tsevi Mazeh, and Frederick J. Vrba. The Rotation Period Distribution of Pre–Main-Sequence Stars in and around the Orion Nebula. *Astron. J.*, 117(6):2941–2979, jun 1999. ISSN 00046256. doi: 10.1086/300881. URL http://stacks.iop.org/1538-3881/117/i=6/a=2941.

Martin Still and Tom Barclay. PyKE: Reduction and analysis of Kepler Simple Aperture Photometry data, August 2012.

A. Strugarek, A. S. Brun, S. P. Matt, and V. Réville. MAGNETIC GAMES BETWEEN a PLANET AND ITS HOST STAR: THE KEY ROLE OF TOPOLOGY. *The Astrophysical Journal*, 815(2):111, dec 2015. doi: 10.1088/0004-637x/815/2/111. URL https://doi.org/10.1088/0004-637x/815/2/111.

L. Testi, T. Birnstiel, L. Ricci, S. Andrews, J. Blum, J. Carpenter, C. Dominik, A. Isella, A. Natta, J. P. Williams, and D. J. Wilner. Dust Evolution in Protoplanetary Disks. In Henrik Beuther, Ralf S. Klessen, Cornelis P. Dullemond, and Thomas Henning, editors, *Protostars and Planets VI*, page 339, January 2014. doi: 10.2458/azu_uapress_9780816531240-ch015.

Thanawuth Thanathibodee, Brandon Molina, Nuria Calvet, Javier Serna, Jaehan Bae, Mark Reynolds, Jesús Hernández, James Muzerolle, and Ramiro Franco Hernández. Variable Accretion onto Protoplanet Host Star PDS 70. ApJ, 892(2):81, April 2020. doi: 10.3847/1538-4357/ab77c1.

Thanawuth Thanathibodee, Nuria Calvet, Jesús Hernández, Karina Maucó, and César Briceño. A Census of the Low Accretors. I. The Catalog. AJ, 163(2):74, February 2022. doi: 10.3847/1538-3881/ac3ee6.

Thanawuth Thanathibodee, Brandon Molina, Javier Serna, Nuria Calvet, Jesús Hernández, James Muzerolle, and Ramiro Franco-Hernández. A census of the low accretors. ii. accretion properties. *The Astrophysical Journal*, 944(1):90, feb 2023. doi: 10.3847/1538-4357/acac84. URL https://dx.doi.org/10.3847/1538-4357/acac84.

Andrei Tokovinin, Monika G. Petr-Gotzens, and Cesar Briceño. Statistics of wide pre-main-sequence binaries in the orion ob1 association. *The Astronomical Journal*, 160(6):268, nov 2020. doi: 10.3847/1538-3881/abc2d6. URL https://dx.doi.org/10.3847/1538-3881/abc2d6.

C. A. Tout and J. E. Pringle. Spin-down of rapidly rotating, convective stars. MNRAS, 256: 269–276, May 1992. doi: 10.1093/mnras/256.2.269.

Brandon M. Turner and Trisha Van Zandt. A tutorial on approximate bayesian computation. *Journal of Mathematical Psychology*, 56(2):69–85, 2012. ISSN 0022-2496. doi: https://doi.org/10.1016/j.jmp.2012.02.005. URL https://www.sciencedirect.com/science/article/pii/S0022249612000272.

Dmitri A. Uzdensky. Magnetic Interaction Between Stars And Accretion Disks. Ap&SS, 292 (1):573–585, August 2004. doi: 10.1023/B:ASTR.0000045064.93078.87.

L. Venuti, J. Bouvier, A. M. Cody, J. R. Stauffer, G. Micela, L. M. Rebull, S. H. P. Alencar, A. P. Sousa, L. A. Hillenbrand, and E. Flaccomio. CSI 2264: Investigating rotation and its connection with disk accretion in the young open cluster NGC 2264. *Astron. Astrophys.*, 599:A23, mar 2017. ISSN 0004-6361. doi: 10.1051/0004-6361/201629537. URL http://www.aanda.org/10.1051/0004-6361/201629537.

J. Vernet, H. Dekker, S. D´Odorico, Kaper, L., Kjaergaard, P., Hammer, F., Randich, S., Zerbi, F., Groot, P. J., Hjorth, J., Guinouard, I., Navarro, R., Adolfse, T., Albers, P. W., Amans, J.-P., Andersen, J. J., Andersen, M. I., Binetruy, P., Bristow, P., Castillo, R., Chemla, F., Christensen, L., Conconi, P., Conzelmann, R., Dam, J., De Caprio, V., De Ugarte Postigo, A., Delabre, B., Di Marcantonio, P., Downing, M., Elswijk, E., Finger, G., Fischer, G., Flores, H., François, P., Goldoni, P., Guglielmi, L., Haigron, R., Hanenburg, H., Hendriks, I., Horrobin, M., Horville, D., Jessen, N. C., Kerber, F., Kern, L., Kiekebusch, M., Kleszcz, P., Klougart, J., Kragt, J., Larsen, H. H., Lizon, J.-L., Lucuix, C., Mainieri, V., Manuputy, R., Martayan, C., Mason, E., Mazzoleni, R., Michaelsen, N., Modigliani, A., Moehler, S., Møller, P., Norup Sørensen, A., Nørregaard, P., Péroux, C., Patat, F., Pena, E., Pragt, J., Reinero, C., Rigal, F., Riva, M., Roelfsema, R., Royer, F., Sacco, G., Santin, P., Schoenmaker, T., Spano, P., Sweers, E., Ter Horst, R., Tintori, M., Tromp, N., van Dael, P., van der Vliet, H., Venema, L., Vidali, M., Vinther, J., Vola, P., Winters, R., Wistisen, D., Wulterkens, G., and Zacchei, A. X-shooter, the new wide band intermediate resolution spectrograph at the eso very large telescope. *A&A*, 536:A105, 2011. doi: 10.1051/0004-6361/201117752. URL https://doi.org/10.1051/0004-6361/201117752.

A. A. Vidotto, S. G. Gregory, M. Jardine, J. F. Donati, P. Petit, J. Morin, C. P. Folsom, J. Bouvier, A. C. Cameron, G. Hussain, S. Marsden, I. A. Waite, R. Fares, S. Jeffers, and Jr do Nascimento, J. D. Stellar magnetism: empirical trends with age and rotation. *Monthly Notices of the Royal Astronomical Society*, 441(3):2361–2374, 05 2014. ISSN 0035-8711. doi: 10.1093/mnras/stu728. URL https://doi.org/10.1093/mnras/stu728.

Fábio Wanderley, Katia Cunha, Diogo Souto, Verne V. Smith, Lyra Cao, Marc Pinsonneault, C. Allende Prieto, Kevin Covey, Thomas Masseron, Ilaria Pascucci, Keivan G. Stassun, Ryan Terrien, Galen J. Bergsten, Dmitry Bizyaev, José G. Fernández-Trincado, Henrik Jönsson, Sten Hasselquist, Jon A. Holtzman, Richard R. Lane, Suvrath Mahadevan, Steven R. Majewski, Dante Minniti, Kaike Pan, Javier Serna, Jennifer Sobeck, and Guy S. Stringfellow. Stellar characterization and radius inflation of hyades m-dwarf stars from the apogee survey. *The Astrophysical Journal*, 951(2):90, jul 2023. doi: 10.3847/1538-4357/acd4bd. URL https://dx.doi.org/10.3847/1538-4357/acd4bd.

Jr. Warren, W. H. and J. E. Hesser. A photometric study of the Orion OB1 association. I. Observational data. ApJS, 34:115–206, June 1977. doi: 10.1086/190446.

Dan M. Watson, Nuria P. Calvet, William J. Fischer, W. J. Forrest, P. Manoj, S. Thomas Megeath, Gary J. Melnick, Joan Najita, David A. Neufeld, Patrick D. Sheehan, Amelia M. Stutz, and John J. Tobin. EVOLUTION OF MASS OUTFLOW IN PROTOSTARS. *The Astrophysical Journal*, 828(1):52, aug 2016. doi: 10.3847/0004-637x/828/1/52. URL https://doi.org/10.3847/0004-637x/828/1/52.

Edmund J. Weber and Jr. Davis, Leverett. The Angular Momentum of the Solar Wind. ApJ, 148:217–227, April 1967. doi: 10.1086/149138.

Jonathan P. Williams and Lucas A. Cieza. Protoplanetary Disks and Their Evolution. ARA&A, 49(1):67–117, September 2011. doi: 10.1146/annurev-astro-081710-102548.

S. C. Wolff, S. E. Strom, and L. A. Hillenbrand. The angular momentum evolution of 0.1–10m⊙stars from the birth line to the main sequence. *The Astrophysical Journal*, 601 (2):979–999, feb 2004. doi: 10.1086/380503. URL https://doi.org/10.1086/380503.

Insu Yi. Magnetic Braking in Spin Evolution of Magnetized T Tauri Stars. ApJ, 428:760, June 1994. doi: 10.1086/174283.

C. Zanni and J. Ferreira. MHD simulations of accretion onto a dipolar magnetosphere. II. Magnetospheric ejections and stellar spin-down. A&A, 550:A99, February 2013. doi: 10.1051/0004-6361/201220168.

E. Zari, A. G. A. Brown, and P. T. de Zeeuw. Structure, kinematics, and ages of the young stellar populations in the Orion region. A&A, 628:A123, August 2019. doi: 10.1051/0004-6361/201935781.